

International Scientific-Technical and Production Journal

The Paton WELDING JOURNAL

April
2005
4

English translation of the monthly «Avtomatische Svarka» (Automatic Welding) journal published in Russian since 1948

Founders: E.O. Paton Electric Welding Institute of the NAS of Ukraine
International Association «Welding»

Publisher: International Association «Welding»

Editor-in-Chief B.E.Paton

Editorial board:

Yu.S.Borisov V.F.Grabin
Yu.Ya.Gretskii A.Ya.Ishchenko
B.V.Khitrovskaya V.F.Khorunov
I.V.Krivtsun
S.I.Kuchuk-Yatsenko
Yu.N.Lankin V.K.Lebedev
V.N.Lipodaev L.M.Lobanov
V.I.Makhnenco A.A.Mazur
V.F.Moshkin O.K.Nazarenko
I.K.Pokhodnya I.A.Ryabtsev
Yu.A.Sternenbogen N.M.Voropai
K.A.Yushchenko V.N.Zamkov
A.T.Zelnichenko

International editorial council:

N.P.Alyoshin (Russia)
B.Braithwaite (UK)
C.Boucher (France)
Guan Qiao (China)
U.Diltay (Germany)
P.Seyffarth (Germany)
A.S.Zubchenko (Russia)
T.Eagar (USA)
K.Inoue (Japan)
N.I.Nikiforov (Russia)
B.E.Paton (Ukraine)
Ya.Pilarczyk (Poland)
D.von Hofe (Germany)
Zhang Yanmin (China)
V.K.Sheleg (Belarus)

Promotion group:

V.N.Lipodaev, V.I.Lokteva
A.T.Zelnichenko (exec. director)
Translators:
A.V.Gorskaya, I.N.Kutianova,
T.K.Vasilenko
Editor
N.A.Dmitrieva
Electron gallery:
I.S.Batasheva, T.Yu.Snegiryova

Address:

E.O. Paton Electric Welding Institute,
International Association «Welding»,
11, Bozhenko str., 03680, Kyiv, Ukraine
Tel.: (38044) 287 67 57
Fax: (38044) 528 04 86
E-mail: journal@paton.kiev.ua
<http://www.nas.gov.ua/pwj>

State Registration Certificate
KV 4790 of 09.01.2001

Subscriptions:

12 issues per year;
460\$ — regular, 390\$ — for subscription agencies, 260\$ — for students; postage and packaging included. Back issues available.

All rights reserved.

This publication and each of the articles contained herein are protected by copyright. Permission to reproduce material contained in this journal must be obtained in writing from the Publisher.

Copies of individual articles may be obtained from the Publisher.

CONTENTS

SCIENTIFIC AND TECHNICAL

Dilthey U., Mokrov O. and Pavlyk V. Modeling of consumable-electrode gas-shielded multi-pass welding of carbon steel with preheating 2

Kalina P.P., Yarovitsyn A.V. and Yushchenko K.A. Peculiarities of the microplasma powder cladding process 7

Patyupkin A.V. and Antonyuk D.A. Effect of alloying on cavitation-corrosion resistance of stainless steels and alloys 14

Kulik V.M., Savitsky M.M. and Bursky G.V. Evaluation of delayed fracture resistance of HAZ metal of high-strength steel with modeling of stress relaxation 17

Podola N.V., Rudenko P.M. and Gavrilash V.S. Algorithms for compensation of electrode wear in resistance spot welding 23

INDUSTRIAL

Shlepakov V.N. and Naumejko S.M. Self-shielded flux-cored wires for welding low-alloy steels 28

Tararychkin I.A. and Voskresensky A.S. Design of compression drive for longitudinal arc welding of thick-walled shells 30

Kornetsky O.Yu. Role of testing laboratories in providing quality control in production of welding consumables 33

Kot A.N. New developments of concern ESAB OK AristoRod and MarathonPac for MAG welding 36

Rosert R., Alimov A.N. and Mikitenko A.M. Organizing seamless wire manufacturing in Ukraine 38

BRIEF INFORMATION

Okhotsky V.B. Model of the process of combustion of iron in oxygen during steel cutting 42

Kiselevsky F.N. and Kolyada V.A. Application of object-oriented software package MS DirectShow for modelling of processing technical vision video signals 45

Theses for scientific degree 47



MODELING OF CONSUMABLE-ELECTRODE GAS-SHIELDED MULTI-PASS WELDING OF CARBON STEEL WITH PREHEATING*

U. DILTHEY, O. MOKROV and V. PAVLYK

Institute of Welding and Joints, Aachen University, Aachen, Germany

Certain features of simulation of gas-shielded consumable-electrode multi-pass welding with item preheating are considered. The paper shows the differences of the improved model from that of single-pass welding (SimWeld program package). Weld geometry and temperature cycles obtained through simulation, are in good agreement with the experimental data.

Keywords: *multi-pass arc welding, consumable electrode, shielding gas, simulation, heat mass transfer, temperature field, form of weld, modulation*

A considerable progress has been observed in the last two decades in the sphere of modeling and computer simulation of the gas-shielded welding process. Important tasks of computer simulation include projection of the temperature field and calculation of sizes and forms of the weld regarding condition (welding speed and wire feed speed), characteristics of pulses and other technical parameters, properties of the material, wire diameter, geometric characteristics of the joint (type of joint, size of gap, spatial position). The work [1] reviews the state of the art in this sphere and considers the process of single-pass gas-shielded welding employed for joining of plates up to 5 mm thick. Thicker plates are welded, as a rule, for several passes with preliminary edge preparation.

High level of developments in the sphere of single-pass welding simulation encourages the use of computer technologies in the industry for modeling and simulation of this process. Fillet welding is considered as a final production stage in manufacturing of angle sections of carbon steel St45 in the collective

research project «Integral Simulation of Materials» SFB 370 (<http://lx1.imm.rwth-aachen.de/sfb370/html/index.html>), which has already for several years been implemented at the Aachen University. The model presented in this article was developed under this project.

Experimental procedure. Diagram of the weld is shown in Figure 1. To provide full penetration and to prevent formation of defects in the weld root the K-groove was used. The first pass was carried out from the inside. Preheating up to 180–200 °C and keeping the same interpass temperature were used to prevent formation of hardening cracks. The newest digital inverter power supply CLOSS Quinto II of the CLOSS Schweißtechnik Company (Figure 2) in pulse regime with I/I -modulation was applied for welding, which provides high stability of the process.

The weld from the inside is shown in Figure 3. Jig fixed the welded plates allows a fast turning of the item between passes to prevent cooling below the interpass temperature. Temperature of the HAZ was measured by thermocouples placed into the drilled blind holes, which permits controlling preheating and interpass heating, as well as obtaining experimental curves of heating and cooling for verification of the model. Plates 8.65 mm thick of steel St45 (0.49 wt.% C) were welded into K-groove (angle of

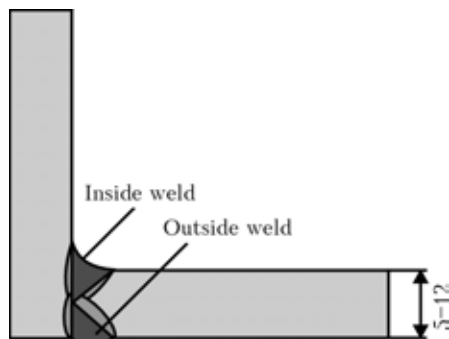


Figure 1. Scheme of fillet joint with K-groove welded in two passes

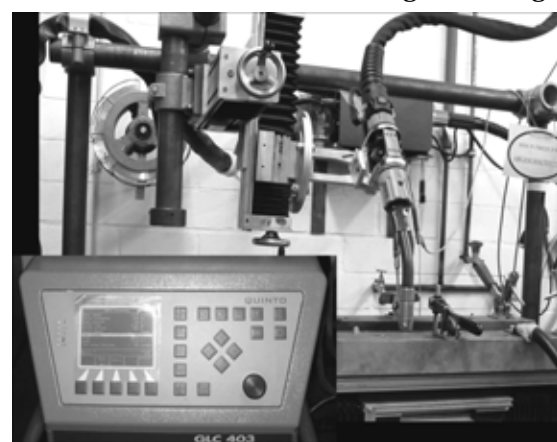


Figure 2. Experimental unit with digital inverter power supply CLOSS Quinto II and welding torch of the CLOSS Schweißtechnik Company

* From materials of the report presented at the Second International Conference on Mathematical Modelling and Information Technologies in Welding and Related Processes (Katsiveli, Crimea, September 13–17, 2004). — Kiev: PWI.



Parameters in outside and inside welding

Parameter	Weld	
	Inside	Outside
Welding speed, cm/min	45	54
Wire feed speed, m/s	8	8
Pulse duration, s	1.9	1.9
Frequency, Hz	180	180
Base current, A	50	55
Pulse current, A	450	460
Arc length coefficient, %	76	70

preparation is 45°; width of root gap --- 0.9 mm) with wire 1.2 mm in diameter. Contact distance was 15 mm. The other parameters for both passes are given in the Table.

Simulation. The following interrelated problems were consecutively solved for calculation of the temperature field and form of the weld. The main components of these problems were described previously [1, 2]:

- finding of the integral characteristics of the heat source (arc);
- finding of the heat distribution in the welded joint;
- finding of the exposed surface of the weld pool.

Multi-pass welding has two basic differences from single-pass welding from the simulation standpoint. It considers, first, preheating of the item and heating by the previous passes and, second, geometry of edge preparation and previous beads as well as their effect on distribution of the heat introduced from the arc source.

If the temperature prior to welding is controlled experimentally as in the described case, then it is trivially considered in the numerical solution by presetting the initial temperature of the item before the next pass. In case when the interval between the passes is preset, then the length of the calculated domain within the stationary model should be sufficiently large to be able to determine to what temperature the item is cooled down before the next bead deposition. Items of small dimensions require solution of the non-stationary problem.

In case of edge preparation the distribution of the heat flow on the edges of the item differs from that in the arcing on the plane surface. Strong effect of the geometry of the edge preparation on the plasma column is most vividly pronounced under short arc burning in the space limited from the sides. In this case accurate calculation of the distribution of the heat flow is possible only within the connectivity model «arc-cathode», which is currently under development stage [3]. Therefore, a simplified approach was applied in this work for describing the distribution of the heat flow on the surface of the item.

As it was previously described [1, 2] the heat capacity of the arc Q_{arc} is composed of three components:

$$Q_{arc} = Q_c + Q_a + Q_{col}, \quad (1)$$

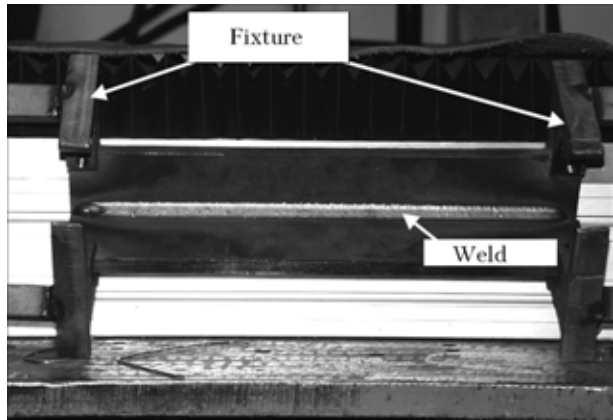


Figure 3. Inside weld and fixture

where Q_c is the heat capacity in the effective cathode spot; Q_a is the heat capacity of the electrode metal drops; Q_{col} is the heat capacity of the arc column.

Distribution of the cathode component of the heat flow q_c on the plane surface was assumed as a square-modified Gaussian distribution (Figure 4):

$$q_c(r) = \frac{6Q_c}{\pi^{3/4} r_s^2} \exp\left(-\left(3 \frac{r^2}{r_s^2}\right)^2\right), \quad (2)$$

where r is a distance from the source axis; r_s is the Rykalin radius of the source. Then this distribution was projected on the preparation line, i.e. the coordinate r in (2) was replaced by the distance l along the edge from the point of intersection of the torch axis with the item to the point on the preparation (Figure 4). Normal distribution of the heat of drops Q_a with radius r_a and uniform distribution of the part of the arc column power Q_{col} in the circle with radius r_{col} were similarly projected. Empirical radii of r_c , r_a and r_{col} distributions corresponded in this case to the single-pass welding without edge preparation.

Submodel of the heat source [1, 2] was modified by two directions. One-dimensional model of the heat

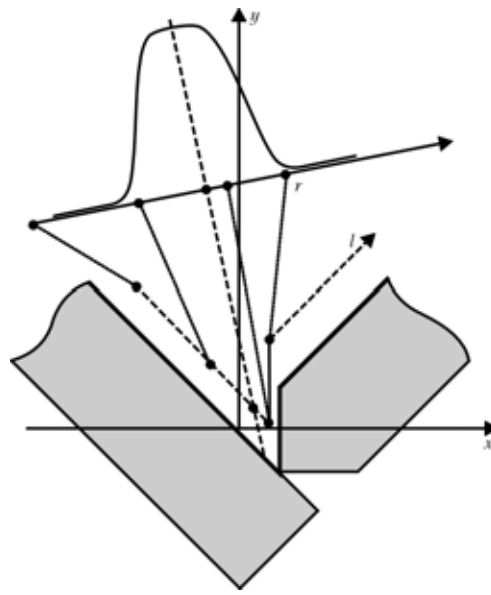


Figure 4. Diagram of heat flow distribution in the fillet weld with edge preparation

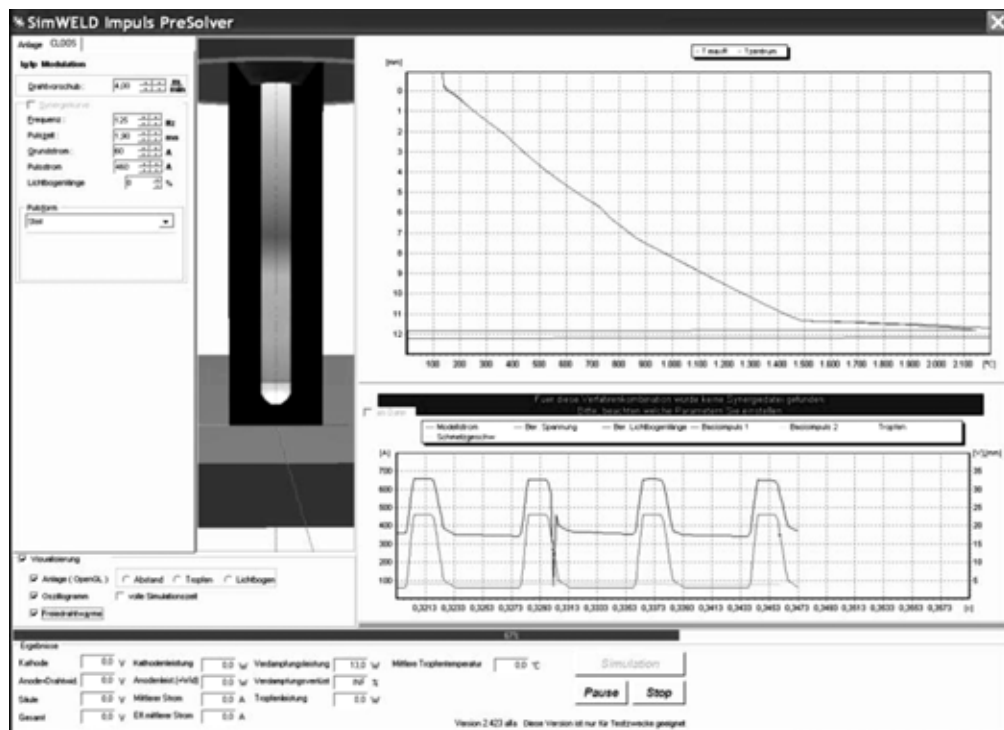


Figure 5. PreSolver module of the SimWeld software package

transfer in the wire was expanded to two-dimensional axially symmetric model. This allowed describing the temperature field in the drop regarding its shape, which is of crucial importance. For example, in case of short arc and large volume of the molten metal at the end of the wire the one-dimensional model may lead to short circuit because liquid metal (by definition) may occupy only cylindrical volume with radius equal to that of the wire. In two-dimensional model regarding the width of the drop its height will be less than the height of the imaginary cylinder, so the short circuit will not occur.

Then the external regulator of the arc length under pulse welding condition with I/I -modulation is included into the model. This mode in one form or another is implemented in many modern power sources. External regulation of the arc length when presetting the current is necessary since natural self-regulation under current (not voltage) presetting does not lead to arc length stabilization. Mathematical model of the regulator of the welding source CLOSS Quinto II was integrated into submodel of the heat sources in cooperation with the CLOSS Schweißtechnik Company. Length of the arc may be estimated by the measured voltage in the pulse phase. Essence of the arc length regulation consists in modification of the pulse parameters, for example, frequency, base current or duration for this voltage to coincide with preset values. Thus, pulse parameters are constantly changing during welding, which will also be reflected in the simulation results.

Submodel of the heat flow is implemented in the PreSolver module of the SimWeld software package [1, 2]. Interface window and results of the simulation of this module are presented in Figure 5. Parameters

of the process are preset in the left upper part of the window. Rightward one can see the picture of the welding torch, temperature field in the wire and drop and a shape of the drop. Temperature distribution by the length of the wire is graphically displayed in the right upper part. Below one can find oscillograms of the current and calculated voltage. Integral results of the calculation, for example, averaged voltage falls at different arc sites, average current, power on cathode and anode (heat transferred by the drops) are presented in the lower part of the window. These values are the input data for describing the heat source under simulation of the temperature field in the item and calculation of the weld form.

Results and discussions. Results of the simulation of the heat source in the form of current, voltage and electrical power oscillograms are presented in Figures 6–8 as compared to the experimental data. Graphs correspond to the inside welding with pulse parameters indicated in the Table. As it is seen from the current oscillogram (Figure 6), the measured pulse frequency is 210 Hz, though 180 Hz is set in the source. This difference is the result of intervention into the work of the regulator, whose degree of influence is controlled by the parameter called arc length coefficient, which in fact determines the preset (desirable) voltage in the pulse. Numerical model with the same regulator leads to the frequency 235 Hz. Regarding that frequency continuously varies in different sites of the weld and it is not possible to select accurately corresponding sites in the experiment and in the model it is then worth to consider only average-integral values. So, the deviation of the average current from experimental value is 3 %.

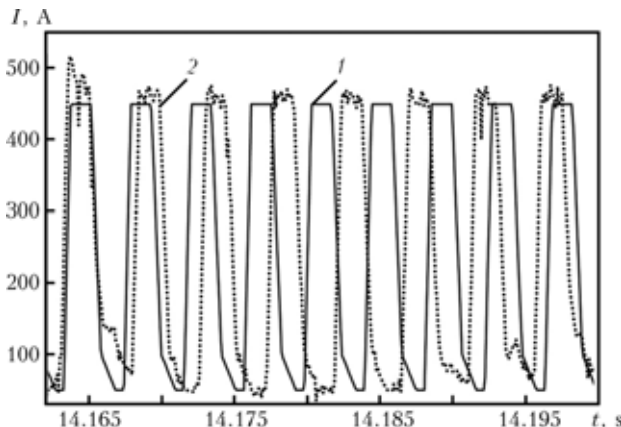


Figure 6. Comparison of calculated (1) and experimental (2) current oscillosograms during inside welding: 1 — $I_{av} = 249$ A, $f = 235$ Hz; 2 — $I_{av} = 241$ A, $f = 210$ Hz

It is followed from the voltage oscilloscopes presented in Figure 7 that frequency of short circuits (negative peaks on the graphs) are higher in the experiment than in the calculation. Besides, the model may give more stable voltage in the pulses and higher frequency. This leads to 6 % overestimation of the calculated average voltage as against the experimental one.

Oscilloscopes of the electric power of the process as a result of the simulation and the experiment calculated as a product of the current and voltage curves are shown in Figure 8. As it is seen, the average power 7.42 kW obtained from the model exceeds the measured one by 20 %. Taking into consideration the complexities of arc processes and the process of the drop transfer as well as the available regulation algorithm it is not possible to receive a more accurate calculation within the current model.

The result of numerical simulation of the weld shape and temperature field under performance of the inside bead with heat flow calculated in the PreSolver module according to the above described submodel of the source is shown in Figure 9. The calculated shape of the cross-section of the inside and outside weld in Figure 10, b is in good agreement with the experimental cross-section (Figure 10, a). Somewhat larger cross-section area of the calculated inside weld as compared to the experimental one is specified by the overestimated value of the calculated heat capacity

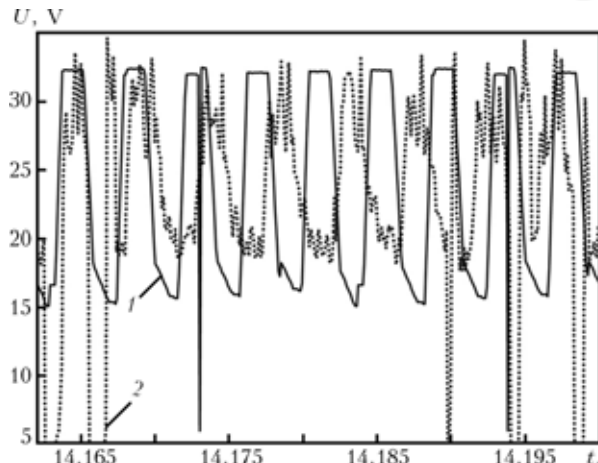


Figure 7. Comparison of calculated (1) and experimental (2) voltage oscilloscopes during inside welding: 1 — $U_{av} = 24$ W, $f = 235$ Hz; 2 — $U_{av} = 22.7$ W, $f = 210$ Hz

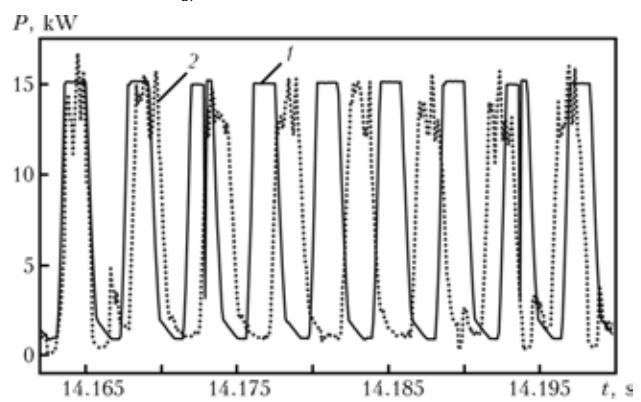


Figure 8. Comparison of calculated (1) and experimental (2) oscilloscopes of instant electrical power during inside welding: 1 — $P_w = 7.42$; 2 — 6.25 kW

of the process, as it was mentioned above. This also leads to higher calculated temperature peaks as against measured ones, which is shown in Figure 11. On the whole the calculated and experimental results are in satisfactory compliance.

CONCLUSION

Expansion of the previously developed model of consumable-electrode gas-shielded single-pass welding for multi-pass welding of thick plates with edge preparation is presented in this work. The main complica-

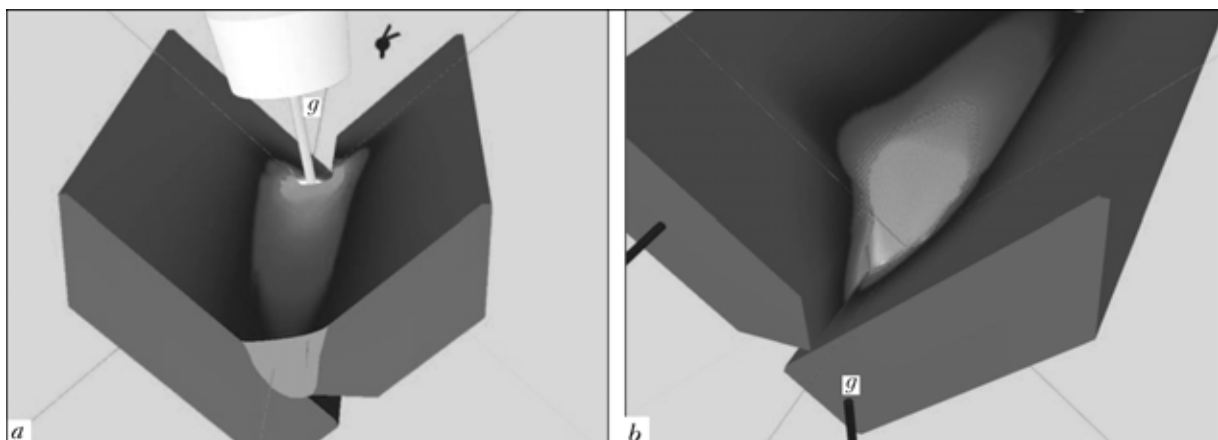


Figure 9. Simulation of form of inside weld and temperature field: a — weld cross-section; b — weld pool with exposed surface

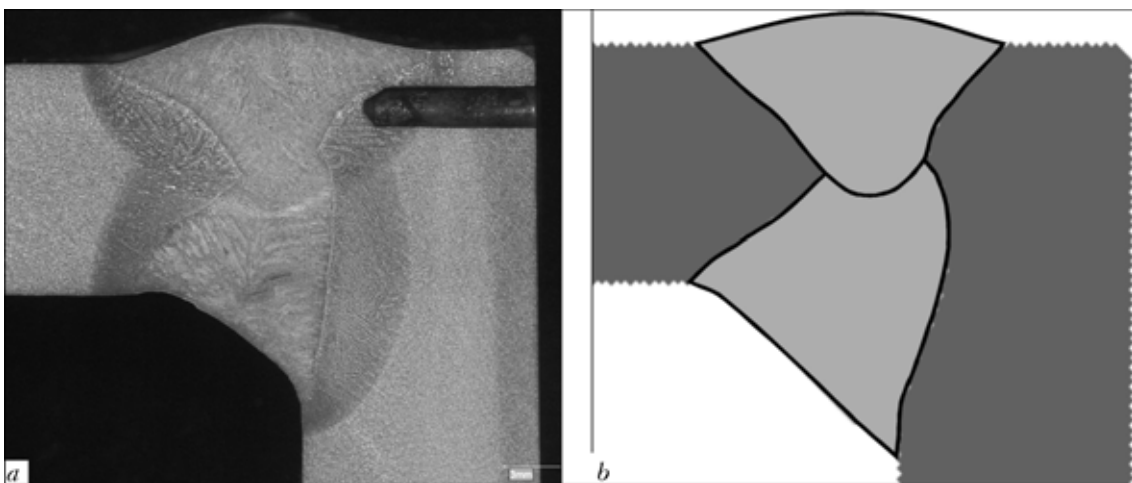


Figure 10. Experimental (a) and calculated (b) form of the weld cross-section

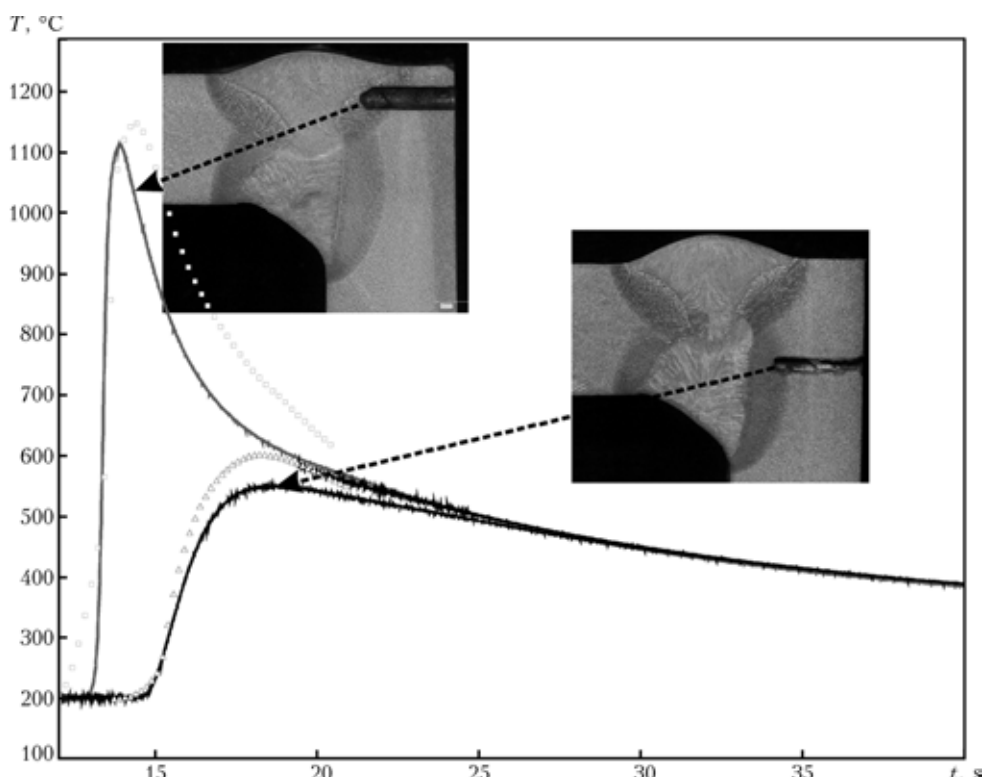


Figure 11. Temperature cycles in different points of tempered steel CH5 (□) and CH8 (Δ) welded joints with inside weld: solid curves — calculated data; symbols — experimental data

tion of the model is connected in this case with the adequate description of the heat flow distribution in the item.

It is shown that assumption of a simple linear representation of the distribution on the surface of the edges in case of the assumed plane surface the simulation may produce a satisfactory agreement with the experiment. Physically substantiated description of the heat flow distribution on the geometrically complex surface may be achieved only in the connectivity models «arc–cathode», which are being currently developed.

Regulating algorithms available in the modern welding sources with digital control and intended for stabilization of the process complicate the adequate simulation of the heat input in the pulse process,

especially in I/I -modulation mode. The developed model of heat mass transfer in the wire and drop regarding regulator allows about 20 % calculation accuracy of heat input under I/I -modulation.

- Dilthey, U., Dikshev, I., Mokrov, O. et al. (2002) Modeling of process and simulating programs for welding in active and inert gases. In: *Proc. of Int. Conf. on Mathematical Modelling and Information Technologies in Welding and Related Processes*, Katsiveli, Crimea, Sept. 16–20, 2002. Kiev: PWI.
- Dilthey, U., Pavlyk, V., Mokrov, O. et al. (2004) Software package SimWeld for simulation of welding process. Part 1. Gas-metal-arc welding of steels and aluminium alloys. In: *Mathematical modelling of weld phenomena 7: Proc. of 7th Int. Seminar on Numerical Analysis of Weldability*, Graz-Seggau, 29 Sept.–1 Oct., 2003. Ed. by H. Cerjak et al. Graz: GTU.
- Fan, H.G., Kovacevic, R.A. (2004) A unified model of transport phenomena in gas metal arc welding including electrode, arc plasma and molten pool. *J. Phys. D: Appl. Phys.*, **37**, 2531–2544.

PECULIARITIES OF THE MICROPLASMA POWDER CLADDING PROCESS

P.P. KALINA, A.V. YAROVITSYN and K.A. YUSHCHENKO

E.O. Paton Electric Welding Institute, NASU, Kiev, Ukraine

Thermal power of the arc, effective efficiency of heating of a workpiece, powder utilisation factor, geometrical parameters of the weld and coefficient of heat flow concentration in microplasma powder cladding were studied. The current and, to a lesser degree, powder consumption were found to be the main technological parameters affecting thermal characteristics of the arc. The coefficient of concentration of heat flow of the plasma arc in microplasma powder cladding is determined primarily by the diameter of the plasmatron nozzle channels, arc length and addition of powder to the arc.

Keywords: *microplasma powder cladding, calorimetry, effective thermal power, effective efficiency of heating of workpiece, heat losses at plasmatron nozzles, heat balance, powder utilisation factor, geometrical parameters of cladding, coefficient of heat flow concentration*

Heat-resistant nickel alloys with a 20–45 % content of the γ -phase are considered to have limited weldability, and those with a more than 50 % content of this phase are considered to be unweldable by the fusion welding methods [1] because of their increased sensitivity to hot cracking [2, 3]. During the last 15 years the arc processes involving a powder additive have been applied to solve the problem of repair welding and cladding of items of special heat-resistant steels and alloys [4, 5]. To provide an efficient control of the process and optimise its parameters, it is necessary to know conditions of formation of a welded joint in order to reduce sensitivity to hot cracking. Knowledge of peculiarities of burning of the powder-containing microplasma discharge and thermal characteristics of a real process of microplasma powder cladding (MPC) makes it possible to model (in the first approximation) the distribution of heat in the HAZ metal for optimisation of cladding conditions favourable in terms of weldability of special steels and alloys [6]. The effect of basic process parameters on thermal characteristics of cladding plasmatrons was studied in detail in [7, 8]. However, these studies did not consider the effect of powder, the addition of which to the plasma arc results in redistribution of heat during the MPC process.

The purpose of this study was to investigate the effective thermal power of the arc, q_s , effective efficiency of heating of a workpiece, η_{work} , heat losses at the plasmatron nozzles, η_n , heat balance for wide and narrow substrates, powder utilisation factor (PUF), geometrical parameters of cladding and coefficient of concentration of heat flow of the arc, k [9], depending upon the MPC process parameters.

The effective efficiency of the arc was determined by the method of dip calorimetry [10] using an experimental unit, the schematic diagram of which is shown in Figure 1. Heat losses at the plasmatron nozzles were evaluated by flow calorimetry through

measuring the difference between the inlet and outlet water temperature in the system used for cooling the nozzles. The accepted method for investigation of heat balance also allows the data on PUF and geometrical parameters of the weld to be generated.

Thermal power of the arc was investigated using a specially developed experimental unit (see Figure 1), which consists of water calorimeter 1 with specimen 3 secured to copper fixture 8. The fixture with the specimen lies on removable support lobes 2 and 7 intended for rapid movement of the specimen to the calorimeter. Removable runoff tab 6 for ignition of the arc is also located on the lobes. Plasmatron 4 is secured to moveable bracket 5 of the AD-228 displacement drive. Calorimeter 1 is a cylindrical vessel having double-layer walls with a heat-insulating material, i.e. foam plastic, located between the layers. Distilled water is a calorimetry body. Mixer 9 serves to level the water temperature. The calorimetry fluid temperature was measured using clinical digital resistance thermometer 10 of the ART.02113 model to an accuracy of 0.1 °F (0.056 °C). Readings of the digital thermometer were calibrated using metastatic

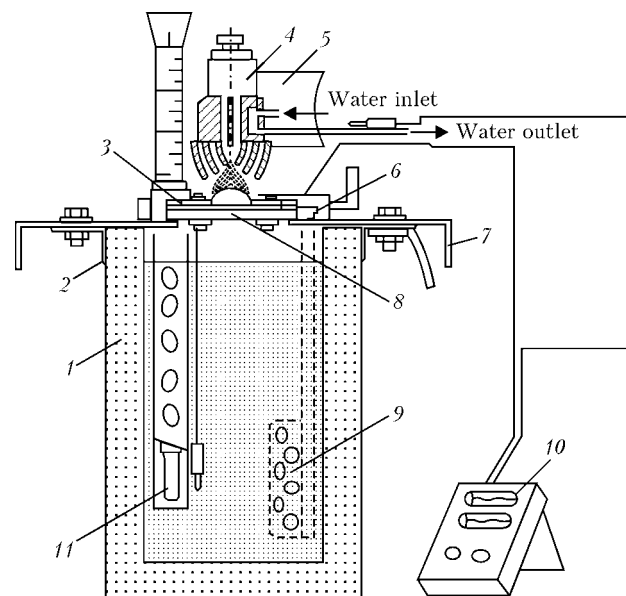


Figure 1. Schematic diagram of dip calorimetry unit (see designations in the text)

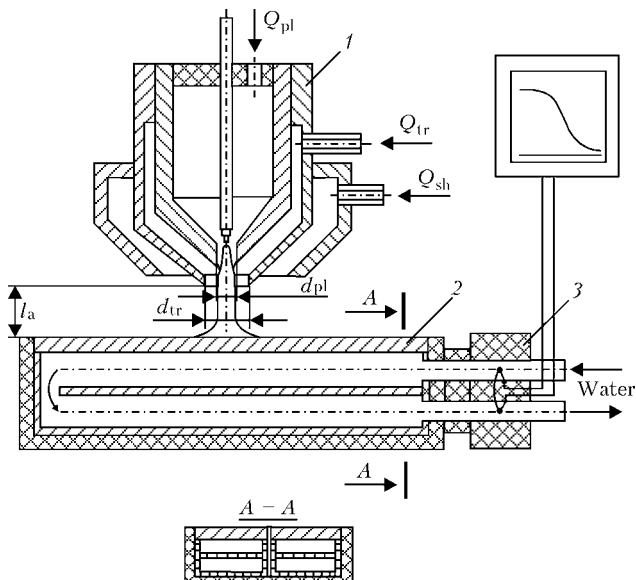


Figure 2. Schematic diagram of experimental unit for two-sectional flow calorimetry (see designations in the text)

Beckmann thermometer 11 with a scale factor of ± 0.01 °C. The calorimeter is designed so that changes in its temperature do not exceed 5 °C under maximal cladding conditions.

The efficiency of heating was determined from the following formula:

$$q_s = K\Delta T' \text{ (J)}, \quad (1)$$

where K is the constant of the calorimetric system (the amount of heat input that causes an increase of 1° in the calorimeter temperature, $K = 8553 \pm \pm 55$ J/°C); and $\Delta T'$ is the change in the calorimeter temperature.

Heat losses at the plasmatron nozzles were estimated from the value of the heat flow taken up by the water-cooled copper nozzles:

$$q_f = c\rho Q_w \Delta T' \text{ (W)}, \quad (2)$$

where c is the heat capacity of water, J/(g·K); ρ is the density of water, g/cm³; Q_w is the water con-

Thermal characteristics and coefficients of concentration of heat flow of the arc for different MPC process parameters

Parameter	Thermal characteristics of arc	Arc heat flow concentration coefficient
Ratio of plasmatron nozzle diameters	2/5.2 2/3.6 2/5.2	1/3.6 2/3.6 2/5.2
Arc current I_a , A	20–140	30–120
Total gas (argon) flow rate Q_z , l/min	21	21
Plasma gas flow rate Q_{pl} , l/min	1.0	0.5–3.0
Arc length l_a , mm	5	5–15
Cladding speed v_c , m/h	4.5	4.5
Powder consumption G_{powd} , g/min	0–12	0–25
Powder particle size d , μm	180–300	180–300

sumption, cm^3/s ; and $\Delta T'$ is the integrated difference of temperatures of water at the inlet and outlet of the cooling jacket, °C.

The cooling water consumption was measured using a measuring vessel, temperature difference $\Delta T'$ --- using digital thermometer 10 with a remote probe. Development of the temperature was read every 10 s. Parameters of the arc (current and voltage) were monitored with the class 0.1 devices.

The effective efficiency of heating of a workpiece, η_{work} , and heat losses at the plasmatron nozzles, η_n , were calculated as a ratio of heat flow to the workpiece and plasmatron nozzle to the arc power. The heat losses for thermal radiation, η_f , were determined as a difference of sum η_Σ of the effective efficiency and heat losses at the plasmatron nozzles from 100 %. PUF was calculated as a ratio of mass of the deposited bead, M_b , to mass of the consumed powder, and geometrical parameters of cladding were determined from macrosections of the clad specimens. The coefficient of concentration of heat flow of the arc was estimated using the two-sectional calorimeter by the method described in [11]. The experimental unit (Figure 2) consists of plasmatron 1, two-sectional flow calorimeter 2 and block of differentiated thermocouples 3. The main difference of the experimental conditions from those used in studies [7, 11] lies in the fact that the working surface of a calorimeter probe is made from stainless steel 04Kh19AFT (instead of copper), and that the powder is added to the arc.

According to this method, the concentration coefficient was calculated using the following equation:

$$k = \frac{1}{2(-y)^2} \left[\Phi^{-1} \left(\frac{q_{(-y)}}{q_s} \right) \right]^2, \quad (3)$$

where Φ and Φ^{-1} are the function and argument of function of the tabulated probability integral [12]; $q_{(-y)}$ is the effective thermal power for part of the heating spot at a deviation of its axis from the joint between two plates by the $(-y)$ value.

Effective thermal power $q_{(-y)}$ and q_s were determined from equation (2). Temperature difference $\Delta T'$ was estimated using differential thermobatteries, each consisting of chromel-copel thermocouples and potentiometer LKS4-003. The temperature scale was calibrated against the clinical digital resistance thermometer ART.02113 with an accuracy of 0.1 °F (0.056 °C). Consumption of the cooling water and parameters of the arc (current and voltage) were monitored as in the case of investigation of heat losses at the plasmatron nozzles.

Experiments on evaluation of the effect of the MPC parameters on thermal characteristics of the arc, heat flow concentration coefficient (Table), PUF and geometrical parameters of the deposited layer in cladding of powder 06Kh13N4 on plates of stainless steel 04Kh19AFT measuring 95 × 45 × 4 mm were conducted by the procedures described in this study. The experiments were performed using the plasma powder



cladding unit UPNS-304 with plasmatron PPS-004 at a powder introduction angle of 20°. Argon was used as a plasma, transporting and shielding gas. Each experiment was repeated not less than four times. Regression equations in the form of the second-order polynomials were derived as a result of statistical processing of the experimental data:

$$q_s(I_a, G_{\text{powd}}) = 222.9 + 5.84I_a - 5.92G_{\text{powd}} + \\ - 0.038I_aG_{\text{powd}} + 0.013I_a^2 - 0.11G_{\text{powd}}^2 \quad (4)$$

$$\text{PUF}(I_a, G_{\text{powd}}) = -0.422 + 0.012I_a + 0.025G_{\text{powd}} - \\ - 1.59 \cdot 10^{-4} I_aG_{\text{powd}} - 2.83 \cdot 10^{-5} I_a^2 - 2.56 \cdot 10^{-5} G_{\text{powd}}^2 \quad (\%) \quad (5)$$

$$h_b(I_a, G_{\text{powd}}) = 0.615 - 0.01I_a + 0.2G_{\text{powd}} + \\ + 1.562 \cdot 10^{-3} I_aG_{\text{powd}} - 7.26 \cdot 10^{-6} I_a^2 - 6.45G_{\text{powd}}^2 \quad (\text{mm}) \quad (6)$$

As can be seen from the dependencies in Figure 3, a plotted on the basis of regression equations, the effective thermal power grows in direct proportion with increase in the arc current. Addition of powder to the plasma arc column leads to an almost 90 W decrease in q_s as a result of decrease in the arc voltage (because of increased conductivity in the arc gap), as well as reduction in the arc gap due to the deposited bead. Decrease in the effective thermal power with increase in a powder consumption from 4 to 12 g/min is attributable to the heat losses (for powder) as a result of decrease in PUF.

Increase in the arc current is accompanied by decrease in the effective efficiency of heating of a workpiece (Figure 3, b), which leads to higher constriction of the plasma arc by the plasmatron nozzles and higher heat losses at the nozzles (Figure 3, c). With increase in the powder consumption, η_{work} can be described by a drooping curve (especially for a current below 80 A). As the arc current is varied from 80 to 120 A, η_{work} changes from 68 to 60 %. With increase in the current to more than 120 A, the effective efficiency of heating of a workpiece can be described by an almost horizontal straight line and ranges from 59 to 61 % at a powder consumption of 4 to 12 g/min. Decrease in η_{work} with increase in the powder consumption is attributable to the dissipation of heat with the powder that does not participate in formation of a cladding bead.

As the powder consumption is increased, the heat losses at the plasmatron nozzles vary from 25 to 40 % at a current range of 80–120 A and powder consumption of 4–12 g/min, and can be described by the curve with a maximum (Figure 3, c). At a powder consumption of more than 6 g/min the heat losses decrease. This is attributable to removal of heat from the plasma arc with the powder, which, in turn, decreases heat removed by the plasmatron nozzles.

Figure 4, a and b shows results of investigations of heat balance in MPC using no powder. The experimental data show a good agreement of the heat balance for all the experiments. As seen from the dependencies

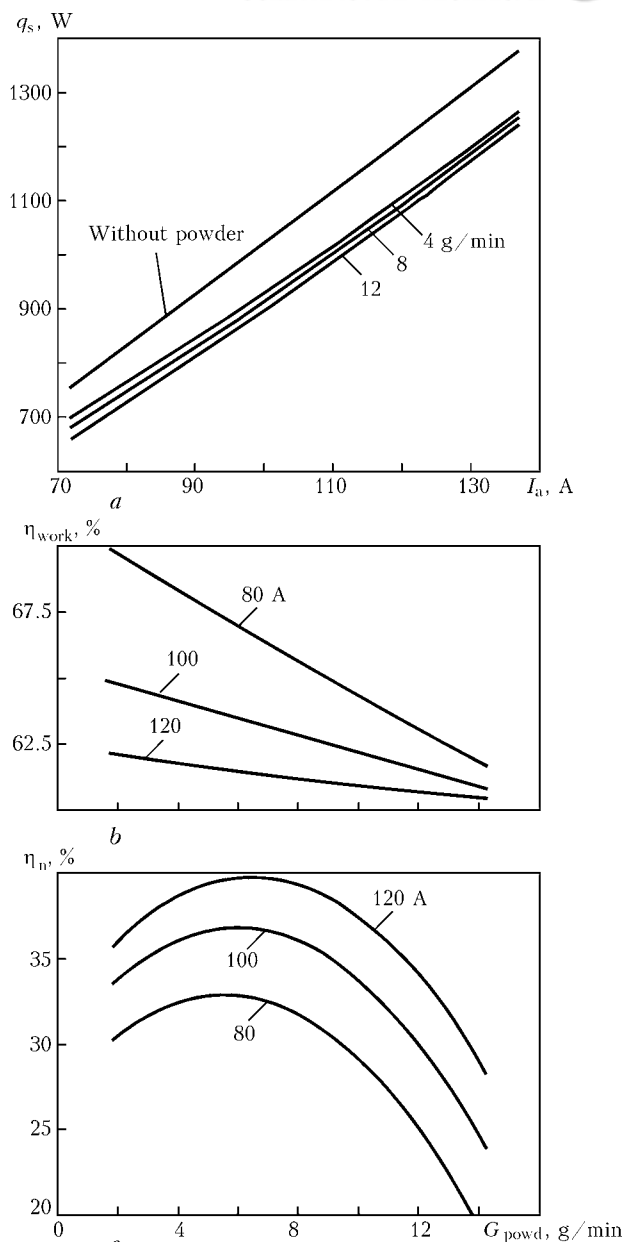


Figure 3. Dependence of the effective thermal power of the arc (a), effective efficiency of heating of a workpiece (b) and coefficient of heat losses at the plasmatron nozzles (c) upon the arc current and powder consumption

plotted on the basis of regression equations, increase in the current is accompanied by decrease in the effective efficiency of heating of a workpiece from 80 to 60 % within the investigated range of the process parameters. Drop of η_{work} is associated primarily with growth of the heat losses mostly at the plasmatron nozzles from 15 to 30 %, as well as heat losses for thermal radiation. The process conditions being identical, in MPC on a narrow substrate 4 mm wide (Figure 4, b) the heat losses for thermal radiation are 5–10 % higher than in the case of the arc burning on a wide substrate, which is caused by splitting of the plasma arc by the narrow substrate.

The heat balance changes to a certain degree with an addition of powder to the plasma arc (Figure 4, c, d). In cladding on a wide substrate the effective efficiency of heating of a workpiece decreases (Fi-

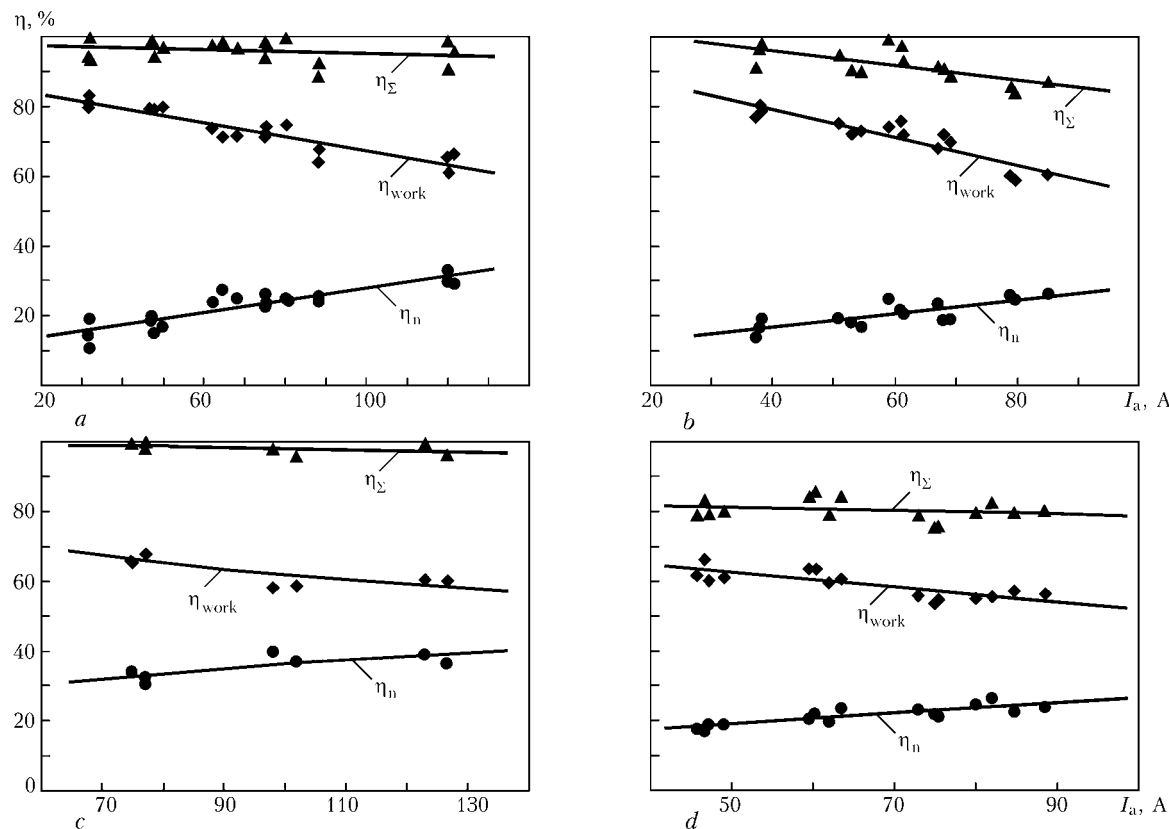


Figure 4. Effect of the arc current on thermal balance of MPC without (a, b) and with powder (c, d) (ratio of the plasmatron nozzle diameters is 2/5.2): a, b — wide and narrow substrate, respectively (without powder); c — wide substrate, $G_{\text{powd}} = 8 \text{ g/min}$; d — narrow substrate, $G_{\text{powd}} = 5 \text{ g/min}$

Figure 4, c) within a range of 58–68 %, the heat losses for thermal radiation also decrease (1–4 %) as a result of removal of heat from the plasma jet with the powder, whereas the heat losses at the plasmatron nozzles grow to 30–40 % within the range under investigation. In cladding on a narrow substrate (Figure 4, d), η_{work} drops to 55–65 % with an addition of powder, η_n hardly changes, and the heat losses for thermal radiation grow to 16–22 %.

PUF strongly depends upon the arc current and, to a lesser degree, upon the powder consumption (Figure 5). As the current is increased from 70 to 140 A,

PUF grows from 0.35 to 0.75. This is attributable to the fact that increase in the current is accompanied by increase in the amount of heat stored in the weld pool, as well as thermal power of the plasma arc, thus allowing a larger amount of the powder to be melted. Growth in PUF with increase in the powder consumption is provided by an increased concentration of the powder that gets into the weld pool. With further growth of the powder consumption, PUF can be described by the curve with a maximum caused by intensive cooling of the plasma arc and weld pool by the powder additive (Figure 6). Increase in the bead

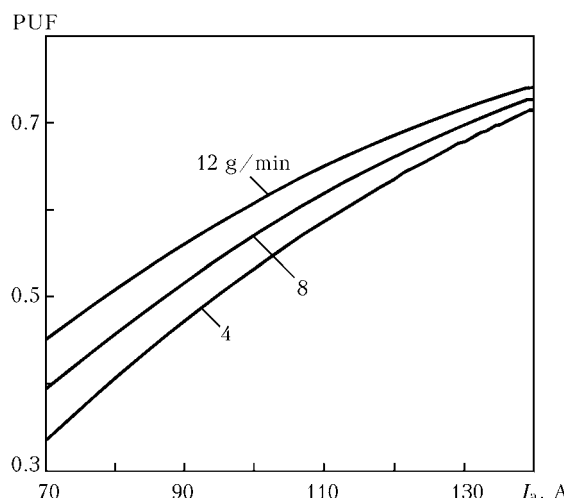


Figure 5. Dependence of PUF upon the arc current and powder consumption

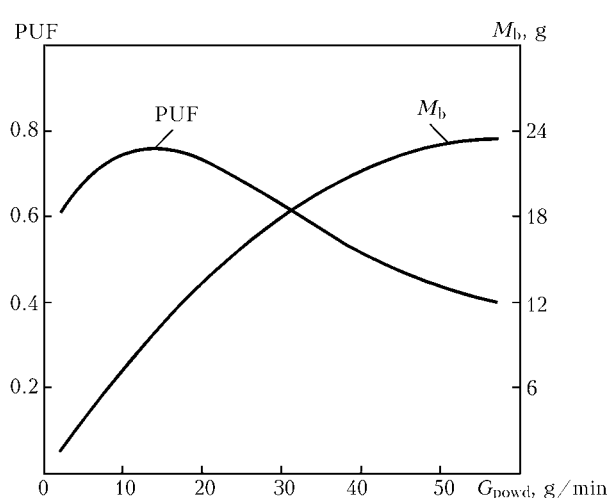


Figure 6. Dependence of PUF and bead mass M_b (cladding for 1 min, $I_a = 120 \text{ A}$) upon the powder consumption

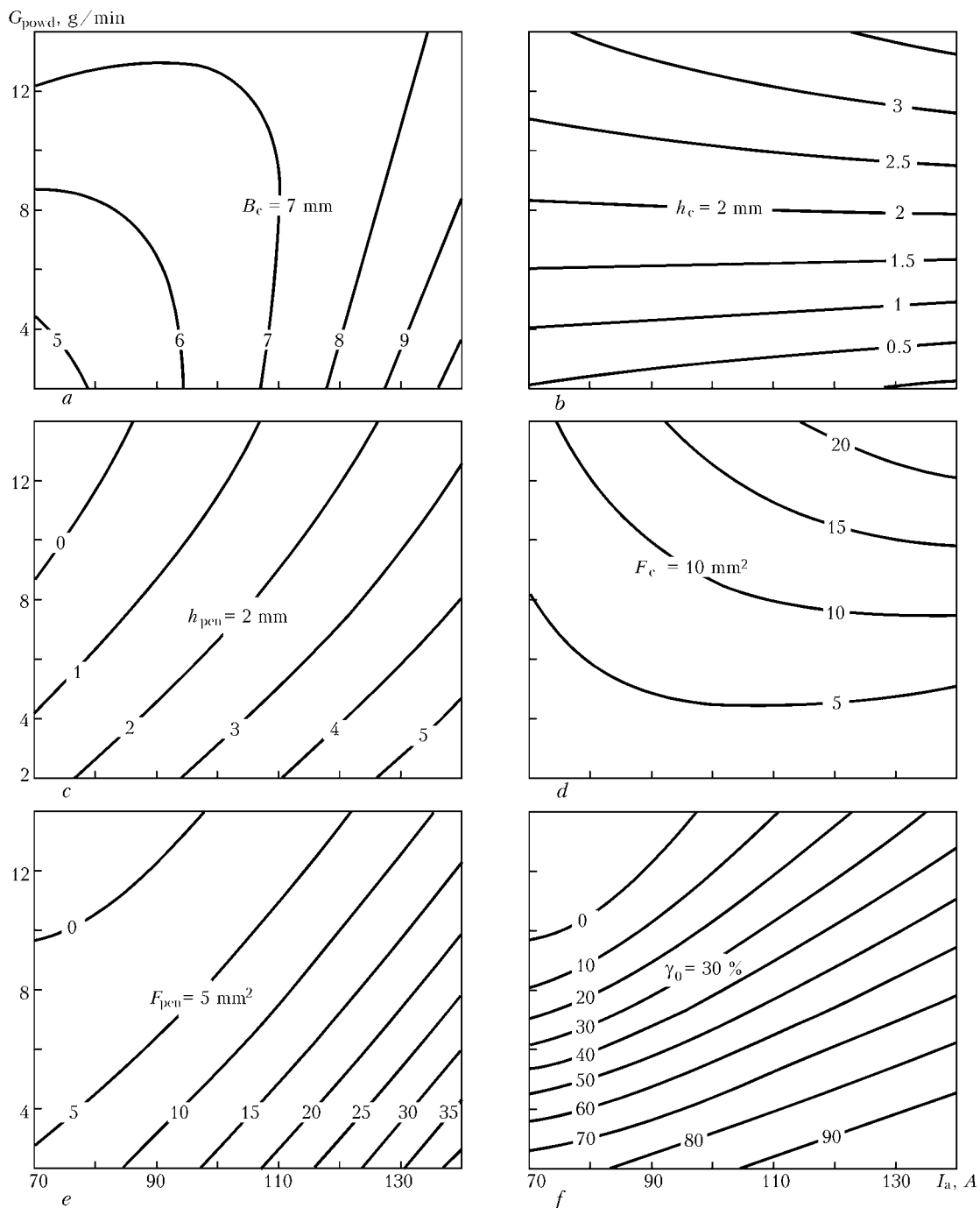


Figure 7. Dependence of the weld width (a), cladding height (b), penetration depth (c), cladding area (d), penetration area (e) and base metal content of the deposited layer (f) upon the arc current and powder consumption

mass within the range under investigation is decelerated with a simultaneous deterioration of quality of the bead formation.

Along with investigation of thermal characteristics and PUF, investigated also was the effect of the arc current and powder consumption on geometrical parameters of cladding (Figure 7), such as width B_c and height h_c of cladding, maximal penetration depth h_{pen} , as well as cladding and penetration areas F_c and F_{pen} , respectively. Thus, increase in the arc current is directly proportional to growth of the weld width (Figure 7, a) and penetration depth (Figure 7, c), especially at a low powder consumption, which results from increase in the concentration of heat input. With

increase in the powder consumption the growth of B_c and h_{pen} is decelerated, which is caused by decrease in heat input into the base metal because of increase in heat removal for heating and melting of the powder additive. Under the considered conditions only an increase in the powder consumption leads to increase in the cladding height (Figure 7, b), whereas a change in the current hardly affects the bead height. This is explained by the fact that increase in the weld width (at increase in the current) is accompanied by an increase in PUF, which, taken together, hardly changes the cladding height. Growth of the penetration area (Figure 7, e) as a result of a more localised heat input into the base metal with growth of the arc

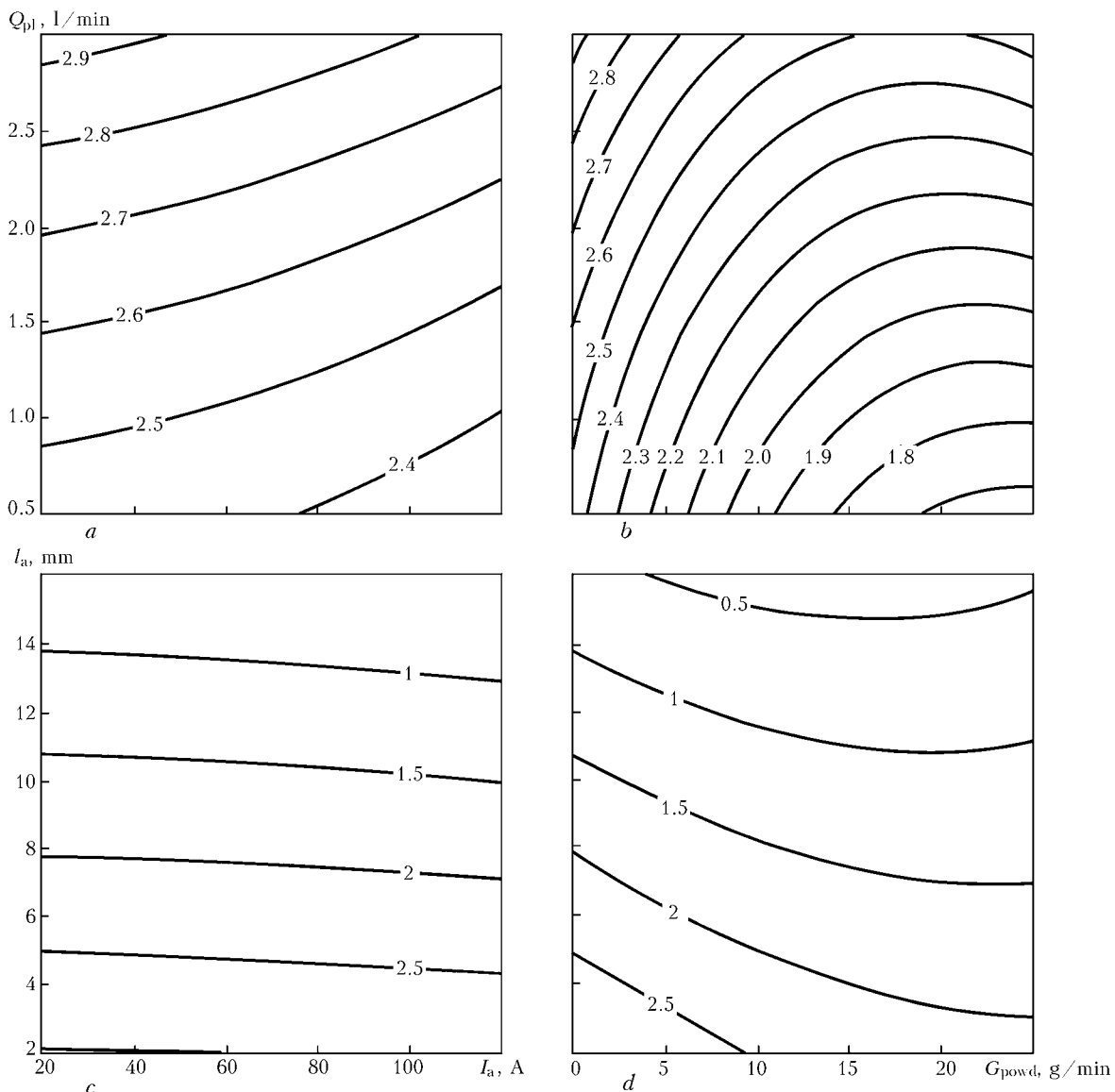


Figure 8. Effect of plasmatron operational parameters (a–d) on heat flow concentration coefficient at a ratio of the plasmatron nozzle diameters equal to 2/5.2

current causes increase in the base metal content of the deposited bead, γ_0 (Figure 7, f). However, increase in the powder consumption, along with growth of the penetration area (Figure 7, d), results in removal of heat from the plasma arc and weld pool. The latter

minimises heat input from the arc to the base metal, which leads to decrease in γ_0 .

As follows from analysis of the experimental dependencies, the effective thermal power of the arc and effective efficiency of heating of a workpiece depend but insignificantly upon the powder consumption, while the total effect by the powder addition consists in redistribution of heat in energy balance during the MPC process.

The coefficient of concentration of heat flow in MPC hardly depends upon the arc current. Thus, k diminishes by 0.2 cm^{-2} with increase in the current from 30 to 120 A (Figure 8, a, c). The basic process parameters are as follows: $I_a = 30 \text{ A}$, $Q_{pl} = 0.8 \text{ l/min}$, $l_a = 5 \text{ mm}$. Increase in the plasma gas flow rate from 1.0 to 2.5 l/min leads to a growth of 0.3 cm^{-2} in the coefficient of the heat flow concentration (Figure 8, a, b). This is caused by increase in the degree of constriction of the arc by the gas flow. A decisive effect on k is exerted by the arc length and diameter of the nozzle channels. Thus, variation in the arc

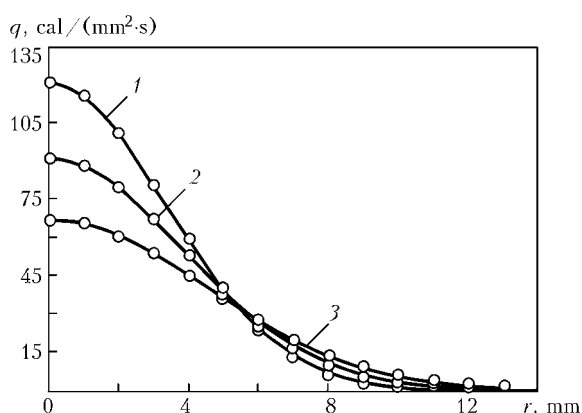


Figure 9. Distribution of heat flow of the plasma arc along a heating radius depending upon the ratio of the plasmatron nozzle diameters: 1 — 1/3.6; 2 — 2/3.6; 3 — 2/5.2



length from 5 to 15 mm results in decrease of 1.5 cm^{-2} (~60 %) in the concentration coefficient (Figure 8, c, d). As the nozzle channel diameters are decreased, the degree of constriction of the arc column by the channel walls grows, this leading to growth of the heat flow concentration and, in turn, to increase in density of the heat flow of the plasma arc (Figure 9). Under the preset conditions $k = 4.2 \text{ cm}^{-2}$ at a ratio of the nozzles equal to 1/3.6, $k = 3.3 \text{ cm}^{-2}$ at 2/3.6, and $k = 2.5 \text{ cm}^{-2}$ at 2/5.2. Addition of powder to the plasma jet leads to decrease in the heat flow concentration coefficient (Figure 8, b, d), and at a powder consumption increased from 5 to 25 g/min k decreases by 0.5 cm^{-2} (~25 %). This is indicative of the fact that an addition of powder results in a more uniform distribution of heat across the jet. The results of investigation of the heat flow concentration coefficient are in good agreement with the data of study by P.V. Gladky [7].

Therefore, a minimum penetration characteristic of the MPC process is achieved by decreasing the heat flow concentration through increasing the nozzle channel diameters and arc length, decreasing the flow rate of the plasma gas, and adding powder to the arc column.

The resulting values of thermal characteristics of the arc, PUF and heat flow concentration coefficient can be used to model the propagation of heat in the HAZ metal and assign the favourable MPC parameters in terms of weldability of special steels and alloys.

CONCLUSIONS

1. The effective efficiency of heating of a workpiece and heat losses at the plasmatron nozzles depend primarily upon the arc current, and in a range of 70–140 A they are 59–65 and 20–40 %, respectively.

2. Increase in the consumption of powder added to the plasma arc leads to drop of the effective efficiency from 5 to 10 % and growth of the heat losses at the plasmatron nozzles from 5 to 8 % for the range of the process parameters under consideration.

3. PUF depends mainly upon the arc current, and at its increase from 70 to 140 A PUF grows from 0.35 to 0.75. PUF can be described by the curve with a maximum at a certain value of the current with increase in the powder consumption.

4. Increase in the current causes a marked increase in the weld width and penetration depth. Growth of the powder consumption raises the height of cladding and decreases the base metal content of the deposited bead.

5. The concentration coefficient for characteristic parameters of microplasma powder cladding is 1–5 cm^{-2} . It depends primarily upon the diameter of the nozzle channels, arc length, addition of powder to the arc and its amount.

1. Savchenko, V.S., Yushchenko, K.A., Makhnenko, V.I. et al. (1993) Influence of physical characteristics of cast nickel heat-resistant alloys on development of thermal-deformation processes in fusion welding. *Avtomatich. Svarka*, **11**, 6–9.
2. Adam, P. (1981) Welding of high-strength alloys for gas turbines. In: *Heat-resistant alloys for gas turbines*. Ed. by P. Shalin. Moscow: Metallurgiya.
3. Sims, Ch., Hagel, V. (1976) *Heat-resistant alloys*. Moscow: Metallurgiya.
4. Savchenko, V.S., Yushchenko, K.A., Savolej, N.I. et al. (1993) Special features of welding of high-nickel precipitation-hardening heat-resistant alloys and repair of pieces made from them. *Avtomatich. Svarka*, **10**, 31–33.
5. Saltsman, G.A., Sahoo, P. (1991) Application of plasma arc welding surfacing in turbine engines. In: *Proc. of 4th Nat. Thermal Spray Conf.*, Pittsburg, May 4–10, 1991.
6. Yushchenko, K.A., Yarovitsyn, A.V., Kalina, P.P. (2002) Study of thermal balance of plasma-powder surfacing. In: *Proc. of Int. Conf. on Mathematical Modeling and Information Technologies in Welding and Related Processes*, Katsiveli, Ukraine, Sept. 16–20, 2002. Ed. by V.I. Makhnenko. Kiev: PWI.
7. Gladky, P.V. (1999) Thermal characteristics of arc of cladding plasmatrons. *Avtomatich. Svarka*, **6**, 13–17.
8. Zubkov, N.S., Terentiev, V.A. (1982) Power characteristics of reverse polarity plasma arc and effect of heat flow distribution on technological parameters of the cladding process. *Svarochn. Proizvodstvo*, **2**, 17–20.
9. Rykalin, N.N. (1951) *Calculations of thermal processes in welding*. Moscow: Mashgiz.
10. Popov, M.M. (1954) *Thermometry and calorimetry*. Moscow: Metallurgizdat.
11. Demyantsevich, V.P., Mikhajlov, N.P. (1973) Study of microplasma arc heat distribution in displacement of the heat spot center from axis of a joint. *Svarochn. Proizvodstvo*, **6**, 1–3.
12. Ventsel, E.S. (1960) *Theory of probability*. Moscow: Nauka.



EFFECT OF ALLOYING ON CAVITATION-CORROSION RESISTANCE OF STAINLESS STEELS AND ALLOYS

A.V. PATYUPKIN and D.A. ANTONYUK

Zaporozhie National Technical University, Zaporozhie, Ukraine

Presented is a mathematical model developed on the basis of experimental data to describe the effect of nickel and chromium equivalents on cavitation and cavitation-corrosion resistance of stainless steels and alloys.

Keywords: cavitation, cavitation-corrosion resistance, stainless steels, mathematical model

A process of cavitation of materials in fresh and synthetic sea water, NaCl solutions and technological media of food industry was considered in a number of works [1–5] devoted to the study of cavitation-corrosion wear of high-alloyed steels and alloys. However, the majority of technological equipment of chemical productions (titanium-manganese, non-ferrous metallurgy and others) mostly operate in the acid solutions of different concentration, which leads to intensive destruction of machine parts, such as rotors, cones of chlorine compressors, scrolls of centrifugal pumps, stop valves and others. With this in mind it is important in selecting the wear-resistant

material for production of wearing parts for chemical apparatuses to consider its cavitation and corrosion resistance in technological acidic solutions. In view of a wide range of stainless steels and alloys recommended for operation in the acidic media and a high degree of their alloying the alloying of different systems by the nickel and chromium equivalent was studied for its effect on cavitation-corrosion resistance of metals. Equivalents of chromium and nickel were determined by the procedure described in [6].

Cavitation and cavitation-corrosion tests were carried out on a special impact-erosion stand [7]. Specimens $20 \times 15 \times 5$ mm in size were cut from the deposited metal. Deposition was carried out on a plate of steel 10Kh18N10T in two layers with forced cooling

Cavitation-corrosion resistance of the deposited metal

Series of the specimen	Deposited metal	Ni_{eq}	Cr_{eq}	Weight losses of specimens, g	
				$I_2\hat{I}$	H_2SO_4
1	10Kh18N10T	21.20	15.60	0.61	1.96
2	07Kh14N20	22.66	15.33	0.37	1.65
3	07Kh15N21Y	23.36	15.70	0.39	1.63
4	08Kh15N21M6	23.40	21.60	0.42	0.79
5	08Kh17N24M3D	27.13	22.13	0.37	1.37
6	08Kh18N24M3D	27.10	23.10	0.35	1.31
7	12Kh18N25M3	28.66	23.30	0.27	0.82
8	10Kh15N21M6Y	23.90	22.23	0.30	0.68
9	10Kh14N29M5	32.23	21.30	0.38	0.61
10	10Kh14N29M6	32.16	21.40	0.43	0.57
11	08Kh15N30	32.56	16.70	0.52	1.26
12	07Kh16N30	32.23	17.20	0.48	1.37
13	14Kh19N25M3D	28.60	26.57	0.26	0.92
14	06Kh23N18	22.40	24.23	0.31	0.65
15	08Kh23N18M5	23.40	28.37	0.17	0.50
16	08Kh23N28M2T	31.80	30.80	0.31	0.71
17	06Kh23N28M3D3T	30.70	31.13	0.30	0.46
18	06Kh24N21	23.20	25.13	0.20	0.59

Notes. 1. Tests were performed in H_2O at the temperature 25 °C; in 92 % solution of H_2SO_4 at the temperature 50–60 °C. 2. Duration of the tests in each medium was 10 h.



of the back side of the specimen. H_2O was used as a working liquid for cavitation tests and 92 % solution of H_2SO_4 was used for cavitation-corrosion tests. Resistance of the materials was evaluated from the weight losses of the specimens with error $1 \cdot 10^{-4}$ g. Each series included 3–5 specimens.

The experimentally obtained data (Table) allowed constructing mathematical models of the effect of the equivalents of nickel Ni_{eq} and chromium Cr_{eq} on the weight loss of the specimen as a result of cavitation and cavitation-corrosion effect:

$$P_{H_2O} = f(Ni_{eq}, Cr_{eq}), \quad (1)$$

$$P_{H_2SO_4} = f(Ni_{eq}, Cr_{eq}), \quad (2)$$

where P_{H_2O} and $P_{H_2SO_4}$ is the weight loss of the specimens under cavitation and cavitation-erosion wear, respectively.

Empirical dependences were found by the least-square method [8–10]. The closest theoretical curve was selected from the experimental data. Equation for this curve is presented in [8]:

$$\begin{aligned} y = & b_0 + b_1x_1 + b_2x_2 + b_3x_1x_2 + b_4x_1^2 + \\ & + b_5x_2^2 + b_6x_1^2x_2 + b_7x_1x_2^2 + b_8x_1^3 + b_9x_2^3. \end{aligned} \quad (3)$$

This equation describes functional and correlation dependence between the studied values. Solution of the problem was based on application of the matrices

$$Y = X \times B, \quad (4)$$

$$\text{where } Y = \begin{pmatrix} y_1 \\ y_2 \\ y_3 \\ \dots \\ y_{18} \end{pmatrix}$$

is the matrix whose elements are the results of the experimental data on the weight losses of the specimens under cavitation (in the first case) and cavitation-corrosion (in the second case) effects;

$$X = \begin{pmatrix} x_{00} & x_{10} & x_{20} & x_{10}x_{20} & x_{10}^2 & x_{20}^2 & x_{10}^2x_{20} & x_{10}x_{20}^2 & x_{10}^3 & x_{20}^3 \\ x_{01} & x_{11} & x_{21} & x_{11}x_{21} & x_{11}^2 & x_{21}^2 & x_{11}^2x_{21} & x_{11}x_{21}^2 & x_{11}^3 & x_{21}^3 \\ \dots & \dots \\ x_{017} & x_{117} & x_{217} & x_{117}x_{217} & x_{117}^2 & x_{217}^2 & x_{117}^2x_{217} & x_{117}x_{217}^2 & x_{117}^3 & x_{217}^3 \end{pmatrix}$$

is the matrix of the values of nickel equivalent x_1 and chromium equivalent x_2 where the second coefficient indicates the number of deposited metal specimen;

$$B = \begin{pmatrix} b_0 \\ b_1 \\ b_2 \\ \dots \\ b_9 \end{pmatrix}$$

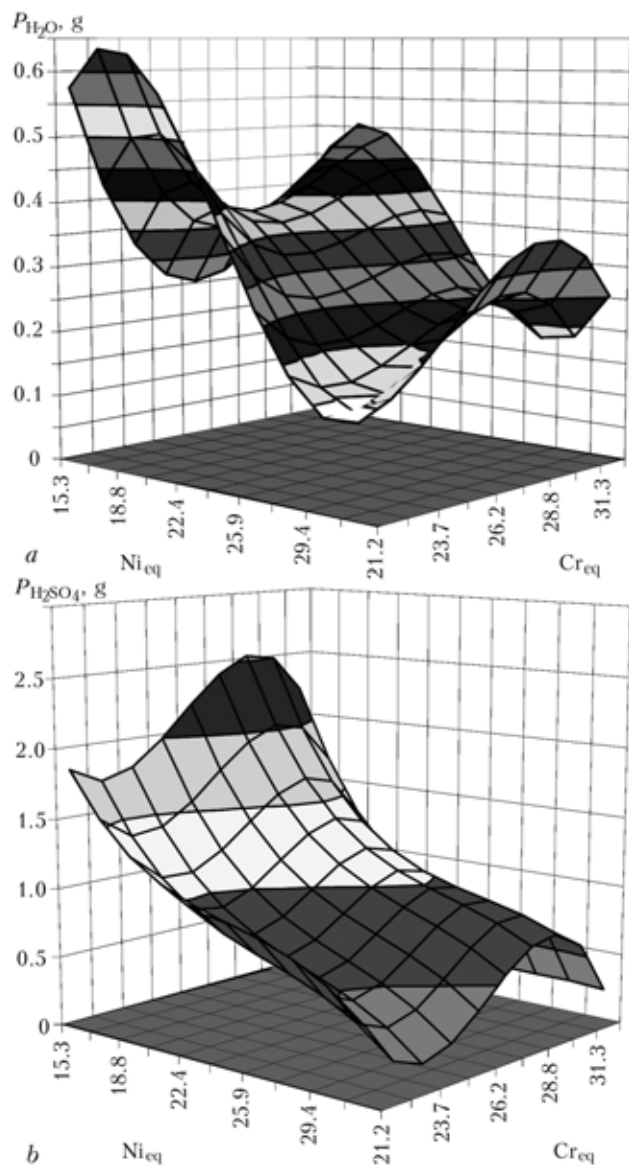
is a matrix of the unknown coefficients in the equation (4).

The desired coefficients were found from the expression

$$B = (X^\dagger X)^{-1} (X^\dagger Y), \quad (5)$$

where X^\dagger is the matrix found by transposing the matrix X .

The obtained results allowed constructing hyperplanes of cavitation and cavitation-corrosion resistance of materials depending on the Ni_{eq} and Cr_{eq} (Figure). With Ni_{eq} increase the weight losses of the specimens noticeably decrease both in H_2O and in 92 % of H_2SO_4 solution, which is explained by an increase of nickel content and thus toughness (plasticity) and corrosion resistance of metal reinforced with carbides under micro-impact effect of the working liquid. With Cr_{eq} decrease down to 20–21 the metal resistance increases since the chromium content within 20–22 provides, according to the author [11], optimal strength characteristics of steels and alloys. At Cr_{eq} 30–31 the weight loss of the specimens also decreases, which is related to the additional introduction of copper, molybdenum and titanium into the



Effect of Cr_{eq} and Ni_{eq} on cavitation P_{H_2O} (a) and cavitation-corrosion $P_{H_2SO_4}$ (b) resistance of stainless steels and alloys



deposited metal, which facilitates an increase of yield point, hardness and corrosion resistance of metals in acidic media under cavitation and cavitation-corrosion action [12–14].

Experimental data were processed by the methods of mathematical statistics [8, 15]. A degree of connection between the variables were judged by the values of the correlation coefficient $r_{x,y}$:

$$r_{x,y} = \frac{n \sum_{i=1}^n x_i y_i - \sum_{i=1}^n x_i - \sum_{i=1}^n y_i}{\sqrt{n \sum_{i=1}^n x_i^2 - \left(\sum_{i=1}^n x_i \right)^2} \sqrt{n \sum_{i=1}^n y_i^2 - \left(\sum_{i=1}^n y_i \right)^2}}. \quad (6)$$

Correlation coefficient of cavitation characteristic of metal is 0.96 and cavitation-corrosion resistance --- 0.94. In this case the calculated Fischer criterion was 0.72 and 1.95, respectively, which is lower than the Table one (2.33). Mean value of absolute error does not exceed 2.7 %.

The performed tests of stainless steels and alloys in H_2O and in 92 % solution of H_2SO_4 served the basis for determination of optimal values: to provide cavitation resistance --- Ni_{eq} (22–31) and Cr_{eq} (21–24), to increase cavitation-corrosion resistance --- Ni_{eq} (24–31) and Cr_{eq} (23–26 and 30–31). The following steels and alloys are included into the cavitation and cavitation-corrosion resistance domain: 06Kh23N18, 08Kh23N18M5, 06Kh24N21, 08Kh23N28M2T, 06Kh23N28M3D3T.

The constructed mathematical models ($r_{x,y} = 0.94$ –0.96) facilitate selection and justification of

the use of steels for specific structures and allow predicting the perspectives for industrial application of the materials exposed to cavitation and cavitation-corrosion destruction.

1. Petrov, L.N., Soprunok, N.G. (1991) *Corrosion-mechanical fracture of metals and alloys*. Kiev: Naukova Dumka.
2. Tsvetkov, Yu.N. (1993) Some peculiarities of cavitation wear kinetics of metallic alloys. *Zavod. Laboratoriya*, **10**, 32–34.
3. Stechishin, M.S., Nekoz, A.I., Pogodaev, L.I. et al. (1990) Regularity of cavitation-erosion wear of metals in corrosive media. *Trenie i Iznos*, **11**(3), 454–463.
4. Sukhenko, Yu.G. (1998) Model of corrosion-mechanical wear of materials in process media of food industry. *Problemy Trybologii*, **3**, 108–110.
5. Nekoz, A.I., Sologub, N.A., Stechishin, M.S. (1984) Analysis of relation between corrosion and mechanical factors in cavitation-erosion wear. *Fiziko-Khim. Mekhanika Materialov*, **20**(2), 110–111.
6. Zaks, I.A. (1973) *Welding of dissimilar steels*. Leningrad: Mashinostroenie.
7. Patyupkin, A.V., Rudychev, A.S., Bykovsky, O.G. (2000) Cavitation-corrosion resistance of some deposited stainless steels and alloys. *The Paton Welding J.*, **8**, 37–39.
8. Hartman, K., Letsky, E., Schefer, V. (1977) *Planning of experiment in investigation of technological processes*. Moscow: Mir.
9. Adler, Yu.P., Markova, E.V., Granovsky, Yu.V. (1976) *Planning of experiment in search of optimum conditions*. Moscow: Nauka.
10. Myshkis, A.D. (1967) *Lectures on higher mathematics*. Moscow: Nauka.
11. Kakhovsky, N.I. (1975) *Welding of high-alloy steels*. Kiev: Tekhnika.
12. Perkas, M.D., Kardonsky, V.M. (1970) *High-strength maraging steels*. Moscow: Metallurgiya.
13. Medovar, B.I. (1966) *Welding of heat-resistant austenitic steels and alloys*. Moscow: Mashinostroenie.
14. Milichenko, S.L. (1971) *Repair of cavitation fracture of hydroturbines*. Moscow: Energiya.
15. Zheverzhev, V.F., Kalnitsky, L.A., Sapogov, N.A. (1970) *Special course on higher mathematics for institutes of higher technical education*. Moscow: Vysshaya Shkola.

EVALUATION OF DELAYED FRACTURE RESISTANCE OF HAZ METAL OF HIGH-STRENGTH STEEL WITH MODELING OF STRESS RELAXATION

V.M. KULIK, M.M. SAVITSKY and G.V. BURSKY
E.O. Paton Electric Welding Institute, NASU, Kiev, Ukraine

The rationality of inducing delayed fracture with lowering of the load on a high-strength steel welded joint was substantiated and its features were studied. The effectiveness of various delayed fracture indices for evaluation of cold cracking resistance in the HAZ is considered. It is shown that for increasing the crack resistance of the joint of sheet steel 30KhGSA, it is rational to reduce the cooling rate during TIG welding, in particular by increasing the heat input, applying a moderate mode, increasing the number of passes, performing arc treatment and tempering at the temperature of 150–200 °C.

Keywords: argon-arc welding, tungsten electrode, high-strength steel, welding mode, thermal cycle, cooling rate, metal microstructure, delayed fracture, stress relaxation, cold cracks

Light-weight high performance structures are usually made of thin high-strength steels with application of TIG welding [1]. This process enables producing joints with a smooth transition from the base metal to the weld, and in the case of application of activating flux reducing the filler metal consumption, and providing a more homogeneous joint in terms of chemical composition. The latter in combination with the produced fine-crystalline structure provides equivalent mechanical properties of welded joint and base metal after strengthening heat treatment of the item. In addition, arc activation by a special flux increases the penetration depth 1.5 to 3 times and allows steel welding to be conducted at lower currents, which lowers the probability of formation of a coarse-grained metal structure in the HAZ [2].

Quenching of high-strength steels in air leads to cold cracking after welding. There exist different methods for evaluation of cracking resistance, based on delayed fracture of the welded sample, the most widely used of which is the implant method [3–6]. In this method a ground sample of 6–8 mm diameter is inserted into a through-thickness hole of the same diameter in a technological tab 20 mm thick, is welded up by making a bead from the surface and is subjected to long-term tension under the impact of a constant load, which allows determining the time to sample fracture in the HAZ. Weldability of sheet steel was evaluated using flat samples of 3 × 14 mm cross-section [7–9], cold cracking resistance --- by force criteria σ_{cr} , $\sigma_{cr max}$, σ_{cr}/σ_y , $j = (\sigma_f - \sigma_{cr})/\sigma_{cr}$, $n = \sigma_f/\sigma_{cr}$, etc. [5–10] or energy index A_{red} [9], where σ_{cr} is the minimum stress, below which no delayed fracture of the sample proceeds; $\sigma_{cr max}$ is the maximum stress, at which the sample does not fail for 24 h; σ_y is the proof stress of the tested steel; σ_f is the breaking stress at continuous increase of the load at deformation rate of approximately 2 mm/min; A_{red} is the reduced work of fracture determined by the product of the value of

appropriate displacement and load, referred to a unit of the sample cross-sectional area. Energy index A_{red} is much more sensitive than force $\sigma_{cr max}$ [9]. Improved testing procedure verified on the joints, made with feeding of welding wire to the arc zone, enables evaluation of the work of crack initiation and propagation by acoustic emission signals from a transducer mounted on sample surface [11].

A flat sample can be also placed in a rectangular hole formed by a combination of rectangular slots on narrow faces of technological tabs 20 mm thick [12, 13]. Sample welding is performed by a consumable electrode with making of a weld of a large cross-section in transverse combined groves of the tabs, and loading is provided by a constant tensile force lateral relative to the weld. Depending on distance from the sample to the surface, fusion zone sections different along the sample height can be tested. However, for TIG welding the technological tabs are rather massive, their manufacture is labour-consuming and they do not give the required effect either for the joint quality, or for the thermal cycle.

Cold cracking in welded joints proceeds by the mechanism of delayed fracture under the conditions of stress relaxation [14]. Delayed fracture of quenched steel, including crack initiation, slow propagation up to a critical size and fast growth of the crack [15], proceeds under the impact of a static load, and below a certain value of this load it is absent. Crack initiation is promoted by residual internal stresses, coinciding in their direction with those applied externally, its propagation proceeds along the boundaries of initial austenite grains, softened through martensite transformation, brittle fracture is due to a low brittle fracture resistance of quenched steel. Relaxation is associated with higher strength of quenched steel and transition from brittle to tough fracture.

In keeping with the above, in this study the features of delayed fracture and cold crack formation were investigated in the HAZ metal of welded joints on high-strength steel, allowing for stress relaxation. As the latter is accompanied by plastic deformation, and the relaxation resistance of the material is characterized by stress drop $\Delta\sigma$, it can be simulated by



long-term application of the load to the sample by a spring device.

Steel 30KhGSA was selected as the object of study, which is widely applied as high-strength structural material in modern structures, including pressure vessels [1]. Let us consider the results of delayed fracture testing at lowering of the load on joints of rolled sheets, made by TIG welding with application of activating flux and without it. A test sample of 3×14 mm cross-section is inserted into a rectangular opening between the abutted technological tabs, where recesses of 1.5×14 mm size are prepared on the narrow mated faces (Figure 1, a), and is welded by its end face to the tab surface (Figure 1, b). TIG and ATIG welding in one and two passes was conducted in a special jig in ARK-1 unit with VSVU-315 welding rectifier. Thermal cycles were adjusted by varying the welding modes in the following ranges: $I = 130\text{--}210$ A; $U_a = 9.5\text{--}11.0$ V; $v_w = 5.5\text{--}13.5$ m/h; $q/v_w = 92\text{--}202$ (W·h)/m under the conditions of sample cooling in the jig. Parameter measurement and recording were performed with VR 20/5 thermocouple and N-105 oscilloscope. Macro- and microstructure of welded joints was studied.

Long-term loading of the sample by a longitudinal tensile force at stress below the yield point, was performed in a refitted unit of LTP-1-6 type with a beam used as a spring device with the rigidity $K = 8$ kg/ μm , calibrated up to 3200 kg at elastic deflection up to 400 μm . Load and stress were determined by its deflection measured using an arrow-type indicator, and

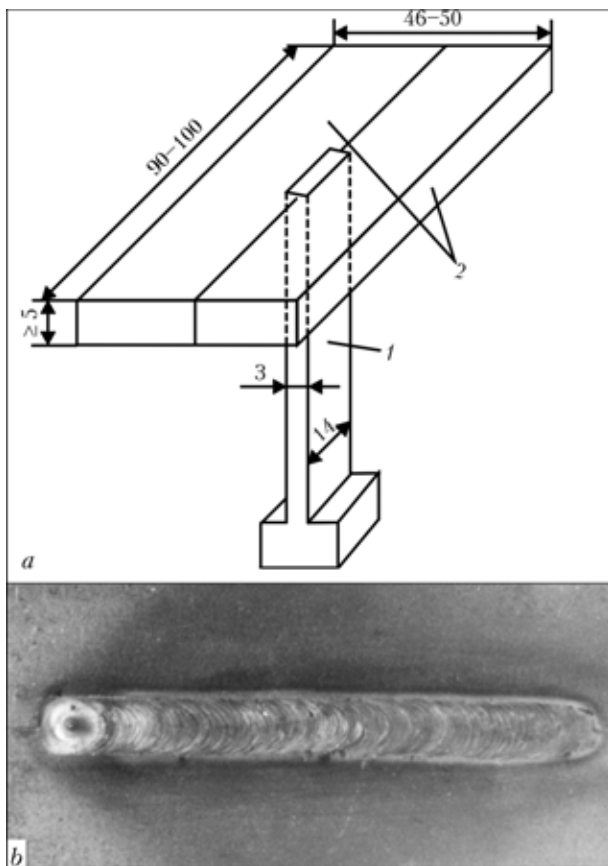


Figure 1. Schematic of fit up for welding of a sample (1) for delayed fracture testing (a) and appearance of a weld on the surface of a butt of technological tabs (2) (b)

sample elongation, load and stress decrease, work of deformation and fracture were determined by reduction of the deflection recorded by KSP-4 potentiometer. HAZ metal hardened in welding was subjected to microplastic deformation and fracture. Microplastic deformation of a welded sample Δl was given by the following formula:

$$\Delta l = \lambda_{in} - \lambda_i, \quad (1)$$

and current stress σ_i by the following formula:

$$\sigma_i = \frac{K}{S} \lambda_i. \quad (2)$$

Here, λ_{in} , λ_i are the initial and current deflection of the beam; S is the cross-sectional area of the sample.

Decrease of stress $\Delta\sigma$ has the following form:

$$\Delta\sigma = \sigma_{in} - \sigma_i = \frac{K}{S} \Delta l, \quad (3)$$

where σ_{in} is the initial stress in the sample.

Work consumed in sample deformation and fracture, is equal to a decrease of the potential energy in an elastically bent beam. Energy content of deformation and fracture reduced to the cross-sectional area of the sample, is equal to

$$A_{red} = \frac{K}{S} \frac{\lambda_{in}^2 - \lambda_i^2}{2}. \quad (4)$$

During earlier studies it was established that an acceptable rigidity of a composite welded sample is preserved during testing at the dimensions of technological tabs of $(23\text{--}25) \times (90\text{--}100)$ mm and not less than 5 mm thickness. Loading of welded joints with less than 1.5 mm penetration depth leads to weld fracture with formation of a through-thickness hole. In order to avoid it, the penetration depth was increased to 2 mm and more by increasing the current and lowering the welding speed.

Parameters of welding, treatment and testing of samples are given in Tables 1–3, appearance, microstructure of the joint metal, typical thermographs of welding, and fracture diagrams in Figures 1–5. Values of testing parameters corresponding to the entire period before fracture, are marked by «fr» index, and those before formation of microcracks, registered by acoustic emission signals from the sample — by «mc» index.

In the given modes of TIG welding of tested samples, cooling of HAZ metal in the temperature range of minimum austenite stability of $600\text{--}400$ °C, proceeds at the rate $w_{6/4} = 4.5\text{--}35$ °C/s. The latter rises at current lowering and increase of welding speed, i.e. at lowering of welding heat input, as well as due to narrowing of penetration depth at arc activation with flux. At the above cooling rates a diffusionless transformation of austenite of 30KhGSA steel and welded joint metal is possible [16, 17]. This leads to formation of a hardening structure, which mostly is a mixture of upper and lower bainite and martensite (Figure 3) [18]. Hardness of welded joint metal is 1.6 to 2.1 times higher than that of the base metal. In the weld, where the metal has a higher stability of austenite formed after weld solidification, the hardness is higher than in the section of HAZ metal overheating (Table 1). A simultaneous lowering of current and welding speed

**Table 1.** Modes of welding, treatment and testing of samples of a welded joint of 30KhGSA steel

I, A	v _w , m/h	q/v _w , (W·h)/m	W _b /4, 1/N/s	Microhardness HV, GPa	
				Weld	HAZ
170	8.0	202	4.5	--	--
130	8.0	154	10	--	--
170	12.5	129	35	3.09–4.05 3.45	3.09–3.56 3.25
170	12.5	129	17	2.58–3.95 3.38	2.60–3.73 3.16
170	13.6	119	--	--	--
130	8.0	154	10	2.88–3.45 3.05	2.78–2.86 2.83

Table 1 (cont.)

Testing parameters								
σ _{in} , MPa	n _{mc} , pcs	τ _{fr} , min	τ _{mc} , min	Δl _{fr} , μm	Δl _{mc} , μm	σ _{fr} , MPa	Δσ _{fr} , MPa	
250	No fracture		--	--	--	--	--	
250	Same		--	--	--	--	--	
380	3	1.5	--	2	--	376	4	756
380	6	40	3–32	18	0–13	346	34	6534
380	3	18	4–16	3	0	374	6	1131
380	13	75	9–53	32	3–21	322	58	11232

Notes. 1. Base metal properties: σ_{0.2} = 445 MPa, σ_t = 650 MPa, δ = 27 %, ψ = 37 %, HV 1.74 GPa. 2. U_a = 9.5 V.

causes a refinement of austenite grain from 6 to 7 points in the section of HAZ metal overheating and lowering of hardness of welded joint metal.

From Table 1 it is seen that at a small initial tension σ_{in} = 250 MPa = 0.56σ_{0.2}, samples made in one pass at cooling rates of 4.5–10.0 °C/s, do not fail during a day or more. At such a load, the sample is elongated by about 4.5 μm during 5 h with stress

Table 3. Influence of tempering and its temperature on the properties and crack resistance of HAZ metal of 30KhGSA steel welded joint

T _t , 1/N	Microhardness HV, GPa		Fracture parameters			
	Weld	HAZ	Δl _{fr} , μm	Δσ _{fr} , MPa	τ _{fr} , min	τ _{mc} , min
Untempered	2.28–3.32 2.72	1.46–2.36 1.82	14	27	8	4
	--	--	6	11.5	75	N/D
100	1.80–2.98 2.33	2.60–3.09 2.82	--	--	NF	80
	2.14–2.68 2.50	1.80–2.43 2.05	--	--	NF	N/D

Notes. 1. σ_{in} = 380 MPa. 2. NF ---- no fracture.

lowering by 8.5 MPa. Sample shortening by less than 1 μm can be observed during the first 10 min of loading with tensile stress increase by 0.5–0.8 MPa.

Increase of initial load up to σ_{in} = 380 MPa = = 0.86σ_{0.2} in combination with increase of cooling rate (lower heat input mostly due to increased welding speed) causes delayed fracture of 30KhSGA steel across the HAZ metal of welded joint within 18–40 min. Microplastic deformation and stress lowering occur right after sample loading and after 5–6 min of the incubation period in a step-like and monotonic manner. Greater lowering of stress Δσ in time with increase of the initial load σ_{in} and in proportion to microplastic deformation Δl confirms the nature of the testing conditions, which are similar to relaxation conditions.

During delayed fracture testing, acoustic emission signals of a high enough intensity are registered that are due to microcrack formation [11, 19]. They are observed during the period of a stable microplastic deformation and stress lowering, as well as during

Table 2. Crack resistance of a welded joint sample depending on second pass parameters (arc treatment)

No.	Welding mode in the second pass			Microhardness HV, GPa			Fracture parameters									
	I, A	v _w , m/h	q/v _w , (W·h)/m	Weld	HAZ	n _{mc} , pcs	τ _{fr} , min	τ _{mc} , min	Δl _{fr} , μm	Δl _{mc} , μm	σ _{fr} , MPa	Δσ _{fr} , MPa	A _{fr} , J/m ²			
1	--	--	--	3.09–4.05 3.45	3.09–3.56 3.25	--	1.5	--	2	--	376	4	756			
2–4	110	12.5	92.5	1.30–3.32 2.07–2.87	1.46–3.45 1.82–3.21	1–3	8–35	4–30	12–18	1–14	346–357	23–34	4423–6534			
5–7	170	13	137	2.68–4.80 2.96–4.48	2.10–4.40 2.30–3.55	--	15–82	15–78	22	20	338	42	7942			
8	210	13	170	2.28–4.05 2.88	3.78–4.05 3.50	--	55	--	--	--	--	--	--			
9	100	5.5	181	6.28–2.78 2.71	1.65–2.60 2.15	--	No fracture	--	--	--	--	--	--			

Notes. 1. First pass was made by ATIG welding (q/v_w = 129 (W·h)/m), second ---- by TIG welding. 2. σ_{in} = 380 MPa. 3. In item 2–4 and 5–7 data are given for three variants.

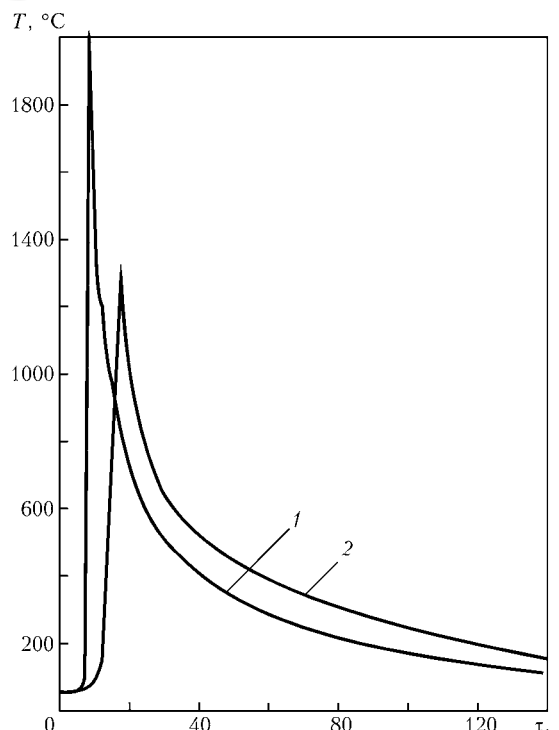


Figure 2. Thermographs of the first (1) and second (2) passes of TIG welding

the incubation period (Figure 4), and are usually accompanied by short-term increase of Δl and $\Delta\sigma$. Different time intervals and magnitudes of plastic deformation between the acoustic emission signals of about the same amplitude, are indicative not of the growth, but of the isolated nature of the formed microcracks at a load which is decreasing on the whole. At the moments of metal shear, acoustic emission signals can be detected, which have an amplitude by an order of magnitude smaller (Figure 4, a), which are regarded as indices of submicrocrack formation.

Brittle fracture without any noticeable narrowing of the sample with fracture orientation normal to the tensile force is completed by a sound effect. Depending on welding conditions, produced structure and hardness of the joint metal, complete fracture (rupture) of the sample proceeds 1.5 to 75 min after microplastic deformation by 3–32 μm at averaged rates of 0.13–0.45 $\mu\text{m}/\text{min}$ and stress lowering by 6 to 61 MPa (to 0.84–0.98 σ_{in}) at averaged rates of 0.8–2.7 MPa/min. In this case work $A_{red} = 756-$

11232 J/m² is performed, which can be equal to 0.92 of the work calculated without stress lowering.

Lowering of the cooling rate of weld metal and HAZ at increase of TIG welding heat input, leads to lowering of welded joint metal microhardness and increased duration of sample testing up to complete fracture, lowering of stress $\Delta\sigma$ and microplastic deformation Δl_{fr} , work of deformation and fracture A_{red} , as well as number of signals of microcrack formation n_{mc} (see Table 1).

Values $\Delta\sigma$ and Δl are the main parameters of welded joint delayed fracture. Their current variation stops simultaneously at achievement of certain values, and after that further application of the load does not lead to fracture, which is characteristic in the case of stress relaxation up to the relaxation limit. Delayed fracture is completed before stopping of the process of microplastic deformation and stress lowering. Dependent on $\Delta\sigma$ and Δl are current and rupture stress

$$\sigma_{i(fr)} = \sigma_{in} - \Delta\sigma = \frac{K}{S} (\lambda_{in} - \Delta l), \quad (5)$$

work of microplastic deformation and fracture

$$A_{red} = \frac{K}{S} (\lambda_{in} - 0.5\Delta l) \Delta l = \frac{S}{K} (\sigma_{in} - 0.5\Delta\sigma) \Delta\sigma, \quad (6)$$

time to complete fracture τ_{fr} and appearance of microcracking signals τ_{mc} , as well as number of these signals, n_{mc} . Reduced work is smaller by the value of 0.5 $\Delta\sigma\Delta l$ than the one which is calculated without stress lowering.

Energy parameter of testing has higher sensitivity than the force parameter, due to its relative change in a certain period from increasing microplastic deformation ($\lambda_{in} >> \Delta l$ and $\sigma_{in} >> \Delta\sigma$). Deformation and relaxation characteristics of testing have an even higher sensitivity that predetermines their use as simpler indices, expressing the essence of the delayed fracture process.

Welded joint with two passes made by TIG welding, develops delayed fracture at decrease of the load, similar to a single-pass weld (Figure 5). Lower hardness and higher grain point of the metal, hardened during welding [18], result in high values of microplastic deformation and lowering of stress, duration and reduced work of deformation up to microcrack initiation and complete fracture (Table 2) during testing, i.e. provide a higher resistance to delayed fracture. Averaged rates of deformation (0.3–

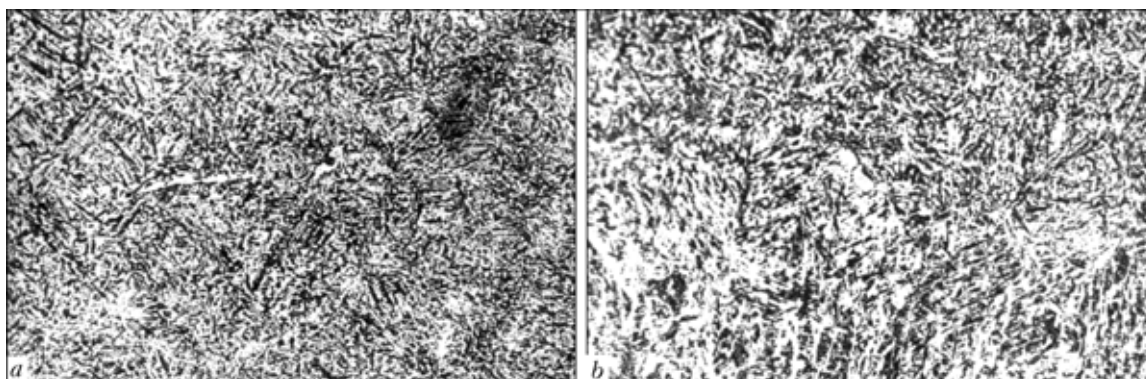


Figure 3. Microstructure of HAZ metal of a sample of the joint welded in one (a) and two (b) passes ($\times 32$)

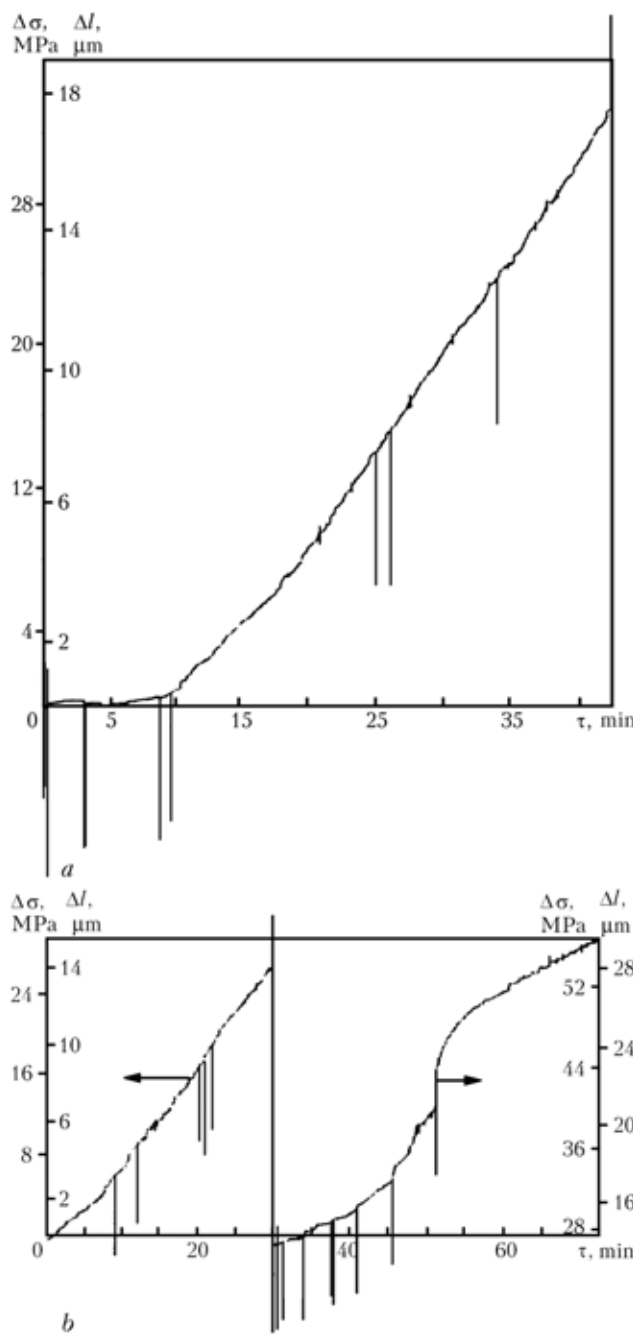


Figure 4. Diagrams of delayed fracture of HAZ metal of 30KhGSA steel cooled at the rate of 17 (a) and 10 (b) °C/s at single-pass welding

1.8 $\mu\text{m}/\text{min}$) and stress change (0.5–3.0 MPa/min), are close to those in a single-pass joint. With increase of welding heat input, the delayed fracture resistance increases in the second pass. Its highest value is achieved in a joint made at low values of welding current and speed.

Tempering at the temperatures of 100–200 °C, without essentially changing the hardness of welded joint metal, increases the time to microcracks initiation and fracture, right up to its prevention (Table 3). It causes a delay and slowing down of microplastic deformation and lowering of stress, leads to fracture at increased stress with less work performed. At temperature of 100 °C, coinciding with the first stage of transformations at tempering, tetragonality of

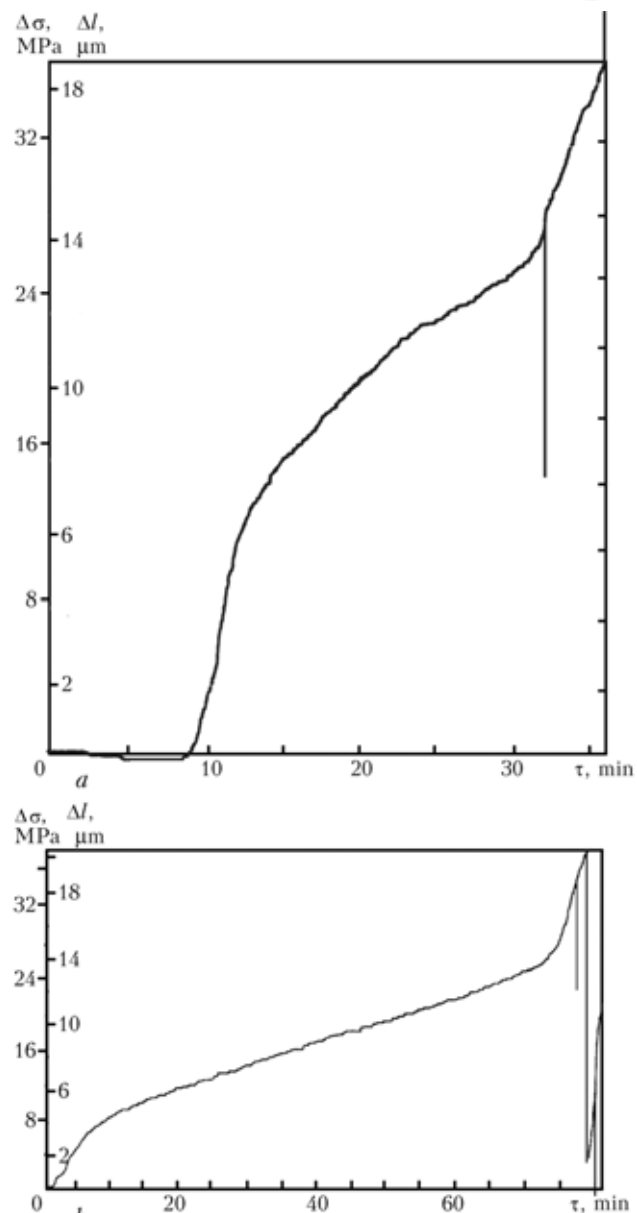


Figure 5. Delayed fracture diagrams of HAZ metal of 30KhGSA steel at two-pass welding with heat input of 92 (a) and 137 (b) (W·h)/m

martensite lattice is reduced, and alongside the initial concentration carbon, it develops regions depleted in carbon, surrounding the formed carbide particles, with strong microdistortions of crystalline lattices of both the phases [20]. Delayed fracture resistance rises essentially, however a proneness to it is preserved. At temperatures of 150–200 °C, when the second stage of martensite decomposition proceeds with strong depletion in carbon, lowering of the degree of tetragonality and defect density in it, a relaxation of internal stresses occurs, primarily of higher local stresses along the grain boundaries. Such tempering prevents delayed fracture of a welded joint on high-strength steel and cold crack formation.

Thus, to increase the crack resistance of a welded joint of high-strength sheet steel 30KhGSA made by TIG welding, it is rational to reduce the cooling rate during welding, also by a certain increase of the heat input, avoiding boosted modes, application of two-



pass welding (arc treatment of a single-pass joint), as well as tempering at temperatures of 150–200 °C.

Cold cracking in the section of HAZ metal overheating proceeds under the conditions of relaxation of stresses reaching (by magnitude) the yield limit of the less strong base metal. It starts along the grain boundaries of hardened metal, where the shear resistance is lower due to violation of the atomic-crystalline structure (amorphization), compared to the grain body [21]. Also found there are the local increases of inherent stresses [22], which, when summed with inherent stresses of the first kind, lead to local microplastic deformation. During this deformation submicrocracks form in local regions with ultimately distorted crystalline lattice, where the atomic planes separate by one interatomic distance [23]. Being not yet dangerous violations of metal continuity, they, on the other hand, facilitate microcracking, the development of which marks the irreversible stage of damage, and initiation and propagation of microcracks.

Microplastic deformation of hardened metal leads to stress lowering in it by lowering of elastic deformation, while stress relaxation causes a weakening of further plastic deformation and longer duration of micro- and macrocracking. Fracture occurs at the stress above the microyield point. Stress drop to this value without exceeding of the microplasticity margin prevents fracture or cold cracking. Increase of welded joint resistance to delayed fracture is promoted by increase of the microyield point and microlasticity, weakening of hardened metal stressed state by lowering of the disordering of the structure and hardness. This is achieved by reducing the cooling rate at increase of heat input in welding, application of moderate modes and multipass welding, performance of postweld tempering.

In conclusion it should be noted that cold cracking in the welded joint of hardening steel proceeds under the conditions of relaxation of stresses from the base metal yield point to the microyield point of the hardened metal of the joint after using the microplasticity margin during microplastic deformation. This is preceded by submicro- and microcracks initiation along the grain boundaries, having a lower shear resistance, which depends on the degree of crystalline imperfection of these regions, where local increases of inherent stresses may be found. At stresses below the microyield point, their relaxation practically does not proceed, and no cold cracks form.

Cracking resistance rises with lowering of the structure disordering, when the microyield limit and the hardened metal microplasticity rise, and inherent stresses decrease. The rate of stress relaxation and microplastic deformation decreases with lowering of the difference between the stress and microyield point, which results in micro- and macrodiscontinuities forming later and in a smaller number.

The most effective indices of delayed fracture of a welded joint at testing with load decrease can be considered to be the values of microplastic deformation and stress lowering that are equivalent and are determined by direct measurement. Energy index A_{red} is less sensitive and more difficult to determine. When complete fracture is reached, these indices do not depend on the applied load, the latter influencing the

stress at complete fracture (force index) and its duration (time index). Duration of delayed fracture also depends on the metal microplastic deformation resistance, i.e. on chemical composition and its structure.

Delayed fracture resistance of the hardened steel joints, welded without the filler metal, rises (right up to fracture prevention) at decrease of the rate of welded joint cooling by lowering welding speed and current, increasing of welding heat input, number of passes, performance of arc treatment and furnace tempering. In this case, cold cracking resistance rises. For a welded joint of sheet steel 30KhGSA tempering at temperatures of 150–200 °C is acceptable.

1. Paton, B.E., Savitsky, M.M., Kuzmenko, G.V. (1994) Prospects of application of high-strength medium-alloyed steels in high-pressure welded cylinders for motor transport. *Avtomatich. Svarka*, **3**, 4–9.
2. Savitsky, M.M., Mielnichuk, G.M., Lupan, A. et al. (2000) Spawanie stali w osłonie gazow owojetnych zuzyciem Topników artywujacych. *Bulletyn Instytutu Spawalnictwa w Gliwicach*, **5**, 61–69.
3. Granjon, H. (1969) The implant method for studying weldability of high strength steel. *Metal Construction and Brit. Weld. J.*, **1**, 509–515.
4. IIW 830–73. Recommendation for the use of implant test as a complementary information test on the cold cracking susceptibility during the welding of steels.
5. Sawhill, J.M., Dix, A.M., Savage, W.F. (1974) Modified implant test for studying delayed cracking. *Welding J.*, **12**, 554–560.
6. Agafonov, V.V., Kroshin, V.A., Sterenbogen, Yu.A. (1987) Improvement of implant method used to evaluate the weldability of steels. *Avtomatich. Svarka*, **7**, 6–10.
7. Sterenbogen, Yu.A., Khripliv, A.A., Gordony, V.G. (1978) Method of evaluation of welded joint resistance to delayed fracture. *Ibid.*, **8**, 66–67.
8. Sterenbogen, Yu.A., Bursky, G.V. (1987) Method of evaluation of resistance of high-strength steel welded joint HAZ to cold cracking. *Ibid.*, **3**, 1–5.
9. Bursky, G.V., Sterenbogen, Yu.A. (1990) Evaluation of resistance of medium-alloyed high-strength steel HAZ to delayed fracture. *Ibid.*, **8**, 33–35.
10. Mikhoduj, L.I., Poznyakov, V.D., Yushchenko, A.K. (2000) Delayed fracture resistance of 12KhGN2MFDRA steel welded joints. *The Paton Welding J.*, **11**, 4–10.
11. Bursky, G.V., Savitsky, M.M., Olejnik, O.I. et al. (1999) Improved procedure of evaluation of HAZ metal resistance to delayed fracture. *Avtomatich. Svarka*, **4**, 31–34.
12. Sterenbogen, Yu.A., Vasiliev, D.V. (1998) New procedure and energy criteria for evaluation of fusion zone metal resistance to cold cracking. *Ibid.*, **6**, 8–12.
13. Sterenbogen, Yu.A., Vasiliev, D.V. (1999) Evaluation of crack resistance of fusion zone in terms of energy intensity of delayed fracture. *Ibid.*, **6**, 6–12, 17.
14. Zemzin, V.N., Chizhik, A.A., Panin, A.A. et al. (1983) Conditions of crack formation in welding. Part 1. On the role of creep in crack formation. *Svarochn. Proizvodstvo*, **11**, 1–4.
15. Sarra, V.I., Filippov, G.A. (1975) Stages of delayed fracture of quenched steel. In: *Problems of fracture of metals*. Moscow: MDNTP.
16. Popov, A.A., Popova, L.E. (1965) *Isothermic and thermokinetic diagrams of overcooled austenite decomposition*. Refer. Book. Moscow: Metallurgiya.
17. Shorshorov, M.Kh., Belov, V.V. (1972) *Phase transformations and variation of steel properties in welding*. Atlas. Moscow: Nauka.
18. Kulik, V.M., Savitsky, M.M., Novikova, D.P. et al. (2004) Features of argon-arc treatment with insipient melting of welded joint on quenching steel. *The Paton Welding J.*, **3**, 15–20.
19. Navolokin, S.N., Ivanov, V.I., Starchenko, E.G. et al. (1984) Application of acoustic emission method for determination of crack formation under the surfaced layer in reheating. *Avtomatich. Svarka*, **5**, 25–28.
20. Kurdyumov, G.V. (1960) *Phenomena of quenching and tempering*. Moscow: Metallurgizdat.
21. Shurakov, S.S. (1961) *Delayed fracture of quenched steel and effect of tempering on its strength*. Syn. of Thesis for Dr. of Techn. Sci. Degree.
22. Sarra, V.I., Suvorova, S.O., Filippov, G.A. (1974) About internal microstresses arising from martensitic transformation in steel. *Metallofizika*, **54**, 94–97.
23. Ostakin, A.I. (1973) *Study of ductile fracture features in metals and alloys*. Syn. of Thesis for Cand. of Techn. Sci. Degree.

ALGORITHMS FOR COMPENSATION OF ELECTRODE WEAR IN RESISTANCE SPOT WELDING

N.V. PODOLA, P.M. RUDENKO and V.S. GAVRISH
E.O. Paton Electric Welding Institute, NASU, Kiev, Ukraine

Various algorithms for compensation of electrode wear at resistance spot welding are considered, and their effectiveness is analyzed. Algorithms are proposed, which provide the required quality of welding at electrode wear under the conditions of production.

Keywords: resistance spot welding, electrode wear, algorithms, autosteppers, spot weld, nugget diameter

In resistance spot welding the electrodes are subjected to cyclic heating and cooling, mechanical shocks at elevated temperatures and contamination of the working surface, particularly in welding of aluminium alloys and coated steels. In this case, the electrode shape changes, and the working surface dimensions increase as a result of increase of electrode diameter d_{el} , i.e. $d_{el,s} > d_{el,f}$, where $d_{el,s}$, $d_{el,f}$ is electrode diameter after dressing at the start of the welding machine operation and after making a certain number of welds, respectively (Figure 1).

Electrode wear depends on the welding mode, cooling intensity, electrode material, manufacturing method, properties of materials being welded, type of surface coating and some other causes. It is quite difficult to determine the degree of electrode wear during welding. Electrode dressing is most often performed after making a certain number of spot welds [1, 2]. As a rule, they are determined experimentally. Work [3] gives the tentative data on the optimum number of spot welds, which do not result in inadmissible contamination of the electrodes, increase of working surface diameter d_{el} by 20 %, or complete wear of electrodes for various materials welded and electrode grades. In welding aluminium alloys the

number of spot welds in the first case is 50–70, and in the second --- 1000–2000, and in welding low-carbon steels 1000–2000 and 5000–7000, respectively.

The objective of the studies was to analyze various algorithms for compensation of the influence of electrode wear, evaluate their effectiveness and develop new algorithms, which allow ensuring the necessary quality of welded joints at electrode wear.

As a rule, increase of the diameter of the electrode working surface by 20–30 % (Figure 2) leads to a reduced current density and inadmissible reduction of the weld nugget ($d_n < 3t$, where t is the thickness of the parts being welded, mm), and, therefore, it decreases the welded structure strength [4].

There exist various methods for evaluation of electrode life [5, 6]. However, most of them are applied in laboratory conditions, and cannot be used in welded structure manufacturing.

Methods and algorithms for compensation of the influence of electrode wear without direct measurement of the working surface diameter, so-called autosteppers are, as a rule, based on a gradual increase of welding current, depending on the number of spot welds.

In the simplest algorithm, the following parameters are assigned: ΔI_w is the step of welding current increment; N is the number of spot welds up to increase of welding current by ΔI_w ; M is the number of intervals, performance of which is followed by electrode replacement or dressing. Values of these parameters, determined experimentally, depend on many factors, mentioned above. When the spot welds are made, the control system counts them, and at an assigned $N_i = N$ the welding current rises by ΔI_w , com-

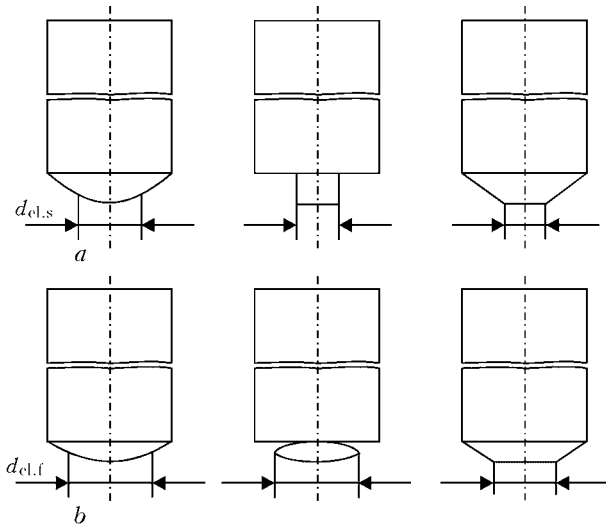


Figure 1. Shape of electrode working surface: a --- initial; b --- final

© N.V. PODOLA, P.M. RUDENKO and V.S. GAVRISH, 2005

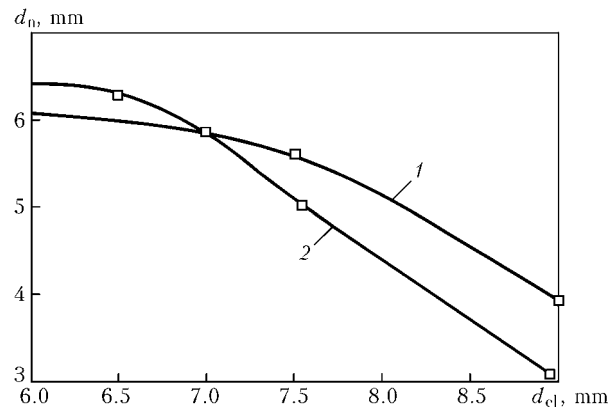
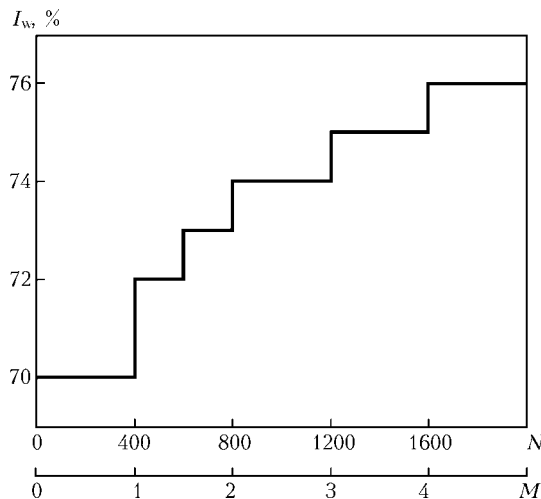


Figure 2. Dependence of d_n on the electrode working surface for MTU 300 (1) and MTP 150 (2) machines; Z_f (2) > Z_f (1)

**Figure 3.** Algorithm of autostepper of the Bosch regulator

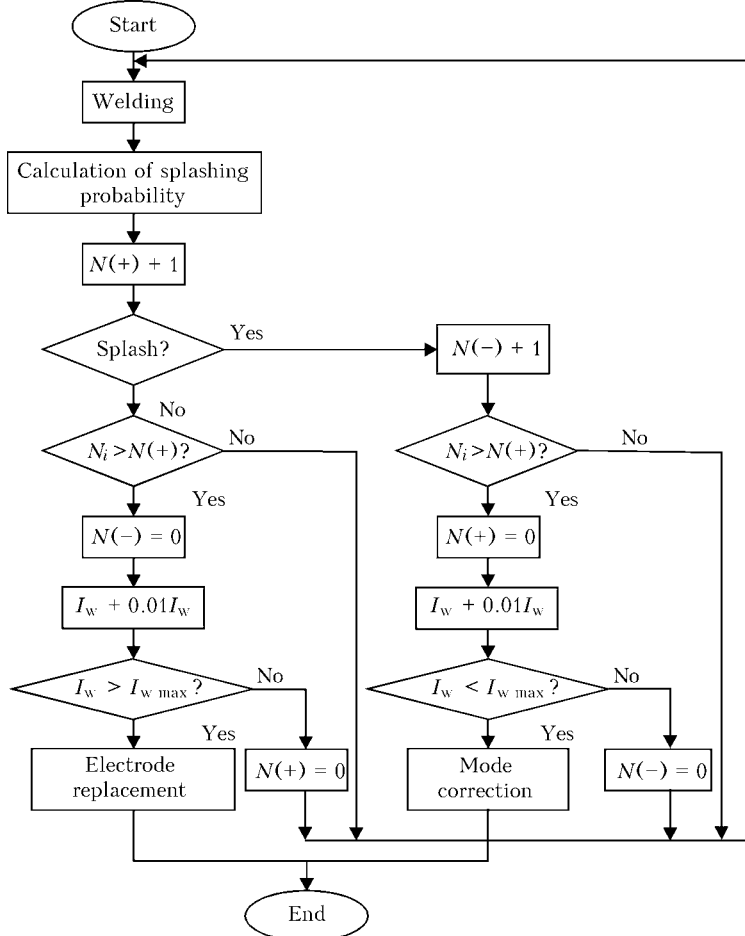
pensating the lowering of the current density. The number of spot welds is divided into several intervals M , each of which is followed by an automatic increase of welding current. The cycle is continued until the number of intervals equals the specified value $M_i = M$. This is followed by electrode replacement or dressing.

A more perfect algorithm was proposed in the quality assurance system of Bosch company (Figure 3). Unlike the previous algorithm, here the assigned parameters ΔI_w and N can have different values for each M interval. This allows compensating for a non-uniform electrode wear during welding performance.

In the autostepper algorithm, applied in the microprocessor regulator RKM-803 of CJSC «Electric-MIKS», just two parameters are assigned, namely the total number of spot welds made before dressing or replacement of electrodes and maximum admissible current $I_{w \max}$ in welding of this item. In this case, the required increment of welding current is calculated by an empirical formula for each spot weld N_i .

The autostepper algorithm applied in DAEWOO regulators, is based on automatic maintenance of welding current at the moment of appearance of splashes in welding (Figure 4). The probability of their appearance is calculated by the curve of dynamic inter-electrode resistance. As welding is performed, the welding current is either increased by $0.01I_w$, or decreased by the same value, depending on the calculated probability of splashing. The assigned values in this case are $N(+)$ and $N(-)$, i.e. number of points of the counter of current increase and decrease, respectively. The algorithm performs until the level of welding current has reached maximum $I_{w \max}$, or minimum admissible $I_{w \min}$ value. In the case of $I_w = I_{w \max}$, the electrodes are replaced or dressed, and at $I_w = I_{w \min}$ the welding mode correction is performed.

Analysis of these algorithms shows that all of them, except for the latter one, use empirical dependencies and data, which are greatly dependent on the specific modes, electrode materials, welding modes, etc. It is natural that under production conditions they need individual correction and further experi-

**Figure 4.** Algorithm of the DAEWOO regulator

mental verification, which requires additional cost and time. The latter algorithm involves application of welding modes, in which metal splashes occur.

Under the conditions of modern production, splashes are inadmissible, given the high requirements to welding quality and product appearance. In addition, in order to increase the quality and stability of welding, the modern computer control systems operate in the mode of stabilization of current, inter-electrode voltage, mains voltage, etc., which practically eliminates the possibility of direct application of the above autostepper algorithms.

We suggested algorithms for wear compensation, which are based on real-time monitoring of welding parameters and variation of welding current by a certain law.

Influence of electrode wear on the quality of welding, related to a change in its shape (contact surface area S_c) can be reduced by correction of the welding mode, in particular welding current, providing a constant value of the density of welding current in the contact, i.e. at increase of contact surface area S_c of the electrodes, the welding current should be increased in proportion.

With an accuracy sufficient for practical purposes, S_c variation can be evaluated by the value of resistance of electrode-electrode area R_{el-el} average over the time of welding current pulse:

$$R_{el-el} \equiv 1/S_c.$$

Considering the random errors of measurement of welding process parameters and gradual wear of the electrodes, in order to determine the importance of variation of area S_c , let us use evaluation of average value of resistance R_{el-el}^{av} over a certain time interval or by the assigned number of successively welded spot welds N :

$$R_{el-el}^{av}(n, N) = \sum R_{el-el,i} / N, \quad (1)$$

where $R_{el-el,i}$ is the resistance of electrode-electrode section R_{el-el} average over the time of the current pulse in i -th welding; $i = n - N, \dots, n$; n is the number of spot welds.

If $R_{el-el}^{av}(n, N)$ statistically significantly differs from the average value of resistances at the start of the working day $R_{el-el}^{av}(0, N)$, i.e. for a normal electrode

$$\Delta R = R_{el-el}^{av}(n, N) - R_{el-el}^{av}(0, N) > 2S_R, \quad (2)$$

where S_R is the root-mean-square deviation $R_{el-el}^{av}(0, N)$, the welding current rises in proportion to the relative variation of the controlled resistance of electrode-electrode section:

$$\Delta I = I_0 \Delta R / R_{el-el}^{av}(0, N), \quad (3)$$

where I_0 is the specified value of welding current, kA.

It is obvious that such an evaluation of the corrective action on welding current is possible at direct measurement of the resistance of electrode-electrode section, for instance by the level of inter-electrode voltage U_{el-el} .

In the case, when inter-electrode voltage U_{el-el} cannot be measured, because of the design features of the welding machine, an indirect evaluation of resistance variation has to be used.

In this case, evaluation of the compensating action depends on the selected algorithm of process stabilization in the used regulator, and proportion of resistances of electrode-electrode R_{el-el} sections, and welding machine secondary circuit impedance Z_f . Impedance can be controlled once a day, and then regarded as unchanged.

Let us consider calculation of the compensating action for the two main algorithms of welding process stabilization, namely welding current stabilization and compensation of voltage fluctuations in the welding transformer primary winding. In the first case, let us use for evaluation of variation of the resistance of electrode-electrode section the estimate of variation of average heating during welding $i_c = I_0 / I_r$, where I_r is the rated welding current, kA; i_c is the current heating, %, corresponding to current I_0 . Heating in relative units i_c is usually used as the driving parameter in regulators, where the welding current sensor is absent.

The regulating action is calculated, using the statistical estimates which are analogous to formulas (1), (2).

If $i_c(n, N)$ statistically significantly differs from mean heating at the start of the working day $i_c(0, N)$, i.e. for normal electrode

$$\Delta i_c = i_c(0, N) - i_c(n, N) > 2S_i, \quad (4)$$

where S_i is the mean-root square deviation $i_c(0, N)$, the welding current rises in proportion to the relative variation of heating:

$$\Delta I = I_r (Z_f / R_{el-el} + 1) \Delta i_c / i_c(0, N). \quad (5)$$

In the case of stabilization of welding transformer power voltage, the measured welding current I_w is used for evaluation of variation of electrode-electrode section resistance.

If $I_w(n, N)$ statistically significantly differs from the average value of current at the start of the working day $I_w(0, N)$, i.e. for a normal electrode

$$\Delta I_w = I_w(0, N) - I_w(n, N) > 2S_i, \quad (6)$$

where S_i is the mean-root-square deviation of $I_w(0, N)$, the welding current rises in proportion to its relative variation

$$\Delta i = i_0 (Z_f / R_{el-el} + 1) \Delta I_w / I_w(0, N), \quad (7)$$

where i_0 is the set value of heating, %, in the mode of compensation of voltage in the welding transformer primary winding.

Difference between i_c and i_0 values in dependencies (4)–(7) is as follows. Level of heating i_c in expressions (4), (5) can be varied from point to point to achieve an unchanged value of welding current I_0 . This is indicated by index «c», i.e. current value. At stabilization of the welding transformer supply voltage, heating is kept constant, i_0 by varying the angle of thyristor contactor switching on. Index 0 shows the constant value of the parameter.



Expressions (5) and (7) show the known effect of self-regulation, depending on the ratio of resistances R_f and Z_f [7].

In the given dependencies at indirect evaluation of resistance R_{el-el} , impedance of the machine secondary circuit is assumed to be constant. However, it is not stable during welding, and may vary due to ageing of detachable joints of the current supply, heating of the current supply by welding current and incorporation of ferromagnetic masses.

Machine short-circuit resistance is adjusted smoothly, and can be monitored by everyday checking. Heating of current supplies during a working shift is rather quickly stabilized and may even be ignored.

In batch production incorporation of ferromagnetic masses may be taken into account. If we choose value N for evaluation of the moving average current or heating, which is a multiple of the number of spot welds on a ferromagnetic item, then the change in the short-circuiting resistance for this reason can be averaged.

General algorithm of compensation for the influence of electrode wear is as follows:

- after mounting new electrodes, their «running-in» is performed, i.e. welding of 20 to 30 spot welds to produce a stable imprint on the working surface;
- mean values are measured of welding current, heating, interelectrode resistance and secondary contour impedance;

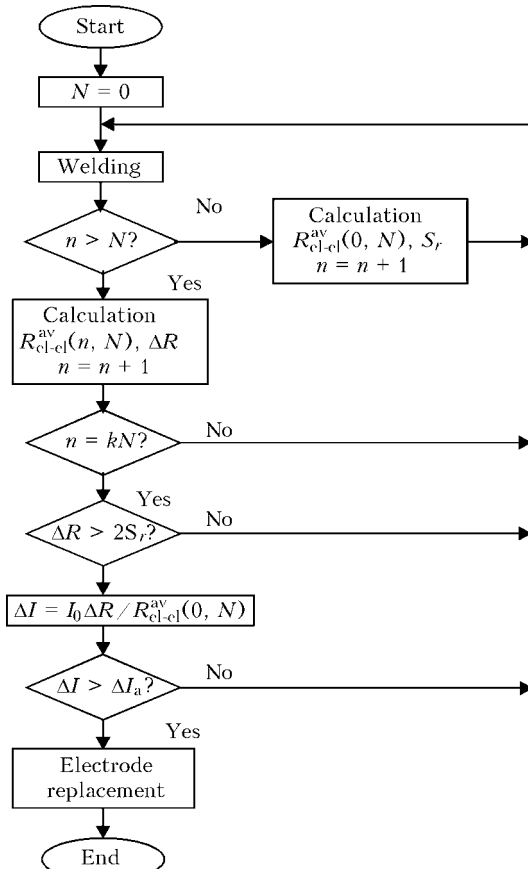


Figure 5. Algorithm of autostepper at U_{el-el} measurement and R_{el-el} calculation; k — integer number (1, 2, ...); ΔI_a — maximum admissible current increment

- during welding, depending on the set algorithm, moving mean of the controlled process parameter is determined and the significance of its deviation from the respective value, obtained in mounting of a new electrode is checked by expressions (2), (4) or (6);

- in case of a significant deviation the corrective action on the welding mode is calculated by equations (3), (5) or (7).

Figure 5 gives an algorithm of compensation for the influence of electrode wear in the case, when R_{el-el} resistance is measured with an inter-electrode voltage sensor.

Mounting of new electrodes is followed by test welding of 20–30 spot welds, by which the average value of interelectrode resistance and its mean-root-square deviation are evaluated. Then during welding of the item the current average resistance is calculated by each points N . Obtained value is compared with the mean evaluation at the start of the work. If their divergence is greater than the doubled mean-root-square deviation, an increase of welding current is calculated for correction.

If a neural network is used in the control system for evaluation of the welded joint quality, its upgrading is possible to calculate the required correction of welding current for compensation of electrode wear (Figure 6). Input parameters of the network were selected to be evaluations of current and voltage between the electrodes in four sections of the welding process, number of spot welds from the start of the shift n and value N for evaluation of the moving mean. Output parameters of the network are diameter of the spot weld nugget and degree of welding current correction.

Experimental studies of electrode contamination in welding of aluminium alloys and zinc-plated low-

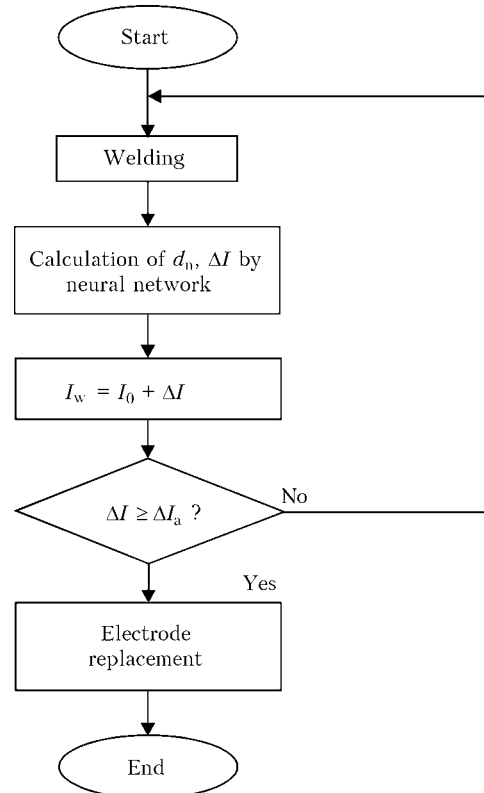


Figure 6. Autostepper algorithm with neural network application

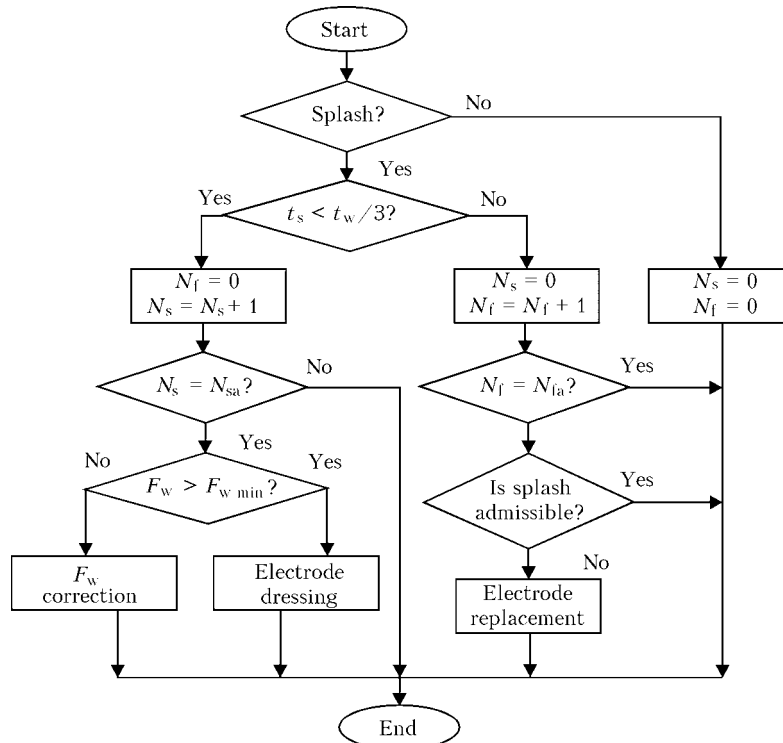


Figure 7. Algorithm of monitoring the condition of electrodes allowing for splashes: N_s , N_f — number of spot welds with initial and final splash, respectively; N_{sa} , N_{fa} — admissible number of points with the initial and final splashes, respectively; F_w — compressive force; $F_{w \min}$ — minimum admissible compressive force

carbon steel showed that the only method to eliminate the wear is timely dressing of the electrodes, performed for aluminium alloys after making a fixed number of spot welds, usually 10–20. For steels inadmissible wear can be determined by a splash at the welding start ($t = t_w/3$). On the other hand, a layer of zinc appearing on the new electrode surface in welding of coated steel is not an indication of inadmissible electrode wear. It is stabilized fairly quickly (10–20 spot welds), and the resistance of electrode-electrode section does not increase.

Figure 7 shows an algorithm of process monitoring by the time of the splash occurrence. Their total number is calculated at emergence of the initial splash. If the set number of welds with the initial splash have already been made in succession, a command is issued for checking the level of the compressive welding force. In the case, if the welding force is within the tolerance, a command is issued for electrode dressing. If the set number of welds with the final splash have been made in succession, a command is issued for electrode replacement.

Effectiveness of the proposed algorithm operation was checked in welding samples of low-carbon steel (1.0 + 1.0) mm thick and with different diameters of the electrode working surface (from 5 to 8 mm). Welding was performed in a spot welding machine of MT-2201 type. Welding mode was selected in keeping with IIW recommendations. Resulting data are given in the Table. From the Table it is seen that application of the algorithm of compensation of the influence of electrode wear provides a stable welding quality (set value of d_n), irrespective of the electrode diameter variation in a broad range (5–8 mm).

I_w , kA	R_{el-el} , μOhm	d_{el} , mm	d_n , mm	ΔI , kA	Note
7.7	151	5	4.8	--	Rated mode
8.8	115	8	3.0	1.1	Without algorithm application
9.8	118	8	5.2	2.1	With algorithm application

Note. Parameter t_w is equal to 8 periods, and F_w — to 275 daN.

Thus, while in the known algorithms based on rigid programs, the parameters are to be chosen allowing for the welding machine characteristics, welding modes and conditions, which is a highly labour-consuming and difficult-to-implement process, in the proposed algorithms such an adjustment is minimized. On the other hand, they enable keeping the welded joint quality within the specified tolerances.

1. (1986) *Technology and equipment for resistance welding*. Ed. by B.D. Orlov. Moscow: Mashinostroenie.
2. Bowers, R.J., Sorensen, C.D., Eagar, T.W. (1990) Electrode geometry in resistance spot welding. *Welding J.*, **2**, 45–51.
3. Waddel, W., Williams, N.T. (1994) The importance of electrode tip growth when welding zinc coated steels. *IIW Doc. III-1032-94*.
4. Sliozberg, S.K., Chuloshnikov, P.L. (1972) *Electrodes for resistance welding*. Leningrad: Mashinostroenie.
5. Satoh, T., Abe, H., Suzuyama, S. (1997) A trail of quality assurance in resistance spot welding by aid neural network and fuzzy reasoning accomplished with detection of top diameter of electrode. *IIW Doc. III-1083-97*.
6. Weber, G. (1998) Electrode wear assessment of spot welding by fuzzy classification. *IIW Doc. III-1111-98*.
7. Lebedev, V.K., Pismenny, A.A. (2001) Power systems of resistance welding machines. *The Paton Welding J.*, **11**, 28–32.



SELF-SHIELDED FLUX-CORED WIRES FOR WELDING LOW-ALLOY STEELS*

V.N. SHLEPAKOV and S.M. NAUMEJKO
E.O. Paton Electric Welding Institute, NASU, Kiev, Ukraine

Advantages and disadvantages of flux-cored wires of the PP-AN60 and PP-AN62 grades developed by the E.O. Paton Electric Welding Institute are considered. Results of metallographic examinations of distribution and composition of non-metallic inclusions in metal of the welds made with wires of the oxide and fluoride types are presented. Recommendations for application of the developed wire grades are given.

Keywords: self-shielded flux-cored wires, deposited metal, chemical composition, mechanical properties, distribution of non-metallic inclusions, welding-technological characteristics

Topicality of tasks in the field of welding using self-shielded flux-cored wire is caused by demand of the national market for materials that provide maximal versatility of the application (possibility of welding different types of the joints in different spatial positions and under different operational conditions). This requires ensuring the desirable level of strength and tough-ductile properties of the joints, as well as high productivity of the welding process.

The E.O. Paton Electric Welding Institute developed the 1.6 mm diameter self-shielded flux-cored wires of the PP-AN60 and PP-AN62 grades for welding structures of carbon and low-alloy steels in any spatial position. Table 1 gives basic characteristics of the wires, and Table 2 gives typical chemical composition of the deposited metal.

Resistance of the weld metal to porosity caused by nitrogen is ensured by alloying the weld metal with aluminium through the core of a self-shielded flux-cored wire.

Flux-cored wire PP-AN60 has a core of the oxide-fluoride type with a high basicity of slag, while the core of wire PP-AN62 is of the oxide type with low basicity. Both wires form rapidly solidifying slag in welding.

Results of metallographic examinations of distribution of non-metallic inclusions in metal of the welds made with wires of the oxide and fluoride types are shown in Figure 1. Metal of the welds made with wire PP-AN60 of the fluoride type is characterised by a relatively uniform distribution of dispersed particles of non-metallic inclusions, which consist mostly of aluminium nitrides and oxides. Non-metallic inclusions in metal of the welds made with self-shielded wire PP-AN62 of the oxide type (Figure 2) consist primarily of aluminium oxides and a small amount (less than 5 vol.%) of silicon and manganese oxides.

Metal deposited with wire PP-AN60 has a low content of sulphur (0.003–0.005 wt.%), which is twice as low as in metal of the welds made with wire of the oxide type (0.009–0.010 wt.%), and much lower than in metal of the welds made with general-application wires and electrodes (~0.0015–

Table 1. Type and characteristics of self-shielded flux-cored wires

Wire grade	GOST 26271	EN 758	Slag base	Polarity of welding current
PP-AN60	PS49-A3U	T5031NiYNiH10	CaO–MgO–Al ₂ O ₃ –R ₂ O–BaF ₂ –LiF	Straight
PP-AN62	PS44-A2U	Ø462SN1H10	MgO–R ₂ O–MnO _x –FeO–Al ₂ O ₃	Reverse

Note. R — alkali element.

Table 2. Typical chemical composition of metal deposited using self-shielded flux-cored wires, wt.-%

Wire grade	C	Si	Mn	Ni	Al	S	P
PP-AN60	0.10	0.12	1.1	1.1	0.70	0.003	0.008
PP-AN62	0.11	0.06	1.2	—	0.25	0.010	0.025

* This information in the form of paper was presented at the III International Conference on Welding Consumables of the CIS countries (Ukraine, Dnepropetrovsk, 1–4 June 2004).

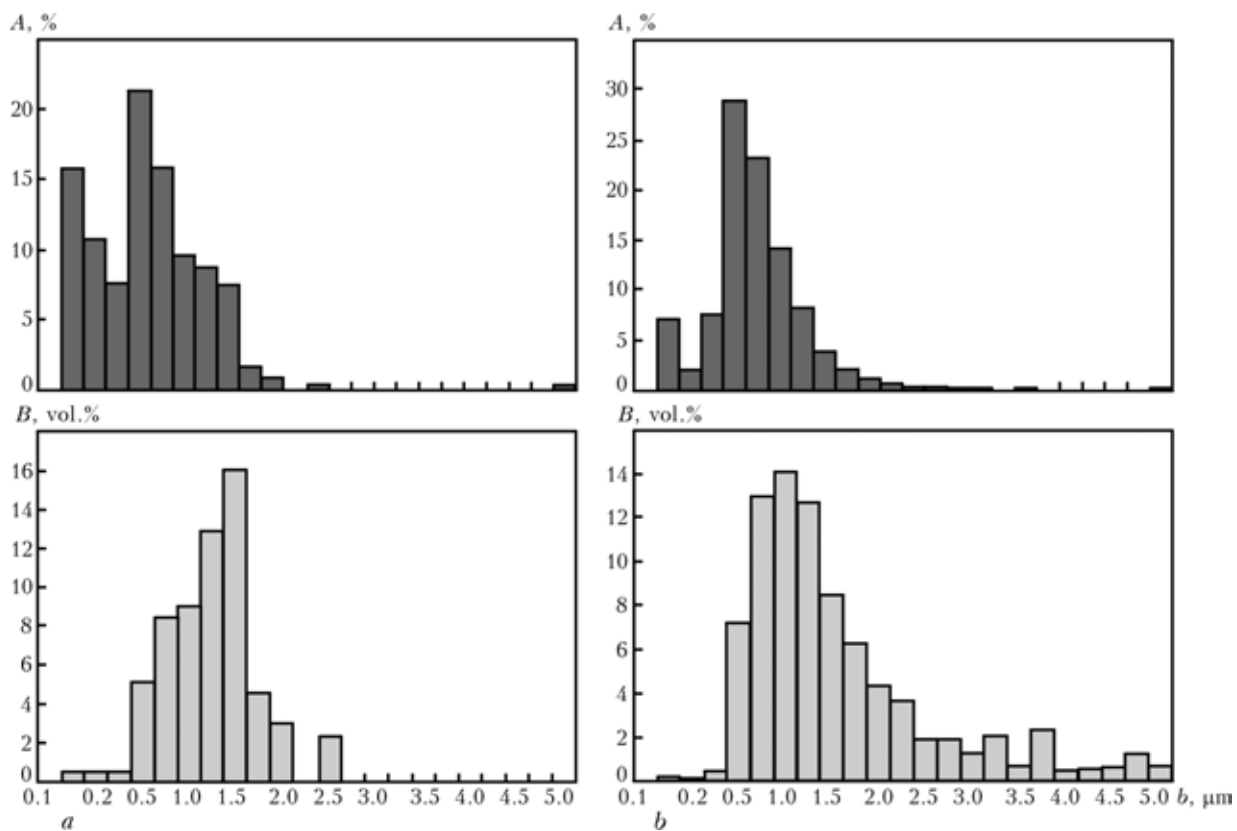


Figure 1. Distribution of non-metallic inclusions *A* and *B* in size *b* in welding using flux-cored wires of fluoride (a) and oxide (b) types

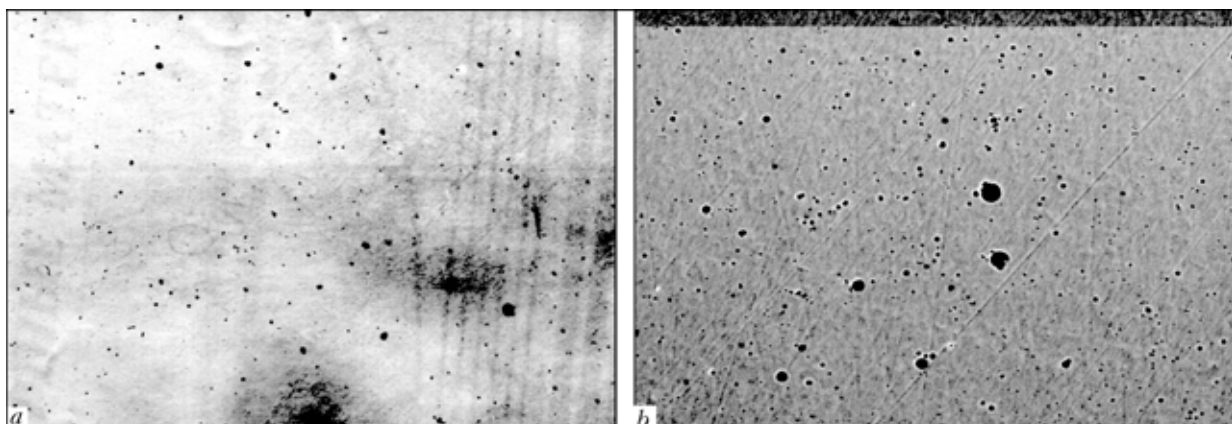


Figure 2. Typical inclusions in metal of the welds made with flux-cored wires of fluoride (a) and oxide (b) types ($\times 750$)

0.0250 wt.%). This is attributable to utilisation of active desulphurising agents in the wire core.

Results of mechanical tests of metal of the welds made with self-shielded flux-cored wires of the fluoride and oxide types are given in Table 3.

Characteristics of productivity of the processes performed with flux-cored wires PP-AN60 and PP-

AN62 under typical welding conditions are given in Table 4.

As to welding-technological properties, the wires are characterised by easy detachability of the slag crust, good shape of the welds and possibility of welding metal over a wide thickness range. They allow welding of metal structures to be performed under

Table 3. Typical mechanical properties of weld metal

Wire grade	σ_t , MPa	σ_y , MPa	δ , %	KCV, J/cm ² , at \dot{O} , $^{\circ}\text{N}$			
				+20	-20	-40	-60
PP-AN60	635.1	525.3	23.3	140.1	68.1	57.5	52.5
PP-AN62	590.0	480.1	22.1	90.0	65.5	35.1	--

**Table 4.** Productivity of welding using self-shielded flux-cored wires

Welding (surfacing) position	PP-AN60	PP-AN62	PP-AN60	PP-AN62
	g/min		cm/min	
Flat	55	47.5	22.5 (5°)	21.8 (5°)
Vertical:				
upwards	40	32.0	7 (8°)	7.5 (6–7°)
downwards	45	39.0	20 (3°)	22.0 (3°)
Overhead	45	--	15 (5°)	--

*Weld leg, mm.

field conditions in all spatial positions (flat, vertical upwards and downwards, overhead). Wire PP-AN60 can be recommended for welding structures of low-carbon and low-alloy steels.

The content of non-metallic inclusions in metal of the welds made with wire PP-AN60 is 0.3 vol.% on the average, while that of the welds made with wire PP-AN62 is 0.85 vol.%.

CONCLUSIONS

1. Versatile self-shielded flux-cored wires were developed for welding structures of low-carbon and low-alloy steels in all spatial positions.

2. Metal of the welds made with wire PP-AN60 of the fluoride type has a relatively uniform distribution of non-metallic inclusions, which consist mostly of aluminium nitrides and oxides, while metal of the welds made with wire PP-AN62 of the oxide type is characterised by the presence of an insignificant amount of silicon and manganese oxides, along with aluminium oxides.

3. Volume content of non-metallic inclusions in the welds made with the oxide type wire is 3 times as high on the average as with the fluoride type wire.

4. Utilisation of active desulphurising agents (calcium and magnesium) in the wire core allows the sulphur content of the deposited metal to be decreased 3–4 times on the average.

5. Alloying of the weld metal with nickel and limitation of its sulphur content (due to addition of AlCa to the core) allow wire PP-AN60 to be recommended for welding structures of low-alloy steels with a yield strength of 490 MPa, and wire PP-AN62 (oxide type) to be recommended for welding steels with a yield strength of 440 MPa.

DESIGN OF COMPRESSION DRIVE FOR LONGITUDINAL ARC WELDING OF THICK-WALLED SHELLS

I.A. TARARYCHKIN and A.S. VOSKRESENSKY
V. Dal East-Ukrainian National University, Lugansk, Ukraine

It is suggested that in longitudinal welding of a thick-walled shell a system of radial forces should be applied to the shell to avoid closing of a gap as a result of development of angular deformations. It has been found that compressive forces need to be adjusted until approximately half of the groove is filled up. Dependencies for design of the pneumohydraulic compression drive are presented, and recommendations for regulation of the compressive force are given.

Keywords: *thick-walled shell, compressive force, multipass weld, angular deformations, welding device, groove preparation, pneumohydraulic drive*

Arc welding of longitudinal joints in thick-walled cylindrical shells can be performed by filling the groove with a multipass weld [1, 2]. The volume of the deposited metal can be reduced and the efficiency of the welding process can be improved through decreasing the included angle of a one-sided groove to 0–7° and providing the gap in a joint equal to 9–15 mm [3]. However, filling of a narrow groove with the multipass weld is hampered because of development of angular deformations and gradual closing of the gap. As reported in [3], the value of reduction of the gap near an upper edge in longitudinal welding of a thick-walled shell can be commensurable with that of the gap proper, and may

lead to sticking of the torch during the welding process. In addition, a change in the gap width leads to systematic disturbances in the welding process, which may be accompanied by formation of technological defects in the form of undercutting, lack of penetration, lack of fusion, etc. The negative effect of closing of the gap on formation of the multipass weld can be diminished using different technological approaches. Thus, according to the technique suggested in [4], a system of radial compressive forces leading to opening of the gap should be applied to the shell, and the welding process should be performed in the following sequence:

- longitudinal joint in the shell is assembled with a set gap $2B$ and parallel groove walls using I-shaped clips;
- after welding of the first layer, an observed angular deformation is measured, and such a radial com-



pressive force is applied that the initial (parallel) position of the groove walls is restored (Figure 1);

- after welding of the second layer, the second measurement of the observed angular deformation is made, and the compressive force is adjusted (increased) so that the initial (parallel) position of the groove walls is ensured.

This sequence of the operations is performed until the groove is completely filled up. Practical realisation of this technique involves to the need to preliminary determine compressive force P , which is capable of ensuring the required deformation of the shell for further selection (design) of the force components of the welding device.

The purpose of this study was to determine radial force P that is capable of compensating for closing of the gap taking place during welding of a longitudinal joint in the shell, as well as to formulate calculation dependencies needed to design a compression force drive. Statistical models suggested in studies [3, 5], which describe the process of development of angular deformations in filling the groove with a multipass weld, were used for a range of mean diameters of the shell equal to $D_{mean} = 0.5\text{--}1.5$ m and thickness of the metal welded equal to $\delta = 60\text{--}120$ mm. The value of the gap, $2B$, in a joint with parallel edges was set depending upon the thickness of the metal welded (Table). Thickness of one layer of the weld, h , should be approximately half of a narrow gap width (on condition of ensuring solidification crack resistance of metal).

Force P provided by the force drive of the welding device is a sum of individual forces Δp_i applied after welding of each layer (except for the last layer):

$$P = \sum_{i=1}^{N-1} \Delta p_i, \quad (1)$$

where N is the quantity of layers necessary for the groove to be completely filled up.

As solution of the deformation problem for a region in the form of a ring with a rectangular cut in a closed shape is not available, the deformed state of the shell was calculated using the finite element system ANSYS. The calculation procedure was performed in two stages. At the first stage reliability of the numerical solution was estimated by comparing values of radial displacements of the internal and external contours of a thick-walled steel shell affected by the external pressure. The calculated displacements of the nodes were compared with results of an exact solution of the problem given in [6, 7]. As found as a result of this estimation, the error of the numerical method for the analysed metal diameter and thickness ranges is no more than 6.5 %, which is acceptable.

The second stage of the calculations was related to determination of the displacements of points A, B, C and D characterising position of the cut (Figure 2), and the corresponding values of Δp_i after completion of each layer. The displacements of nodes G_1 and G_2 , to which the radial compressive force was applied according to the accepted calculation diagram, were also determined (Figure 1).

Results of the calculations allow a conclusion that radial force P should be adjusted until approximately

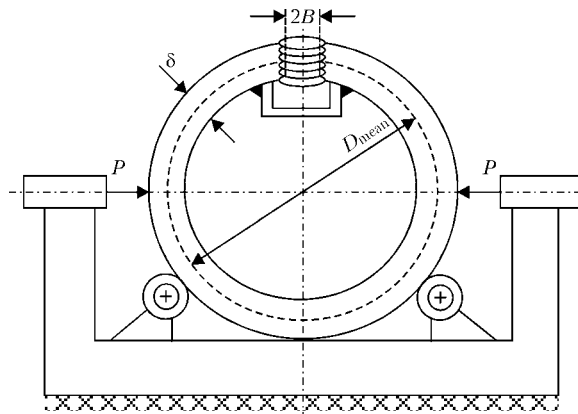


Figure 1. Calculation diagram for application of forces along the generating line of the shell

half of the groove is filled up, as with this approximately 90 % of the residual angular deformation is formed. Further filling of the groove leads to an insignificant closing of the gap, which can be ignored. Therefore, all the calculations associated with determination of force P were made allowing for this circumstance.

Analysis of the calculation results shows that at a constant mean diameter of the shell the value of compressive force P varies insignificantly within a metal thickness range of 60–120 mm. This can be explained by the fact that at a constant mean diameter of the shell [3] an increase in the wall thickness is accompanied by decrease in residual angular deformations of the joint, β_L . Therefore, with growth of thickness δ , despite an increase in rigidity of the shell, the force required for its deformation varies but insignificantly.

The force module of the fixture can be based on standard components (hydraulic drive, moment electric drive, etc.). Independently of the drive used to equip the device, it should meet the following requirements:

- it should develop the force sufficient for deforming the shell of a specified size;
- it should provide the possibility of gradually changing the compressive force over the entire range of working values.

The pneumohydraulic compression drive [8] meets most completely the above requirements. An example

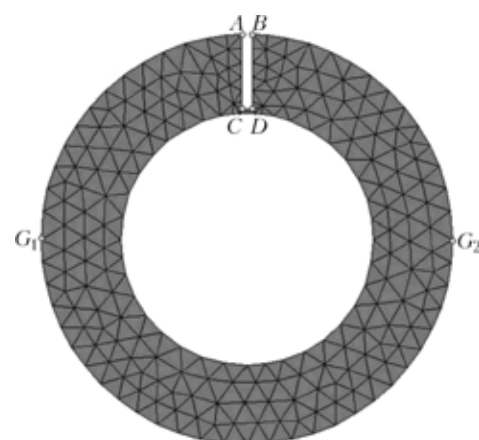


Figure 2. Spacing of the region in the form of a ring with a cut and positions of point A, B, C, D, G_1 and G_2 the displacements of which were estimated by calculations

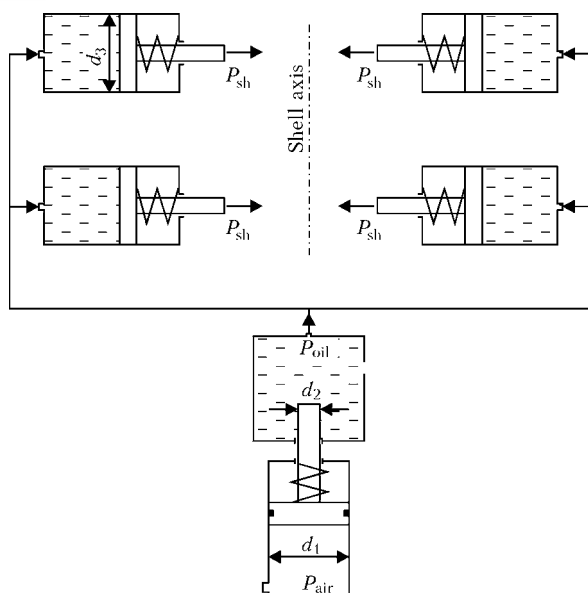


Figure 3. Schematic diagram of pneumohydraulic drive for compression of the shell (see designations in the text)

of the calculation of this drive is given below. Excessive air pressure P_{air} formed in a work chamber of the pneumocylinder leads to increase in oil pressure P_{oil} in the hydraulic system of the drive and is transferred to the actuating rods of the working hydrocylinders (Figure 3).

The force required for deformation of the shell per rod of one hydrocylinder is determined as follows:

$$P_{\text{sh}} = \frac{2P}{k}, \quad (2)$$

where k is the total quantity of the hydrocylinders installed on two sides in one meter of the shell length; and P is the force determined for specified D_{mean} and δ .

The pneumohydraulic drive should be designed so that the sufficient force P_{sh} is ensured at the hydrocylinder rod:

$$P_{\text{sh}} \geq P_{\text{air}} \frac{\pi}{4} \left(\frac{d_1 d_3}{d_2} \right)^2 - W_p \left(\frac{d_3}{d_2} \right)^2 - W_h, \quad (3)$$

where d_1 , d_2 and d_3 are the diameters of the work chamber of the pneumocylinder, rod of the booster and hydrocylinder (see Figure 3); W_p and W_h are the forces developed in a compressed state by the return springs of the pneumo- and hydrocylinders, respectively.

The pressure of oil in the hydraulic system of the drive is as follows:

$$P_{\text{oil}} = P_{\text{air}} \left(\frac{d_1}{d_2} \right)^2 - \frac{4W_p}{\pi d_2^2}, \quad (4)$$

stroke of the pneumocylinder rod is

$$L_p = \left(\frac{d_3}{d_2} \right)^2 l_0 k k_0, \quad (5)$$

stroke of the hydrocylinder rod is

$$L_h = l_0 k_0, \quad (6)$$

where k_0 is the safety factor for stroke of the hydrocylinder rod, allowing for the probable deviation of the shell shape from the cylindrical one, as well as

Parameters of a joint in the shell

Wall thickness δ , mm	Gap value $2B$, mm	Layer thickness h , mm
60–80	9–11	4.5–5.5
80–100	11–13	5.5–6.5
100–120	13–15	6.5–7.5

for the need to ensure the gap between the rod and shell in an inactive state for its installation into the device ($k_0 = 1.5–3.0$).

It is advisable to regulate force P_{sh} during the welding process by gradually varying air pressure P_{air} in the pneumatic system of the drive (e.g. using a gas pressure regulator), and monitor the required compressive force by measuring the distance between the upper edges of the gap in a thick-walled shell.

Therefore, the approach suggested for calculation of the pneumohydraulic drive for compression of the shell should be performed in the following sequence:

- determine values of P and l_0 for the shell of a specified size;
- upon setting the quantity of hydrocylinders, k , installed per meter of the shell length, from formula (2) determine force P_{sh} per rod of one hydrocylinder;
- P_{air} and P_{sh} , as well as forces needed for complete compression of return springs W_p and W_h being known, set (select) the values of diameters d_1 , d_2 and d_3 at which inequality (3) is met;
- determine stroke of the rod for pneumo- and hydrocylinders from formulae (5) and (6).

CONCLUSIONS

1. It has been established that to prevent closing of the gap in longitudinal welding of the shells with a wall thickness of 60–120 mm and mean diameter of 0.5–1.5 m, it is necessary to apply a compressive force of about 48,000 N per meter of the shell length.

2. The compressive force during welding should be adjusted until approximately half of the groove is filled up.

3. The required compressive force before making the next layer should be monitored by measuring the distance between upper edges of the groove of a thick-walled shell.

1. Kurkin, S.A., Khovov, V.M., Rybachuk, A.M. (1989) *Technology, mechanisation and automation of welded structure fabrication*. Manual. Moscow: Mashinostroenie.
2. Renelt, E., Fisher, W. (1981) Untersuchungen zum Engspaltschweißen von Zylindern. *ZIS-Mitt.*, 23 (6), 619–625.
3. Nakajima, H., Ohsawa, M., Nagai, A. et al. (1984) A study on narrow groove MIG welding for heavy wall pressure vessels. In: *Proc. of 5th Int. Conf. on Pressure Vessel Technol.* San Francisco, Sept. 9–14, 1984. New York.
4. Tararychkin, I.O., Voskresensky, A.S. *Method for multipass arc welding of longitudinal joints in thick-wall cylindrical shells*. Pat. 67052A, Ukraine. Int. Cl. B 23 K 9/00. Appl. 13.06.03.
5. Tararychkin, I.A. (2003) Study of angular deformation propagation in multipass narrow-gap welding. Part 2. *Vistnyk VUNU*, 68 (10), 163–169.
6. Podgorny, A.N., Marchenko, G.A., Pustynnikov, V.I. (1981) *Principles and methods of applied elasticity theory*. Kiev: Vyshcha Shkola.
7. (1986) *Strength of materials*. Ed. by G.S. Pisarenko. 5th ed. Kiev: Vyshcha Shkola.
8. Rymorov, E.V. (1988) *New welding devices*. Leningrad: Strojizdat.



ROLE OF TESTING LABORATORIES IN PROVIDING QUALITY CONTROL IN PRODUCTION OF WELDING CONSUMABLES*

O.Yu. KORNETSKY

OJSC «Dneprometiz», Dnepropetrovsk, Ukraine

Practical experience accumulated by the testing laboratory of the Open Joint Stock Company «Dneprometiz» in assuring quality of covered electrodes in compliance with requirements of ISO 9001:2000 and DSTU ISO 9001–2001 is described.

Keywords: welding consumables, production, quality control, testing laboratories, certification

Open Joint-Stock Company «Dneprometiz» is one of the largest produces of metalware in Ukraine. This is a high-technology enterprise with more than 100-year history, its own traditions and developed infrastructure. Despite of financial constrains the enterprise has managed to preserve the structure of the service for providing quality, which includes the central plant laboratory (CPL) with accredited chemical, mechanical and spectral laboratories equipped with modern testing facilities. The service also comprises a net of shop technological laboratories, laboratory of metrology, department of technical control and engineering department.

The main task of the enterprise collective is to insure the output of high-quality products, which maximally meet the demands of the consumers. Engineering and technological personnel is characterized with high intellectual and professional level.

A system of quality management certified by the certification bodies TUV CERT, TUV Rheiland Berlin-Brandenburg and STANKOCERT to meet the requirements of ISO 9001:2000 and DSTU ISO 9001–2001 is developed, operating and permanently improving at the enterprise.

The developed scheme for identification of products at all technological process stages toughly regulating the quality parameters and allowing determination of any discrepancy within the whole technological chain is successfully functioning. Introduction of this system allowed increasing a responsibility of every participant of the technological process and considerably improving the quality of the manufactured products.

Volumes of production and sales of welding electrodes somewhat decreased for the last five years, which had a negative effect on the economy and price of the products. In spite of this, the metal for pro-

duction of electrodes and raw materials for are purchased only from the producer. In this case the purchased materials are subjected to 100 % control irrespective of the lot size, which is sufficiently expensive. However, the quality of wire rod does not allow refusing from the total control of chemical composition of the welding metal. The enterprise practices melt-by-melt supply of metal to the production of both wire and electrodes, which allows taking all necessary preventing and correcting measures in time.

Technology for production of electrodes provides a full cycle including production of wire, rods, processing and preparation of raw materials and charge, production of liquid glass, packing of electrodes, their storage and acceptance tests.

Engineering department, department of technical control, CPL, laboratory of metrology, technological laboratory and personnel of the shop perform the functions of control of the technological process and ready products of the electrode shop.

The enterprise already for many years conducts a 100 % incoming control of the raw materials including verification of the quality certificate by chemical composition and other parameters. After obtaining satisfactory results every type of the raw material is formed into a lot to insure traceability and identification of the products. Then the lot is launched into production.

The results of the incoming control give during the last years a positive result. The enterprise used in 2000–2001 rather large quantities of wire rods from the Makeevka Metallurgical Integrated Plant. The wire rods were characterized with unstable chemical composition and increased sulfur content. The results of the incoming control showed that about 400 t of wire rods did not correspond to the specifications as to sulfur and manganese content, 8 t --- as to silicon content and 8 t had defects in geometrical parameters and microstructure. Then the enterprise had to refuse from purchasing fire rod from this plant.

The Krivoj Rog Metallurgical Integrated Plant has been supplying wire rod to our enterprise during the last three years. But here we also have problems with wire rod of standard carbon steel: many melts of wire rod in one rail car, inhomogeneity of chemical composition and defects of metal microstructure. All

*This material was presented at the 3rd International Conference on Welding Consumables in CIS Countries (Dnepropetrovsk, June 1–4, 2004).



this does not permit providing stable quality of our production. Unfortunately, DSTU 2770-94 does not regulate microstructure indices (segregation, porosity, non-metallic inclusions).

As a result of the performed works the issue of decreasing the number of different melts in one rail car was resolved. Purposeful work is carried out on improvement of the metal quality.

Until 2003 the ferromanganese was purchased from the Nikopol Ferroalloy Integrated Plant. During 2000-2002 nine lots with inconsistent chemical composition (increased silicon content) were supplied, so representatives of the plant were twice called for solution of the issue on replacement of ferromanganese.

Since 2003 the Zaporozhie Ferroalloy Integrated Plant recognized as responsible supplier has been supplying ferromanganese to our enterprise.

The technological laboratory headed by the technologist performs the following functions:

- controls moisture content in materials after drying;
- determines granulometric composition of the raw materials;
- controls quality of liquid glass from the silicate clod;
- determines plasticity of the coating flux;
- controls humidity of ready electrodes;
- determines coefficient of the coating mass;
- prepares the specimens for acceptance control;
- develops technology for producing new grades of electrodes.

The CPL has the following responsibilities:

- to conduct chemical analysis and necessary mechanical tests of raw materials;
- to control quality of semi-products and ready products during analysis and tests;
- to carry out necessary research works;
- to participate in the inspection of technological process in the shops of the enterprises;
- to process statistical data of the studies and analysis.

The CPL was in 2003 attested by the Ukrainian Research Institute of Metals (Kharkov) and received the right to carry out attestation activities.

The CPL includes a chemical laboratory (chemical methods of analysis) and a laboratory on production control (mechanical tests, spectral methods of analysis), proximate-analysis laboratories in the main shops.

Chemical laboratory provides 100 % control of raw materials for production of electrodes and powder wire: different ferroalloys (ferrotitanium, ferromanganese, ferrovanadium, ferrotungsten, ferromolybdenum and others) as well as marble, dolomite, limestone, silicate clod, rutile and ilmenite concentrate, mica and others.

Chemical composition of wire rod and deposited metal was determined by the optical emission spectrometer SPECTROLAB-F based on photoelectric spectrum analysis using excitation of steel element

atoms with electric discharge, decomposition of radiation into spectrum, change of the analytical signals proportional to the intensity or logarithm of the intensity of spectral lines and subsequent determination of the content of elements by the graduation characteristics.

The method of «three standards» based on the comparison of measured intensities of spectral lines by the reproducible measure is used for measuring fraction of total masses of chemical elements in steels. This process is fully automated and controlled by the built-in computer. Standard specimens of the attested composition for spectral analysis were used as the measure.

The CPL developed the programs for analysis of the wire rod, wire 4 and 5 mm in diameter and deposited metal as well as the method for quantitative analysis of wire rod, different steels and zinc on the SPECTROLAB. The laboratory is selecting and developing sets of standard specimens of the enterprise. The use of these specimens solved the problem of the shortage of expensive state standard specimens. The available measuring methods are improved and new measurement methods are created.

The CPL carries out intensive research on development and mastering the technology for production of metalware on the new equipment with the aim of saving main and accessory materials. So, the joint work of the specialists of the engineering department, the CPL and electrode shop allowed considerably decreasing the consumption norms of metal and coating flux during electrode production as well as developing recommendations on the rational use of the coating flux wastes.

In 2002-2003 quality characteristics of the electrodes produced at the enterprise were studied to identify the reason for decrease of the demand for these electrodes at the consumer's market.

Quality characteristics of the electrodes were studied by comparison of the electrodes of the enterprises competitors, such as company ERA, BaDM Ltd. (Dnepropetrovsk), E.O. Paton Experimental Plant of Welding Consumables (Kiev), Vistek Ltd. (Artyomovsk).

As a result of the tests and welding operations with electrodes ANO-4 carried out by two independent welders the preference was given to electrodes of the Open Joint-Stock Company «Dneprometiz» even though the electrodes were produced at the equipment, which is in operation for already 29 years.

The results of the acceptance inspection tests of the electrodes ANO-4 and MR-3 are presented in the Table.

High quality of the welding technological properties of the electrodes ANO-4 was confirmed at the exhibition «Welding in Ukraine» in 2004 in Kiev. Tests were carried out on the German equipment of the company HKS with comparison of the products of Russian and Ukrainian producers.



Chemical composition of deposited metal and mechanical properties of the metal of welds produced by the electrodes ANO-4 and MP-3

Grade of the electrode	Fraction of total mass of the elements, %					Mechanical properties		
	C	Mn	Si	S	P	σ_t, MPa	$\delta, \%$	$Q_i, J/m^2$
ANO-4	0.08–0.09	0.56–0.69	0.09–0.12	0.016–0.022	0.018–0.032	480–520	24–27	100–116
MR-3	0.08–0.09	0.65–0.72	0.020–0.028	0.016–0.022	0.020–0.028	480–520	23–26	90–106

With the aim of improving quality of the welding consumables and the products on the whole the CPL specialists carry out a statistical control by using the methods of numerical data processing ---- test card, histogram, Pareto diagram.

Statistical methods of control are employed to analyze the reasons of receiving the products, which do not meet the relevant standards as well as violations of technological discipline in the shops.

The CPL, department of technical control and engineering department together with main shops analyze the statistical processing of the data and develop correcting measures to improve quality of the products. The Pareto diagrams and histograms are used on the quarterly basis to analyze the output of the low quality products by types and reasons of violations.

Data on the average statistical surface density of zinc on the ready products of the shop of metal products are processed every month during a year and histograms on density distribution by the wire diameters are constructed.

The laboratory of metrology unifies all measurements and carries out all necessary metrological support of the production (calibration of the instruments, verification of the devices, preparation of necessary techniques for measurements). The laboratory includes the following units: site for servicing tools for measurements of mass; laboratory of electric measurements; laboratory of linear-angular SIT; site for instrumentation.

Introduction of high-productive modern equipment at the enterprise is impossible without the use of the automatic control instruments. The number of such instruments grows every year. The laboratory of metrology is responsible for their maintenance. Owing to the reliable operation of instrumentations it has become possible to correct technological processes and to save energy.

The number of necessary tests has increased during the last time because the requirements to the quality of welding consumables have become tougher. The personnel provide performance of such tests by mastering additional professions, upgrading qualification and rational work.

So, in connection with increased requirements of the customers to the quality of the zinc-plated wire (appearance, homogeneity of mechanical properties by the length of the bundle, strength of the coating) the correction measures of technical and organizational character were developed and introduced into practice. The equipment is reconstructed, a scheme of control of technological production is changed, a system of identification is introduced providing a possibility of tracing the production of every bundle of the ready product, methods of control are changed and toughened.

Taking of necessary measures required introducing changes into the structure of quality management. The laboratory of the shop of metal coatings combines the functions of controller and laboratory assistant, complete interchangeability of the personnel is achieved. Calculations necessary for measurements and maintenance of the control log are carried out electronically. This allowed achieving a considerable improvement of the quality of zinc-plated wire (specific luster, heterogeneity of mechanical properties by the length of the bundle, strength of the coating in winding on one diameter) and simultaneously decreasing the norms for zinc consumption.

Therefore, stability of the quality of electrodes is provided by well-equipped testing laboratories and qualified personnel. Our testing laboratories have a sufficient potential for development of production of welding consumables, expansion of the range of products and increase of the production volumes.



NEW DEVELOPMENTS OF CONCERN ESAB OK AristoRod AND MarathonPac FOR MAG WELDING

A.N. KOT
OJSC NISA, Kiev, Ukraine

Recent developments of concern «ESAB International AB» (Sweden) in the field of coatings and packing of welding wire are considered. Advantages of offered developments are analyzed and examples of their industrial application are given.

Keywords: arc welding, welding wire, copperization, spattering, arc stability, machining, coating, wire packing, welding process efficiency

Coppered welding wire is widely used in industry for production of carbon and low-carbon steels structures. Copper coating on welding wires for MAG welding performs a number of important functions. It is used as lubrication when wire is fed, enhances current transfer in welding and protects wire against corrosion under storage. However, the use of copper has essential disadvantages. Gradual accumulation of copper dust and chips causes blockage of wire feed mechanism, thus leading to slip and instable feed, enlarged spattering and finally to a dead stoppage of the welding process.

Relevant maintenance and cleaning of the feed system is vitally needed when using coppered welding wires. However, this is labor-consuming and rather expensive process leading to outage of welding equipment including the one in composition of complex automatic systems. In addition, copper available on the welding wire fosters increased spattering in welding, which, as a rule, deteriorates the properties of the weld metal.

Another essential drawback of copper coating is an increased content of vapors of oxides and other copper compounds in the welding arc, which has a negative impact on environment and health of the personnel. By this reason the use of coppered wire is not recommended in many countries.

OK AristoRod --- a new type of welding wires.

Research workers of the concern ESAB International AB (Sweden) developed a new promising series of welding wires OK AristoRod with unique copper-free coating ASC (Advanced Surface Characteristics) with improved characteristics. ASC is a technology including two main components: special surface machining (calibration of very high degree) and application of micron-thick coating whose composition is the concern ESAB know-how. Wire with improved feeding and welding characteristics on par with corresponding parameters of the coppered wire was for the first time produced by this technology without using copper. ESAB by excluding the operation on removal of copper dust and chips from the welding process eliminated the reason of production equipment outage. In this case the arcing stability increased, spattering decreased, quality of weld metal improved, thus lowering the cost of weld dressing.

Constant and not high electrode wire feed force is advisable in welding (Figure 1). The welding wire OK AristoRod (Table) and high-quality coppered wire were tested in two stages. At the first stage the wires were fed through the straightened channel 4.5 m long, at the second stage the same channel was laid in loops 300 mm in diameter. At the second stage the feed force increased, its increment for both wires is shown in Figure 1, where the feed force for coppered wire is much higher than for OK AristoRod wire.

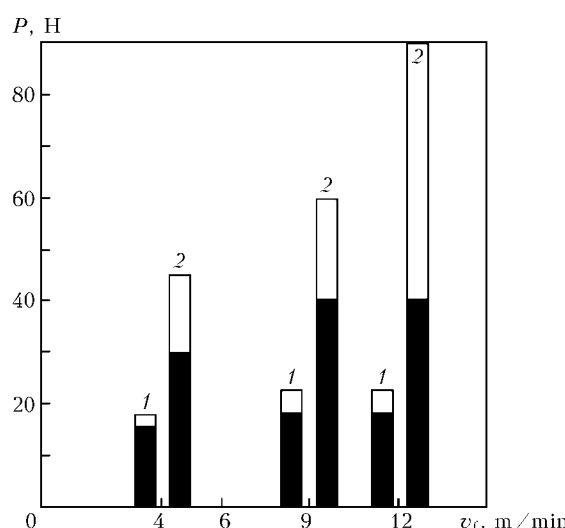


Figure 1. Diagram of feed force of wire 1 mm in diameter through the straightened channel (■) and folded hose (□): 1 — OK AristoRod wire; 2 — coppered wire

Characteristics of the AristoRod wires

Type of wire	Classification			
	Wires		Weld metal	
	AWS A5.18	EN 440	M21	C1
Î K AristoRod® 12.50	ER70S-6	G3Si1	G 42 3	G 38 2
Î K AristoRod® 12.57	ER70S-3	G2Si	G 38 3	G 35 2
Î K AristoRod® 12.63	ER70S-6	G3Si1	G 46 3	G 42 2

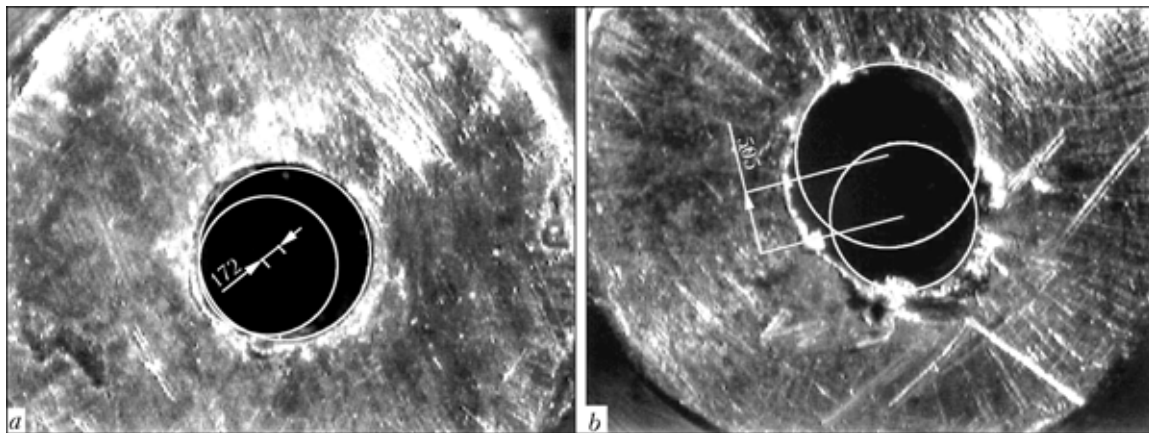


Figure 2. Results of wear tests of current-conducting tips: a --- OK AristoRod 12.50; b --- OK Autrod 12.51

Besides, the wear of current-conducting tip was much lower due to decreased friction forces (Figure 2).

ASC coatings also minimize the risk of wire corrosion during long storage period. The absence of copper on the wire has another advantage, namely the content of copper compounds is minimized in welding fumes and gases (Figure 3), which essentially improves working conditions for welder who only needs to use the protective means for breathing organs.

Therefore, the advantages of OK AristoRod wires at all welding processes are as follows:

- due to less wear of the contact tip less stops are needed for its replacement;
- due to increased arcing stability the spattering is lowered;
- uniform feed of wire fosters increased stability and improved quality of welding;
- the lowered effort allows feeding the wire for longer distances;
- due to the absence of metal dust and chips in the wire feed channels the number of stoppages for maintenance decreases;
- decreased fume content in welding improves the atmosphere for the welder in the working zone;
- improved corrosion protection permits increasing the storage period;
- the all above increases welding efficiency.

MarathonPac --- new type of welding wire packing. The use of MarathonPac has become for many users of ESAB products a key factor for increasing the production efficiency. Actually, MarathonPac allows reducing the equipment stoppage for replacement of the wire bobbin almost by 95 %. The MarathonPac package contains 250 and 475 kg of welding wire.

Another novelty of ESAB is an «infinite» feed of wire connecting several packages of MarathonPac to keep continuous work of wire feed mechanism. In this case the spent wire switches to the feed of the next one and so on, thus forming a continuous feed of the wire.

Special winding technology imparts to the wire elastic torsional deformation, which is compensated when the wire wrap rolls off the package. Therefore the fed wire is not twisted and entangled, which eliminates wandering of the arc and provides high quality of weld in all spatial positions of welding. The wire

untwisting from bobbin is automatic. It requires the use of support equipment and application of additional force for spinning of the bobbin.

MarathonPac is supplied in octagonal paperboard packages of multiple use. **AristoRod and MarathonPac are an optimal combination to increase efficiency of the welding process.** AristoRod and MarathonPac form a combination with which is hard to compete in terms of high efficiency of not only mechanical and automated but also manual welding. Many manufacturers in different branches of industry have appreciated the benefits of increasing production efficiency. For instance, the automobile producers re-

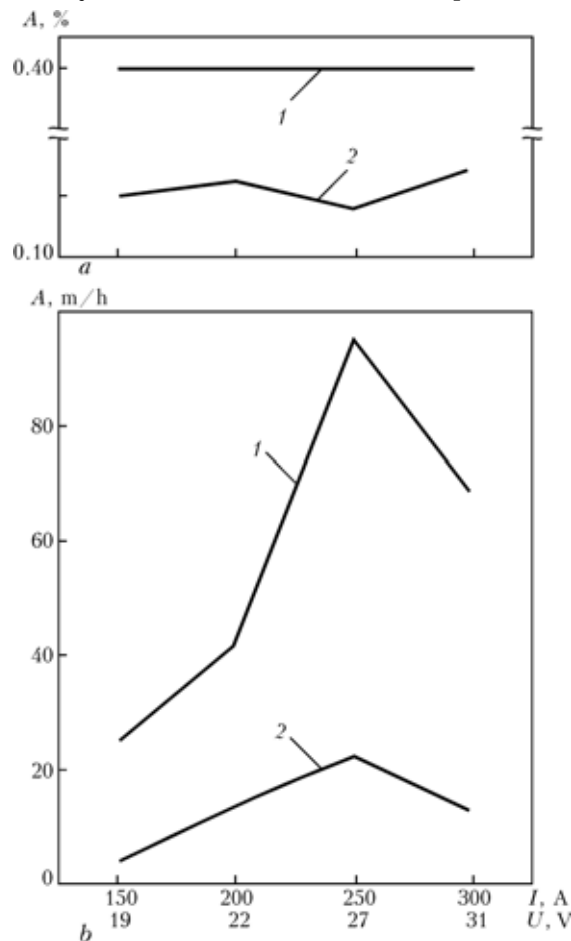


Figure 3. Quantity (A) of copper vapors in welding fume of coppered (1) and OK AristoRod (2) wire



alize the importance of welding efficiency to meet the supply schedule for ready products. That is why the AristoRod and MarathonPac combination first of all has found its application in the motor-car construction. In particular, its use in the production unit VBG in Warneborg specializing in manufacturing of automobiles with load-carrying capacity of more than 16 t allowed increasing the efficiency of welding production line almost by 15 %.

The use of the above combination at the Italian production enterprises Fai Komatsu Industries (Padua) allowed not only essentially increasing the welding efficiency but also obtaining the ISO 14.000 certificate, which toughly regulates the overall effects on the environment.

Here is another interesting example. The use of the package Jumbo MarathonPac at one of the world largest ship-building Kvaerner Masa Yards (Turku) allowed using wire conduits 37 m long without inter-

mediate feeder in production of beams of 22 mm long. The beams were simultaneously welded in both sides using two carriages, each having two welding heads. Three wires are fed into every head, so 12 wires are involved into welding process simultaneously. The beam elements are welded for one pass at high speed by continuous or discontinuous fillet weld with 2.4–8.0 mm leg. Any failures in the wire feed system are inadmissible during such high productive welding. Stoppages of equipment for wire replacement are minimized. Welding wires 1.6 and 2.0 mm in diameter are fed from the 450 kg package of MarathonPac indispensable for such high-speed operational mode.

Growth of economy in Ukraine, particularly such branches as ship- and automobile building, as well as general engineering, allows hoping that new advanced welding technologies will occupy a prominent place in the national industry.

ORGANIZING SEAMLESS WIRE MANUFACTURING IN UKRAINE

R. ROSERT¹, A.N. ALIMOV² and A.M. MIKITENKO²

¹Drahtzug Stein Wire & Welding, Germany

²OJSC ARKSEL, Donetsk, Ukraine

Summarized are the data on establishing in Ukraine the production of small-diameter seamless flux-cored wires for application in ship-building, manufacture of pressure vessels, laying of pipelines and fabrication of engineering structures.

Keywords: arc welding, seamless flux-cored wires, production technology, range, advantages, development prospects

ARKSEL company, Donetsk, Ukraine, together with Drahtzug Stein Wire & Welding, Germany, has mas-



Figure 1. Device for control of the coefficient of ready wire filling with the charge mounted in the line of Megafil wire copper plating

© R. ROSERT, A.N. ALIMOV and A.M. MIKITENKO, 2005

tered full-scale production of flux-cored wires and strips, known under the trade names of Megafil®, Mecufil®, Topline® and Topcore®. Technological process of manufacturing of these welding consumables in ARKSEL completely corresponds to the technology used by Drahtzug Stein both in the head plant in Germany and in the affiliate plants. ARKSEL production lines used for manufacture of seamless flux-cored wires, are fitted with control devices, mounted and commissioned by Drahtzug Stein specialists (Figure 1). The system of product quality control is certified in keeping with DIN EN ISO 9001.

Production program of manufacturing ARKSEL seamless flux-cored wires started with putting into production the most widely used and needed in Europe wire grades Megafil 713R, Megafil 821R and Megafil 710M. Wire specification is given in Table 1, and the effectiveness of their application is illustrated by cost estimate for welding 1 m of weld, given in Table 2. Some operations of wire manufacturing and examples of application of Megafil wires by the users are shown in Figures 2–4.

Metal structure fabricators in shipbuilding, mechanical engineering, construction of bridge and building structures are offered a wide range of seam-

**Table 1.** Characteristics of seamless flux-cored wires

Wire grade, EN classification, certification	Typical composition, %	Typical mechanical properties of deposited metal in as-welded condition	Recommended applications
Megafl 710M T 46 4 I I 1 I 5 \varnothing 1.0–2.4 BV, LR, DNV, RINA, FORCE, GL, DB	0.05C 1.30Mn 0.70Si	$\sigma_{0.2} \geq 470$ MPa $\sigma_t = 550$ –650 MPa $\delta \geq 27$ % $a_n^{-40} > 60$ J/cm ²	Shipbuilding, pressure vessels, pipelines, engineering facilities
Megafl 713R T 46 2 P C 1 H5 T 46 4 P M1 H5 \varnothing 1.0–1.6 TÜV, DB, GL, Controlas, BV, LR, DNV, RINA, PRS, FORCE, ABS	0.05C 1.30Mn 0.50Si 0.20Ni 0.03Ti	$\sigma_{0.2} \geq 460$ MPa $\sigma_t = 550$ –650 MPa $\delta \geq 22$ % $a_n^{-40} > 60$ J/cm ²	Same
Megafl 821R T 50 4 1Ni P C 1 H5 T 50 6 1Ni P M1 H5 \varnothing 1.0–1.6 TÜV, DB, GL, BV, LR, DNV, RINA, PRS, FORCE, ABS	0.05C 1.30Mn 0.50Si 0.70Ni 0.03Ti	$\sigma_{0.2} \geq 500$ MPa $\sigma_t = 550$ –690 MPa $\delta \geq 22$ % $a_n^{-60} > 47$ J/cm ²	»

less flux-cored wires with technological capabilities unique for the market of Ukraine, which are due to the features of the technological sequence of manufacturing. The main stages of the technological process determining the user characteristics of the wires are as follows:

- manufacture of the initial tube by HF welding with subsequent control of welded joint tightness;
- preliminary preparation of the flux filler from a mixture of powder-like components by the agglomeration method;
- filling the calibrated tube by a flux core by vibration method;
- control of filling of the tube inner cavity by the flux core before drawing;
- drawing of a filled billet up to a finished diameter with intermediate annealing;

- applying a copper coating 0.15–0.20 μm thick on the wire surface and its pressing. 100 % control of the finished wire filling after pressing of the copper coating;

- rewinding of finished wire on user coils and its packing.

Operation of light recrystallization annealing of the wire with a tight sheath before the final drawing operation ensures a complete removal of residual moisture from the flux core. Due to wire annealing before drawing to a final diameter, the content of diffusible hydrogen in the deposited metal does not exceed 5 ml/100 g, and usually is in the range of 2–3 ml/100 g in welding in CO_2 and gas mixture ($\text{Ar} + 18\% \text{CO}_2$).

Technical, process and economic advantages of flux-cored wires, compared to solid wires in gas-

**Figure 2.** Precision winding of flux-cored wire on user reels**Figure 3.** Wire in the packing before shipment to customer

**Table 2.** Effectiveness of flux-cored wire application instead of solid wire Sv-08G2S in welding of a 20 mm thick butt joint (typical calculation)

Parameter	Symbol	Unit of measurement	Formula
Diameter	\emptyset	mm	--
Cost of salary, power, equipment, etc.	Z	Hr/h	--
Arc voltage	U	V	--
Welding current	I	A	--
Amount of molten wire per 1 h	P	kg/h	--
Duration of operation (duty cycle) per 1 h	PR	h	--
Price of 1 kg of wire	K	Hr/kg	--
Wire consumption coefficient	K_c		--
Price of 1 kg of shielding gas	G_c	Hr/l	--
Gas flow rate per 1 min	G_f	l/min	--
Gas flow rate per 1 kg of weld	G_w	l/kg	$G_w = 60 \times G_f / P \times PR$
Weight of 1 m of weld 20 mm thick	M	kg/m	$M = V \times 7.85$
Cost of 1 kW·h of power	E_k	Hr/kW	--
Power consumption per 1 kg of weld	E_c	kW	$E_c = I \times U \times PR / 1000 \times P$
Cost of gas per 1 kg of weld	E_g	Hr/kg	$E_g = G_c \times G_w$
Cost of filler materials per 1 kg of weld	E_f	Hr/kg	$E_f = K \times K_c$
Production cost per 1 kg of weld	Z_w	Hr/kg	$Z_w = Z / P \times PR$
Power cost per 1 kg of weld	E_p	Hr/kg	$E_p = E_c \times E_k$
Total cost per 1 kg of weld	Z_{tot}	Hr/kg	$Z_{tot} = Z_w + E_f + E_g + E_p$
Welding cost per 1 m of weld		Hr/m	$Z_{tot} \times M$

Table 2 (cont.)

Parameter	Welding position				
	Downhand		Upward		
	Sv-08G2S	Megafil 710M	Megafil 713R	Sv-08G2S	Megafil 713R
Diameter	1.6	1.6	1.6	1.2	1.2
Cost of salary, power, equipment, etc.	32	32	32	32	32
Arc voltage	27	30	30	23	25
Welding current	250	330	330	180	250
Amount of molten wire per 1 h	3.4	6.3	6.5	2.7	4.5
Duration of operation (duty cycle) per 1 h	0.7	0.7	0.7	0.7	0.7
Price of 1 kg of wire	7.2	18	18.5	7.4	19
Wire consumption coefficient	1.17	1.08	1.12	1.15	1.12
Price of 1 kg of shielding gas	0.03	0.03	0.03	0.03	0.03
Gas flow rate per 1 min	18	18	16	15	13
Gas flow rate per 1 kg of weld	453.78	244.90	210.99	476.19	247.62
Weight of 1 m of weld 20 mm thick	2.45	2.45	2.45	2.45	2.45
Cost of 1 kW·h of power	0.23	0.23	0.23	0.23	0.23
Power consumption per 1 kg of weld	1.39	1.10	1.07	1.07	0.97
Cost of gas per 1 kg of weld	12.71	6.86	5.91	14.29	7.43
Cost of filler materials per 1 kg of weld	8.42	19.44	20.72	8.51	21.28
Production cost per 1 kg of weld	13.45	7.26	7.03	16.93	10.16
Power cost per 1 kg of weld	0.32	0.25	0.25	0.25	0.22
Total cost per 1 kg of weld	34.89	33.81	33.91	39.97	39.09
Welding cost per 1 m of weld	85.49	82.83	83.07	97.94	95.77

Notes. 1. Volume of deposited metal (V) for a butt-welded joint 20 mm thick 1 m long was taken to be equal to 312 cm^3 . 2. Flux-cored wire Megafil 710M --- wire with metal powder core (without slag). 3. Flux-cored wire Megafil 710R --- wire with quickly solidifying slag of rutile type. 4. Calculation did not take into account the cost of cleaning the HAZ to remove spatter and grinding the weld surface before painting for Sv-08G2S wire. In welding with Megafil 710M and Megafil 710R wire these costs are eliminated.



shielded welding, are well known. These are an essentially higher welding efficiency, good formation of the bead surface, absence of fusion defects, lower dependence of welded joint quality on welder qualifications, etc. Let us mention just some advantages of seamless flux-cored wires compared to rolled-in wires that do not have a tight longitudinal butt joint:

- absolute protection of the flux core from possible saturation with moisture from the atmosphere during storage or use even without packing for a long time;
- no need to perform repeated baking before use;
- possibility of copper plating of the surface and improvement of wire sliding along the guide in welding equipment;
- improved feeding of the wire, no need to use a four-roller feed system, ability of working with semi-automatic machines designed for solid wires;
- lower wear of the current-carrying tip and more stable arcing due to a constant reliable contact of the moving wire with the tip;
- higher ductility and impact toughness of weld metal due to a superlow content of diffusible hydrogen in the deposited metal (less than 5 ml / 100 g).

The plans of Drahtzug Stein and ARKSEL companies for further development of joint production of seamless flux-cored wires envisage a gradual mastering of a wider range of welding consumables, meeting the demands of the Ukrainian market. A complete list of welding consumables scheduled for production includes:



Figure 4. Welding with Megafil 713R wire in shipbuilding plant of Damen Shipyard «Okean» in Nikolaev, Ukraine

- Megafil ---- a family of flux-cored wires with a rutile and basic-type core, as well as with metal-powder core for gas-shielded welding;
- Megafil A ---- a family of flux-cored wires for wear-resistant repair and reconditioning surfacing in shielding gases and without additional shielding;
 - Mecufil ---- a family of flux-cored wires for arc (consumable electrode) or plasma brazing;
 - Topline ---- a family of flux-cored strips for consumable electrode submerged arc welding and surfacing;
 - Topcore ---- a family of flux-cored wires for submerged arc welding and surfacing.



MODEL OF THE PROCESS OF COMBUSTION OF IRON IN OXYGEN DURING STEEL CUTTING

V.B. OKHOTSKY

National Metallurgical Academy of Ukraine, Dnepropetrovsk, Ukraine

The paper described the model of combustion of iron-base metal in oxygen, including in cutting by oxygen jets. Calculation and experimental data are in good agreement.

Keywords: cutting, oxygen jet, iron-base steels, combustion process, combustion rate, oxygen mass transfer, model

Combustion of iron in oxygen, in its pure form, takes place, e.g. in cutting of iron-base metal. This process determines the speed of cutting and productivity of handling of scrap, cutting of billets using continuous casting machines, and conditioning of metal in rolling production.

Combustion of iron in oxygen and the speed of cutting of iron-base metal were studied under field [1] and laboratory conditions by conducting experiments on cutting of rods [2] and combustion of horizontal [3–6] and vertical [7] wires. Combustion of iron was investigated both under rarefaction and increased pressure [4–6], using both alloyed steels [5, 6] and cast irons [6].

Combustion of metal with the dominant iron content underlies the steel melting processes with oxygen lancing, which was another reason for its investigation [8].

The purpose of this study was to develop a model of the process of iron-oxygen combustion. Considering differences in experimental procedures [1–8], it was necessary to develop the model of the process for specific conditions.

Combustion of wire of iron-base metal located horizontally [3–6] or vertically [7] is characterised by formation of a molten drop at the hot tip, which periodically detaches from the tip. As the processes of formation of bubbles (when gas flows to a liquid) or a drop (when liquid flows to gas) occur in a similar way [9], given that diameter of the jet of a melting metal and iron combustion products is the initial diameter of wire, d , and that the flow of the melting products has a very low rate, it can be assumed that the drops are formed in the gravity-capillary mode, in which the diameter of the forming drops is $D = d(4/B_0)^{1/3}$ [10], where $B_0 = \Delta\rho gd^2/\sigma$ is the Bond criterion; $\Delta\rho = \rho_l - \rho$; ρ_l and ρ are the densities of liquid and gas, respectively; g is the gravity acceleration; and σ is the surface tension of liquid.

If the metal combustion process is limited by an external transfer of oxygen in the gas phase to the surface of a formed drop, during combustion time dt the following mass of oxygen is transferred:

$$dm_{O_2} = (\beta_{O_2} p_{O_2} F/RT_g)d\tau, \quad (1)$$

where β_{O_2} is the coefficient of mass transfer; p_{O_2} is the partial pressure of oxygen in the gas phase related to the atmospheric one; $F = \pi D^2$ is the surface area of the formed and growing drop; R is the universal gas constant; and T_g is the temperature of the gas phase.

The relative velocity of the drop and environment being neglected, it holds that

$$\beta_{O_2} = ShD_{O_2}/D,$$

where $Sh = 2$ [11]; $D_{O_2} = D_{O_2}^0(T_b/273)^{1.8}(1/p)^{1/2}$ is the coefficient of molecular diffusion of oxygen in the gas phase [12]; $D_{O_2}^0$ is the same but under normal conditions; T_b is the temperature of the boundary layer equal to $(T_g + T_c)/2$; T_c is the temperature of metal combustion; and $1/p$ is the ratio of normal atmospheric pressure to actual pressure in the gas phase, p .

Increase in mass of the molten drop as its size changes is

$$dm_l = (\rho_l \pi D^2/2M_{Fe})dD. \quad (2)$$

As

$$dm_l = dm_{O_2}(\Delta H_c/\Delta H_l)(m_M/m_{O_2}), \quad (3)$$

where ΔH_c is the thermal effect of metal combustion; ΔH_l is the heat content of the molten drop; m_M and m_{O_2} are the quantities of moles of metal and oxygen, respectively, participating in the combustion reaction, then, substituting equations (1) and (2) to formula (3) and integrating the resulting expression for increase in size of the drop, dD , during time $d\tau$ within a range of $D = 0$ at $\tau = 0$ and $D = D$ at $\tau = \tau$, yield the time necessary for the drop to reach size D :

$$\begin{aligned} \tau &= \rho_l(\Delta H_l/\Delta H_c)RT_g(p/1)^{1/2} \times \\ &\times D^2/M_{Fe} 3\delta_{O_2} 2D_{O_2}^2(T_b/273)^{1.8}. \end{aligned} \quad (4)$$

Transforming a change in size of the drop to the critical one, at which the drop detaches, and wire combustion rate v yields

$$\begin{aligned} v &= (m_\mu/m_{O_2})M_{Fe}^{2/3}(\Delta H_c/\Delta H_l)(1/p)^{1/2} \times \\ &\times 2D_{O_2}^0(T_b/273)^{1.8}\sigma^{1/3}p_{O_2}/\rho_s RT_g \Delta\rho^{1/3} g^{1/3} d^{5/3}, \end{aligned} \quad (5)$$



where ρ_s is the wire metal density; and M_{Fe} is the atomic mass of iron.

At end cutting of a metal layer with the oxygen jet moving at rate w [2], or cutting through a metal lump with thickness δ [1], the coefficient of oxygen mass transfer can be determined using the Danquerts model $\beta_{O_2} = (D_{O_2}/\tau^*)^{1/2}$ [11], where the surface renewal time is $\tau^* = \delta/w$ and, therefore, $\beta_{O_2} = (D_{O_2}w/\delta)^{1/2}$. Under the experimental conditions [8], $\delta = d/2$ at an oxygen flow coaxial to the burning metal rod with diameter d , and at an opposing oxygen flow, compared with cleaning one [1, 2], the metal combustion rate increases 2.5 times.

Unlike the model of a spontaneous combustion of metal in oxygen [3–7], cutting with the oxygen jet is performed in a steady-state mode (in terms of space) at a constant reaction surface area.

Specific intensity of an external mass transfer of oxygen to the combustion surface is equal to

$$i_{O_2} = \beta_{O_2} p_{O_2} / RT_g, \quad (6)$$

which, in terms of the cutting speed, yields the following expression:

$$v = p_{O_2} (m_M/m_{O_2}) (\Delta H_c/\Delta H_l) \times M_{Fe} (D_{O_2} w/\delta)^{1/2} (1/p)^{1/2} / \rho_s R T_g \quad (7)$$

As reported in [13], where the data of numerous studies are generalised, in oxygen cutting of iron-base metal the cutting products contain both iron oxides and a metal melt. It can be assumed that combustion occurs until FeO or Fe₃O₄ is formed, and that composition of the cutting products varies from a pure iron metal to pure oxides FeO or Fe₃O₄. Calculations of value v from expressions (5) and (7) were made using the data given in [11, 14, 15].

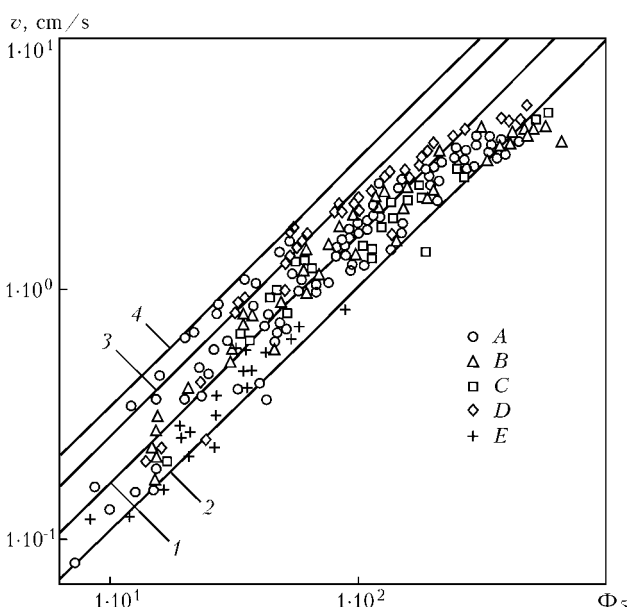


Figure 1. Rate of combustion of metal wire in oxygen (see designations in the text)

In Figure 1, the rate of combustion of iron-base metal wire is shown as a function of a variable part of expression (5):

$$\hat{\phi}_5 = p_{O_2} (1/p)^{1/2} d^{5/3} \text{ atm/cm}^{5/3}$$

at the following variants of input data: combustion of iron occurs to form FeO with melting of iron (curve 1) or melting of FeO (curve 2), or to form Fe₃O₄ with melting of iron (curve 3) or melting of FeO₄ (curve 4). Figure 1 was plotted using the following experimental data on combustion of metal in oxygen:

- steel with 0.024–0.044 % C; 0.29 % Mn; ≤ 0.02 % Si; $\delta = 0.5$ –2 mm; $p = 0.25$ –1 atm [3];
- iron $\delta = 1$ and 2 mm; $p = 1$ –100 atm [4];
- steel with 0.33 % C; 1.6 % Cr; 0.25 % Mn; 1.11 % Ni; $\delta = 1$ and 2 mm; $p = 1$ –200 atm [5];
- steel with ≤ 1.1 % C; 0.25–1.29 % Mn; 1.33–1.51 % Si; 22.4–27.9 % Cr; 0.44 % Mo; 11.6 % Ni; $\delta = 2$ mm; $p = 5$ –150 atm;
- cast iron with 3.48–3.73 % C; 0.39–0.70 % Mn; 1.86–2.35 % Si; 2 × 2 and 2 × 3 mm²; $p = 1$ –26 atm [6];
- iron $\delta = 1$ mm; $p = 1.8$ and 2 atm [7].

These data are broken into groups: steels with ≤ 0.1 % C (A), 0.1–0.5 % C (B), > 0.5 % C (C), stainless steel (D) and cast iron (E).

It is not difficult to notice that decrease in the carbon content of metal causes increase in the combustion rate at a constant value of Φ_5 , which is especially pronounced in transition from cast iron to steel. It can be assumed that both carbon and elements with a higher affinity for oxygen, compared with iron, (e.g. silicon contained in cast iron in marked concentrations) raise the probability of combustion of iron to form FeO, which provides a lower thermal effect than in combustion to form Fe₃O₄ and, accordingly, a lower combustion rate.

In general, the results calculated from formulae (5) and experimental data are in satisfactory agreement, which proves the assumption that the combus-

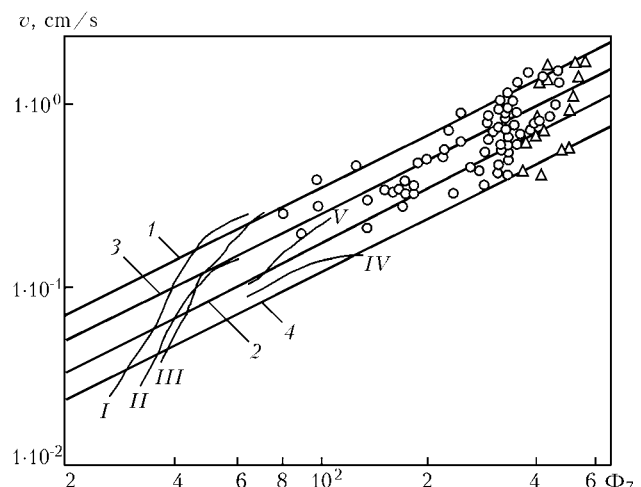


Figure 2. Speed of cutting of metal with oxygen jets (see designations in the text)



Cutting device	Pressure at nozzle, atm	δ , mm	Curve in Figure 2
Laval nozzle	3.5	350–1350	III
Cutter R-100-2 (converging nozzle)	3.5 and 2.0	350–1350	II
Cutter R-100	3.75	300–2000	I
Cutter R-100-1 (converging nozzle)	2.5	75–350	IV
Cutter R-100-1 (Laval nozzle)	5.0	150–525	V

tion process is limited by an external transfer of oxygen in the gas phase. An experimental finding of [3] that $v \sim p_{O_2}^{1/2}$ can be explained by the fact that the coefficient of molecular diffusion in gases is inversely proportional to pressure p in a system, which, in the case of using pure oxygen ($p_{O_2} = p$) in experiments [3–6] and the combustion rate dependence of $v \sim p_{O_2}(1/p)^{1/2}$ from model (5), yielded $v \sim p_{O_2}^{1/2}$ in the experimental results.

The relationship fixed in [3], similar to $v \sim F^{-1}$, is represented in model (5) by the $v \sim d^{-5/3}$ dependence, which is close in exponent.

Figure 2 shows the results of calculation of the metal cutting speed from model (7) depending upon variable $\hat{\Omega}_7 = p_{O_2}(wD_{O_2}/\delta)^{1/2}$ at the same variants of composition of the combustion products (FeO or Fe_3O_4) and melting products (iron or its oxides) as in the first case.

The experimental data [1] on oxygen jet cutting, including special steel containing chromium and tungsten, are given in the Table.

The data on friction of rods 6.4, 9.5, 12.7 and 25.4 mm in diameter, made from armco-iron, low-, medium-, high-alloy and high-speed steel, using oxygen with a purity of 86.5 and 99.7 % fed through a slot-like nozzle at a rate of 14.8–328 m/s [2] (points O), as well as mild steel (≤ 0.1 % C) in the form of rods 3 and 5 mm in diameter at a counter-current jet of pure oxygen moving at a rate of 133–200 m/s [8] (points Δ), are given in Figure 2.

Using data of study [16] on distribution of temperature through metal thickness within the cut zone, it can be assumed that at a sufficient heating of a cut metal [2, 8, 1] at $\Phi_7 > 50$ and a heating flame capacity of 15–20 % of total heat of the cutting process, the

speed of the latter is limited by mass transfer of oxygen to the cut surface according to model (7). At the same time, at $\Phi_7 > 50$ [1] and a larger thickness of the cut metal the cutting speed (see Figure 2, curves I–III) falls faster with decrease in the Φ_7 value than results from expression (7). Apparently, the heating flame capacity of 15–20 % is insufficient, and a limiting link of the process is the required level of metal heating. Probably, increase in the heating flame capacity in the case reported in study [1] can bring the process back to the state where the limiting link of the process is again the mass transfer of oxygen to the cut surface with increase in the cutting speed.

Therefore, the rate of combustion of iron-base metal in oxygen, including in cutting with oxygen jets, can be limited by an external mass transfer of oxygen to the combustion surface. It is likely that at $\Phi_7 < 50$ the cutting speed is determined by the value of heat input due to the heating flame.

- Khrenov, K.K., Bort, M.M. (1953) Oxygen cutting of thick steel. In: *New methods for metal welding and cutting*. Kiev: Gostekhizdat Ukr. SSR.
- Wells, A.A. (1955) The iron-oxygen combustion process. *Brit. Welding J.*, 2(9), 392–400.
- Kirschfeld, L. (1959) Die Brennbarkeit von Metallen in Sauerstoff. *Angew. Chem.*, 2, 663–667.
- Kirschfeld, L. (1961) Die Verbrennungsgeschwindigkeit von Eisendraehten in Sauerstoff von hohes Druckes. *Arch. Eisen.*, 32(1), 57–62.
- Kirschfeld, L. (1965) Einrichtung fuer Verbrennungsversuche an Metallen unter Sauerstoffdrucken bis 200 atm und Brennbarkeit von Eisendraht in Hochdrucksauerstoff. *Ibid.*, 36(1), 823–826.
- Kirschfeld, L. (1968) Brennbarkeit von Stahl und Gusseisen in Sauerstoff bei Druecken bis 150 atm. *Ibid.*, 39(7), 535–539.
- Harrison, D.L., Yoffe, D. (1961) The burning of metals. *Proc. Roy. Soc.*, 261A(1306), 357–370.
- Hauttmann, H. (1961) In discussion. *J. Iron & Steel Inst.*, 198(1), 410–411.
- Okhotsky, V.B. (1988) Formation of drops with a jet of liquid flowing to the other liquid. *Inzh.-Fiz. Zhurnal*, 54(2), 203–211.
- Okhotsky, V.B. (1997) Size of gas bubbles formed in liquid. *Teoret. Osnovy Khim. Tekhnol.*, 31(5), 458–464.
- Okhotsky, V.B. (1993) *Physical-chemical mechanics of steelmaking processes*. Moscow: Metallurgiya.
- Bretschneider, S. (1966) *Properties of gases and liquids*. Moscow-Leningrad: Khimiya.
- Vasiliev, K.V. (1963) *Electric cutting of metals*. Moscow: Mashgiz.
- Elliott, J., Gleiser, M., Ramakrishna, V. (1969) *Thermochimistry of steelmaking processes*. Moscow: Metallurgiya.
- Esin, O.A., Geld, P.V. (1962) *Physical chemistry of pyrometallurgical processes. Part 1*. Sverdlovsk: Metallurgizdat.
- Von Hofe, H., Wirtz, H. (1967) Neue Erkenntnisse zum Ablauf des Brennschneidvorganges. *Schweissen und Schneiden*, 19(5), 203–209.



APPLICATION OF OBJECT-ORIENTED SOFTWARE PACKAGE MS DirectShow FOR MODELLING OF PROCESSING TECHNICAL VISION VIDEO SIGNALS

F.N. KISELEVSKY and V.A. KOLYADA

E.O. Paton Electric Welding Institute, NASU, Kiev, Ukraine

Method is suggested for calibration of triangulation optical sensors used in automation of welding processes. This method allows calibration of the sensors after mounting them on a welding unit under factory conditions.

Keywords: video data flow, image processing, video capture device, band-pass filter, video camera, line generator

Automation of welding processes involves many problems. One of the key components of any modern automatic welding system is a system for acquisition of data on parameters of a welded joint. Preference is given to the data acquisition systems that are based on technical vision devices. At the initial stage of development of such a system it is necessary to decide on the type of a sensor that is an «eye» of the system and method for video data processing, as well as estimate probable errors in measuring values of the required parameters. It is apparent that a developer also needs the experimental data, in addition to the analytical ones. The object-oriented software package MS DirectShow is best suited to modelling of the process of operation of some types of the sensors. Its component structure allows the developer to easily and rapidly process the video data flow, receive the experimental data and estimate them on the basis of assigned criteria.

MS DirectShow is an object-oriented software package intended for reproduction, conversion and storage of data in different formats. The component structure of MS DirectShow facilitates the work of the developer with new formats of the data, makes it possible to generate new user effects and convert the standard format data [1].

The DirectShow technology is based on the modular system of components (filters) united into a structure called the filter graph. Each filter can be applied as a conventional object, having its properties and methods. With the availability of a program code of a filter, its internal structure can be modified to suit developer's requirements. The standard DirectShow filters include the Image Effects data conversion filter, the input program codes for which are contained in the software package. Each image frame from the video camera is transmitted to the Image Effects filter in the form of a 24-digit pixel picture of a fixed size. Each pixel of the image is characterised by the RGB palette, meaning that three colours, i.e. red, green and blue, having different intensity (from 0 to 255) correspond to each pixel. As the black-and-white video cameras are primarily employed in TV sensors to measure joints of welded structures, in this case all the three colours of each pixel have an identical intensity. Therefore, input data for the Image Effects filter have the form of a sequence of integer number matrices. The developer has just to enter the program code into the filter to process an integer number matrix following a certain algorithm. The processing result is automatically fed to the filter output.

The triangulation method for measuring parameters of a welded joint is based on video filming of region of the joint with a narrow light band projected

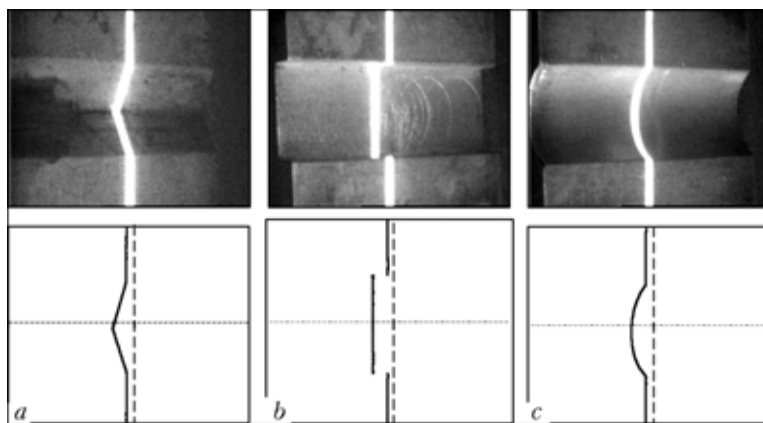


Figure 1. Frames of initial and mathematically processed images of joints with V- (a), rectangular (b) and oval (c) groove

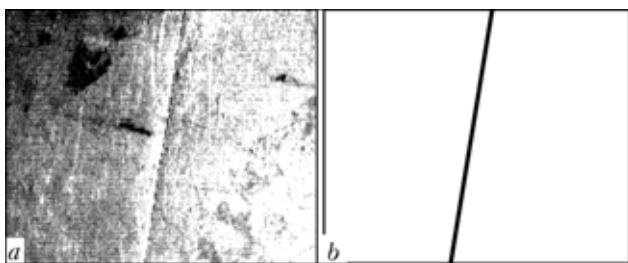


Figure 2. Frames of initial (a) and mathematically processed (b) images of joints

on its surface, which enables estimation of shape and size of the groove elements and measurement of variations in distance between the sensor and workpiece with respect to some initial relative position [2].

Image from the video camera is transmitted through the video capture device to the computer for processing. In the computer, the DirectShow software arranges a flow of video data through the filter graph. With the triangulation method of measuring parameters of a welded joint the most important steps are correct location of the profile of projection of the light band and its entering into some 2D coordinate system.

The Image Effects filter is designed so that it can transmit video data with and without processing from input to output. Figure 1 shows frames of image of welded joints with the most common groove shape. The found profiles of projection of the light band are entered into the 2D coordinate system with origin at the image centre. Therefore, each image frame that passed through the filter graph has a 2D array of x - x and y - x coordinates of points of the light band projection profile, from which it is not difficult to calculate all parameters of the joint required for each particular case.

The zero gap sensor was developed specifically to guide the electrode to the square butt joint with a gap between the parts welded close to zero [3]. The sensor consists of a video camera, band-pass filter and matrix of infra-red light-emitting diodes. Image of

the joint illuminated by the light-emitting diodes is transmitted through the band-pass filter matched with the wavelength of the light-emitting diodes to the video camera objective (Figure 2, a). Processing of image of the joint in this case consists of determination of coordinates of the joint points in pixels and plotting the approximating curve from them to determine position of the joining line with respect to the sensor and, hence, to the welding device (Figure 2, b). This information is sufficient to form a signal for transverse correction of the position of the welding device. The DirectShow software was also used to model operation of the zero gap sensor. The modelling results allowed a conclusion of the feasibility of using the technical vision devices for automatic adjustment of position of a welding device in welding of joints with a gap close to zero.

The object-oriented software package DirectShow makes it possible to readily and rapidly model operation of different types of the sensors, as well as check efficiency of different methods intended for measuring parameters of welded joints to solve specific problems. The major drawback of this software package is a low data transmission rate limited by capabilities of available hardware. If there is no need to ensure a high rate of acquisition of video information (10–15 frame/s), then, as shown by practice, the DirectShow software tools can be applied to develop the full-blown automatic welding systems using the technical vision devices. Such systems developed by the E.O. Paton Electric Welding Institute have been commercially used to advantage for welding of metal structures, including straight-line and roll butt welds in different-diameter pipes of aluminium and steel alloys.

1. Goncharov, D., Salikhov, T. (2001) *DirectX7.0 for programmers*. Training aids. St.-Petersburg: Piter.
2. Boillot, J., Noruk, J. (2002) The benefits of laser vision in robotic arc welding. *Welding Technique*, **8**, 33–34.
3. Kiselevsky, F.N., Butakov, G.A., Dolinenko, V.V. et al. (2003) Optical sensor for butt following at gap sizes close to zero. *The Paton Welding J.*, **2**, 48–50.



THESIS FOR SCIENTIFIC DEGREE

**Volgograd State Technical University (VolgGTU),
Volgograd, Russia**



S.N. Vlasov (VolgGTU) defended on June 24, 2004 master's thesis «Study and Development of Technology for Non-Consumable Electrode Helium-Arc Welding of Thin-Plate Elements of Chromal-Type Alloys».

The work is devoted to solution of the urgent task of welding thin-plate elements of precision Fe-Cr-Al alloys of Chromal type. Welding of small-ampere arc with non-consumable electrode in helium is proposed as a method providing a high level of mechanical and operational properties of the joints.

The following new scientific results are obtained in this work:

- Correlations between electrophysical peculiarities of small-ampere arcing with non-consumable electrode in helium and heat conditions in the welding zone, which finally determine strength properties of welded joints of thin-plate alloys of Chromal type are established. In this case application of the helium-arc welding decreases a degree of overheating and

increases the number of the weld metal grain and near-weld zone, facilitates heat destruction of surface oxide film at the account of increasing the arc concentration by 1.9–3.3 times as compared with arc in argon;

- It is shown that one observes a decrease of resistance of the activated non-consumable electrodes exposed in formation of knobs and destruction of working sites specified by a change of physical properties of the electrode material as a result of formation of multi-component solid solutions on the basis of tungsten, which contain elements of the electrode and those evaporating from anode;

- It is for the first time shown that a voltage jump observed under increase of helium content in the Ar-He mixture up to 75–80 % (up to 3 V) is conditioned by an increase of not only cathode but also anode fall of potential, which only slightly ranks bellow the first in value and may achieve 1.0–1.5 V. In this case the potential gradient in the arc column remains practically unchanged.

- The developed method for determination of the arc column diameter by transversal probing with a double horizon probe allows establishing that a maximal compression of the arc column in helium occurs not in the close proximity but at a certain distance from anode. A change of structural parameters of the working site of the electrode and gas consumption allow within a wide range controlling a shape and a size of the arc column in helium influencing its concentration and penetration ability

The results of the studies serve as the basis for development of the technology for repair welding of the resistance elements of the tram for Production Association «Volgogradelektrotrans».



THESIS FOR SCIENTIFIC DEGREE

**Volgograd State Technical University (VolgGTU),
Volgograd, Russia**



I.E. Lapin (VolgGTU) defended on November 18, 2004 the Doctor's thesis «Increase of Technological Properties of Arc in TIG Welding».

The scientific novelty of the work is in resolution of an urgent scientific problem for creation of theoretical fundamentals for formation of the welding arc with diffusion cathode spot (DCS) in welding with non-consumable electrodes in the inert gasses or in their mixtures within a wide range of currents. The findings became the basis for development of methods and tools for controlling technological properties of the arc as applied to welding conditions on DC and AC for different types and classes of structural materials for a wide range of the thickness of welded parts.

A decisive role of emission cooling of cathode and Joule heat release whose required level in the working zone is achieved under current densities of not less than $45\text{--}50 \text{ A/mm}^2$ and should exceed the energy that comes from the arc to the electrode is theoretically proved.

It is established that resistance of non-consumable electrodes under welding with DCS arc in helium and Ar-He mixtures is on par with their resistance under welding in pure argon while efficiency of the metal heating with the heat input energy of more than 650 kJ/m is characterized by a presence of thermody-

nical minimum specified by a growth of arc power under increase of the helium concentration, on the one hand, and decrease of its power effect, on the other. Joint effect of these factors provides an increase of penetration ability under helium concentration of more than 25–30 % and improves weld formation under its concentration for more than 50 %.

Regularities of arcing processes with DCS determined under theoretical and experimental studies and under simulation of heat processes allow formulating conditions for simultaneous increase of temperature and decrease of the temperature gradient in the working zone of the electrode providing an increase of physical and spatial stability of the discharge and increase of the electrode stability to the heat action of the arc preventing the formation of knobs and crown.

A possibility is shown and conditions are determined for formation of the arc with DCS under welding with AC with rectangular form of pulses (RFP). It is established that under changes of current rates above $(2.5\text{--}3.0) \cdot 10^6 \text{ A/s}$ a powerful gas-dynamic effect on the weldpool related to a sharp change of the arc pressure under the change of polarity increases its penetration ability.

Studies of electrophysical and technological characteristics of arc in the inert gases and their mixtures allowed developing ways and methods for increasing resistance of non-consumable electrodes and stability of small-ampere arc, improving formation of welds, increasing of penetration ability of the arc and productivity of welding of structures of high-alloy steels and non-ferrous metals. Technological recommendations and relevant software are created for optimization of arc properties in solution of specific tasks in welding with non-consumable electrodes. High-effective welding and surfacing processes with non-consumable electrode are developed. They are introduced on the S.P. Korolyov Rocket Space Corporation «Energiya» (Korolyov, Moscow oblast), Federal State Unitary Enterprise «Barrikady» (Volgograd) and others.